Big Bang Nucleosynthesis and Evolution of Dark energy

一政, 遼太郎

https://doi.org/10.15017/1806810

Thesis

Big Bang Nucleosynthesis and Evolution of Dark Energy

Theories of Particle Physics,
Nuclear Physics and Astrophysics/Astronomy,
Department of Physics, Graduate School of Science,
Kyushu University
Advisor: Prof. Masa-aki Hashimoto

March 2017

Ryotaro Ichimasa

Abstract

The standard model of cosmology based on the Big Bang theory is established as the theory which can reproduce many astrophysical phenomena because of dramatic improvements of observations in recent years. Cosmic Microwave Background (CMB) radiation, type Ia supernovae, abundances of light elements and determination of H_0 by observing the Cepheid variables are the representative observations. In particular, CMB is observed using WMAP satellite and Planck satellite up to the redshift, $z \sim 1000$, which includes the oldest information we can currently obtain. These observations have revealed that only 4% of baryons is present as the component of the current universe. Others are consist of dark matter (28%) and dark energy (68%). In order to describe correctly the evolution of the universe, it is necessary to accurately predict the time evolution of these components. Although current composition ratios among baryons, dark matter and dark energy are determined exactly, more detailed observation and analysis are required to clarify their properties.

Helium-4 and deuterium are the most important elements that are synthesized in the early universe: so-called Big Bang nucleosynthesis (BBN). Observation of helium-4 has large ambiguity because the primordial quantity is evaluated using models of chemical evolution of the galaxy. In addition, there exist crucial uncertainties for observations. Two groups give different observational results.

On the other hand, the abundance of deuterium is estimated from the absorption spectrum due to the backward quasar which is considered to be the primitive galaxy at the early stage of its formation; and the abundance is determined with very high accuracy. In order to predict accurately these abundances of light elements which are assumed to be synthesized by BBN, it is necessary mainly to determine the nuclear reaction rates, the lifetime of neutrons, and the number of neutrinos.

Since the present universe is dominated by dark energy, the nature of dark energy characterizes the evolution of the universe. Clarifying its feature is one of the important studies in cosmology. There are many theoretical predictions as the candidates for dark energy. One of them is a cosmological term. It can be interpreted as a static dark energy which is introduced by Einstein. For the other candidates, dynamical dark energy models, such as quintessence field and phantom field, are also theoretically predicted. Thus, there

are many kinds of method to describe the characteristics of dark energy. In addition to these models, dark energy can also be characterized by using a modified gravity field theory and an equation of state. In recent years, many discussions are performed for the availability of gamma ray bursts to limit the properties of dark energy, in addition to adopt type Ia supernova data. The supernova data have been used to constrain the properties of dark energy. If gamma ray bursts become available, we can constrain the character with use of 7 times wider range of the redshift $z < 10$.

It is assumed in these models that dark energy conserves its energy independently from other components. It is necessary to clarify the presence or absence of energy transport among them. There have been many studies on the interaction between dark energy and dark matter. Although, the latest observational data indicate that the interaction between them is not allowed, energy transport may exist between dark energy and photons may exist. Improvement of observational accuracy makes it possible to determine the temperature of the CMB photons at low redshift within 3% precision. Furthermore, it is suggested that the energy density of the CMB photons may not be conserved with 1σ confidence level. There have been proposed models with interaction between dark energy and photons which influence BBN. However, if there is an interaction between dark energy and photons, there arises a possibility of influencing Big Bang nucleosynthesis.

In the present study, firstly we investigate BBN. For the nuclear reaction rates of our calculations we adopt astrophysical nuclear reaction rates (NACRE-II) using the latest experimental value and 880.1 $\pm$ 1.1 s (J. Beringer et al. 2013) for neutron lifetime. We take observations of Izotov *et al.* (2013) and Aver *et al.* (2013) for helium-4 abundance.

Our result is consistent with the observational value of Aver *et al.* (2013). As for the observational value of Izotov *et al.*, if we include degenerate electron neutrinos we can find a plausible range of the baryon density with 1σ confidence level.

Secondly, using a specific equation of state, we investigate the density evolution of dark energy to clarify its feature in the low redshift universe. Taking account of the observational values of type Ia supernovae and gamma ray bursts, we can exclude a dark energy model in which cosmological behavior changes from a phantom-like model to quintessence-model with 2.4σ confidence level.

Contents

1 Introduction

What is the composition of our universe? How did the universe begin and evolve? These are the most basic questions. In the past few decades, our common sense for the universe has changed drastically. Einstein established the theory of general relativity and enabled a physical approach to the universe in 1916. The theory described not only the gravitational field, but also the evolution of the universe. Moreover, the theory predicts the steady, expanding, and contracting universe. Thereafter, George Gamow introduced the Big Bang model which describes the universe from the beginning to the end. Big Bang model has predicted three observational evidences:

1) Our universe is not stationary, but expanding.

2) Light elements were synthesized at the early universe.

3) Cosmic Microwave Background Radiation is a relic of hot Big Bang.

Currently, there are many observational results that roughly support above predictions. However, these arise some cosmological problems, such as lithium problem, cosmological constant problem, flatness problem, horizon problem, and monopole problem. It is well known that the last three problems can be solved by adopting an inflation model. However, the others remain as unsolved serious issues. To make matters worse, recent observational results on the abundance of light elements cause a new serious problem.

In Sec. 1 we introduce the conventional approach to the cosmology and current problems what we focus on. In Sec. 2 we summarize the current situation of the Big Bang nucleosynthesis and observed abundances of light elements. In Sec. 3 we present our models and calculational results for dark energy, which is the alternative conjecture of a cosmological constant. Summary and discussions are given in Sec. 4.

1.1 Historical Review

Newton's gravitational theory cannot explain Mercury's perihelion shift. In 1916, the theory of general relativity is presented by Einstein in 1916 [1]. This theory succeeded in

explaining the above perihelion shift. After completion of the general theory of relativity, a number of scientists tried to apply this theory to the universe. Scientists made a simple assumption that universe is homogeneous and isotropic, where the fluids behave as the perfect fluid. This is so-called Cosmological Principle. Under this hypothesis, dynamics of our universe can be written in a simple formula. In 1922, Friedmann provided the cosmological solution of the Einstein equation under the ideal conditions [2]. After that in 1927, Lemaître also solved the equation with a cosmological term and put forward the expanding universe [3]. This theory suggests that the universe can take not only a steady state, but also take expanding and contracting stages. These studies are the foundation of the Big Bang model. Finally, correctness of the expanding universe was proved by the observation of Hubble in 1929 [4]. Hubble observed that the farther the astrophysical objects locate, they move away faster (see Fig. 1.1). Therefore, he derived the famous Hubble's law $v = H_0 d$. Here v, H_0 and d are the speed at which the object moves away from the earth, the Hubble constant and the distance from the earth. This observation is the first evidence of the Big Bang model.

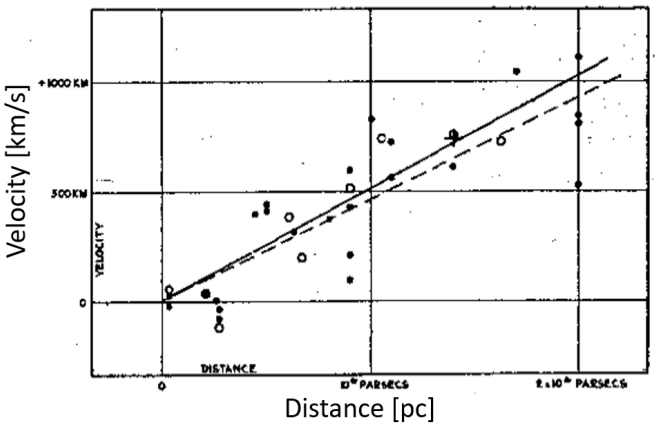

Fig. 1.1: Hubble diagram. The distance is measured in units of parsec (pc).

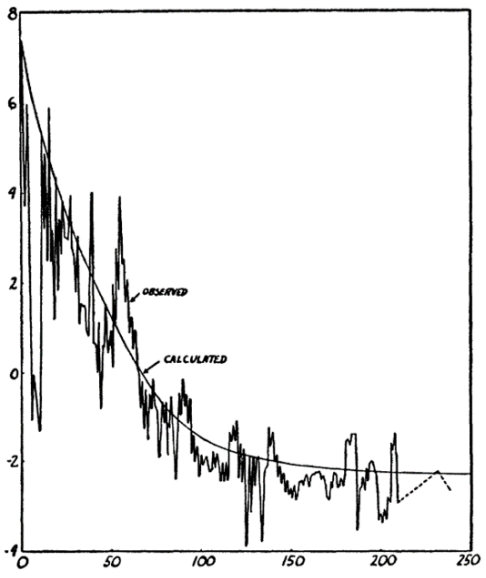

FIG. 1.
Log of relative abundance

Fig. 1.2: Comparison between the caluclation by $\alpha\beta\gamma$ theory and the solar system abundances.

In 1946, Gamow introduced firstly the Big Bang model [5]. He assumed that the uni-

verse was expanding, and thought that the early epoch of the universe occupied the high temperature and high density states. Thereafter, Alpha, Bethe, and Gamow proposed the so-called $\alpha\beta\gamma$ theory [6]. They assumed that all of nuclei are destroyed and only neutrons can exist in such a high energy condition. Furthermore, they thought that nuclei in the present universe were generated at this epoch (Fig. 1.2). However, their theory had fatal mistake and Hayashi pointed out following two points [7, 8]: (i) Neutrons and protons are in β-equilibrium via the weak interactions. (ii) Heavy elements ($A > 8$) will not be synthesized since there is no stable nuclide of the mass number $A = 8$. In the mean while, many scientists have tried to improve the theory.

The Big Bang model suggests another prediction. It is isotropic cosmic blackbody radiation, so-called Cosmic Microwave Background (CMB) radiation. The radiation could be seen only in the expanding universe, but not be seen in the steady universe. In 1964, Penzias and Wilson accidentally discovered the radiation [9] (see Fig. 1.3), but it could not give the details. Robert Dicke and James Peebles have got the same result as Gamow

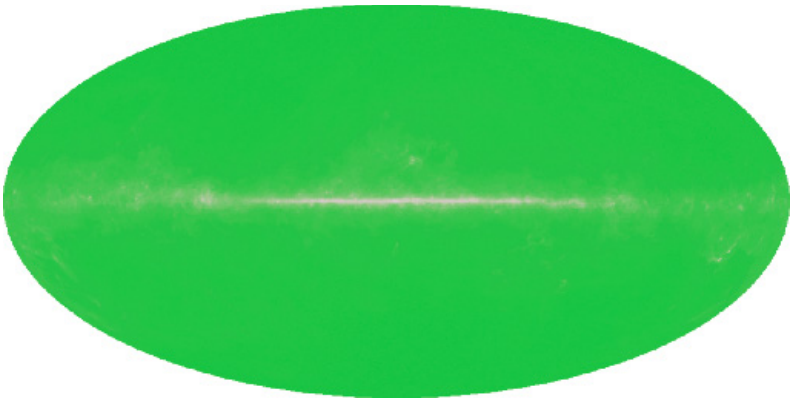

Fig. 1.3: The first measurements of the CMB radiation. The horizonal thin area is due to the radiation from our Galaxy. https://www.cosmos.esa.int/web/planck/picture-gallery/

had obtained long ago. They assumed that the wave length of the radiation in the early universe, which has high energy, is extended as the evolution of our universe, and then we can measure it as the radiation of 3 K. Namely, this measurement discloses that our universe were begun with the high temperature and high density.

To explore details of CMB, in 1990s, Cosmic Background Explorer (COBE) satellite (launched in 1990) measured the CMB spectrum over the whole sky (see Fig. 1.4). The COBE disclosed the following two facts;

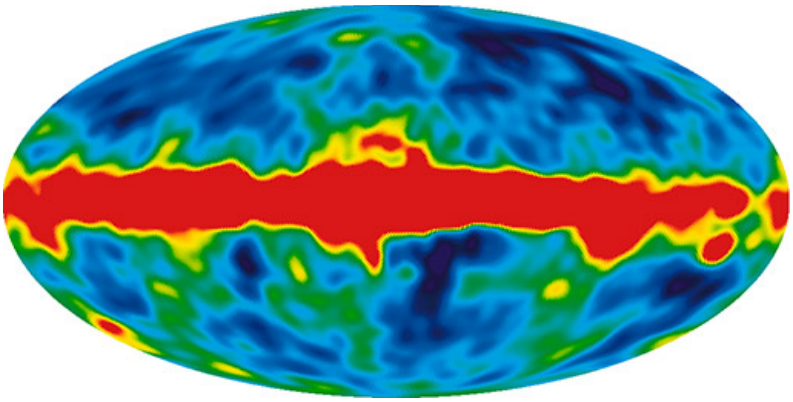

Fig. 1.4: CMB radiation by COBE-4yr. The holizontal red and yellow areas are due to the radiation from our Galaxy. https://www.cosmos.esa.int/web/planck/picture-gallery/

- CMB is nearly isotropic and homogeneous with a constant temperature.
- There are small fluctuations in the CMB temperature, $\delta T_{\rm CMB} \sim 10^{-5}$.

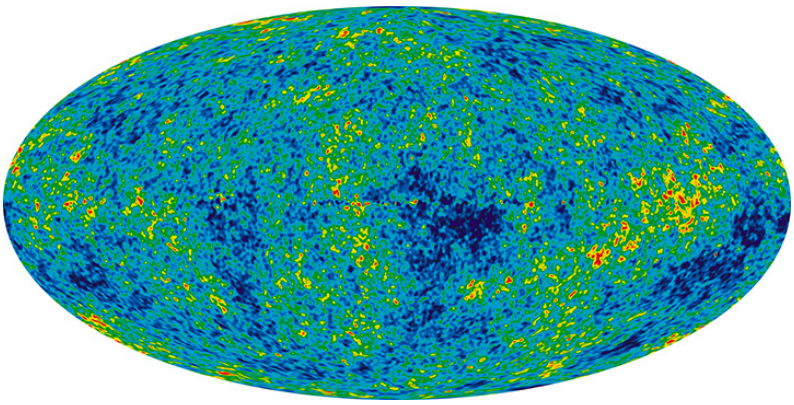

Fig. 1.5: WMAP-9yr result of CMB radiation. It shows the CMB temperature and fluctuation from -300μK (dark blue) to 300μK (red).

As the measurements have been improved, our knowledge of the universe has been progressed. CMB has many kinds of physical information such as the Galaxy synchrotron and dust radiation (foreground radiation), lensing by the structure on large scales (secondary), scattering by reionization, the CMB polarization, and gravity waves which are the main fluctuations generated in the early universe as predicted by an inflation theory.

Wilkinson Microwave Anisotropy Probe (WMAP) satellite (launched in 2001) measured CMB and its fluctuation in more detail. The small fluctuations are caused by the

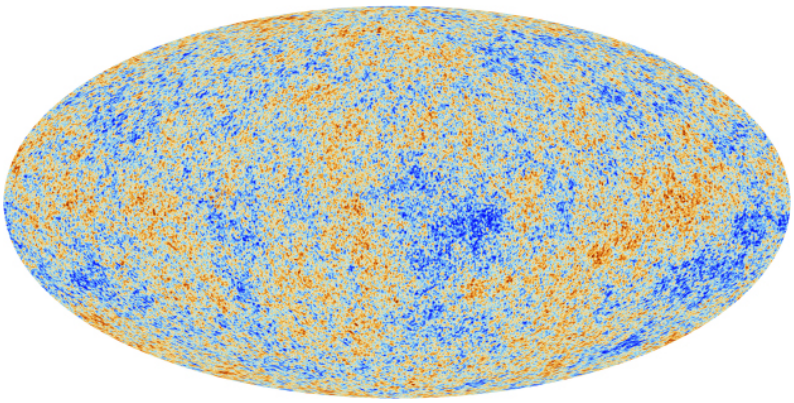

Fig. 1.6: CMB observed by *Planck*. It shows the temperature fluctuation in more detail from -300μK (blue) to 300μK (red). [10]

tiny density variations of the universe just after the Big Bang, the more a dense region tends to attract, the more matter results in a dense region. The process led to the formation of the first stars, galaxy and large scale structure. *Planck* satellite (launched in 2009) was the latest observation instrument. It has 2-3 times higher resolution compared to that of WMAP. It surveyed whole sky 5 times and finished the operation in 2014 (see Fig. 1.6).

Additional prediction is made by Zwicky in 1933, when he analyzed the relative motion between galaxies in the Comae Berenices. However, he could not explain why these galaxies are gravitationally bounded, contrary to the high speed of motion of galaxies. There should be more than 100 times larger mass to be bounded in the cluster of galaxies. That is why they called this mass as 'Missing Mass', which could exist but we do not know the true character yet. Currently the Missing Mass is called dark matter. There is another fundamental prediction for Big Bang model. Riess *et al.* (1998) studied Hubble diagram (see Fig. 1.7) for type Ia supernovae. They revealed that the current universe is dominated by dark energy. It brought the current universe in the accelerated expansion epoch [11].

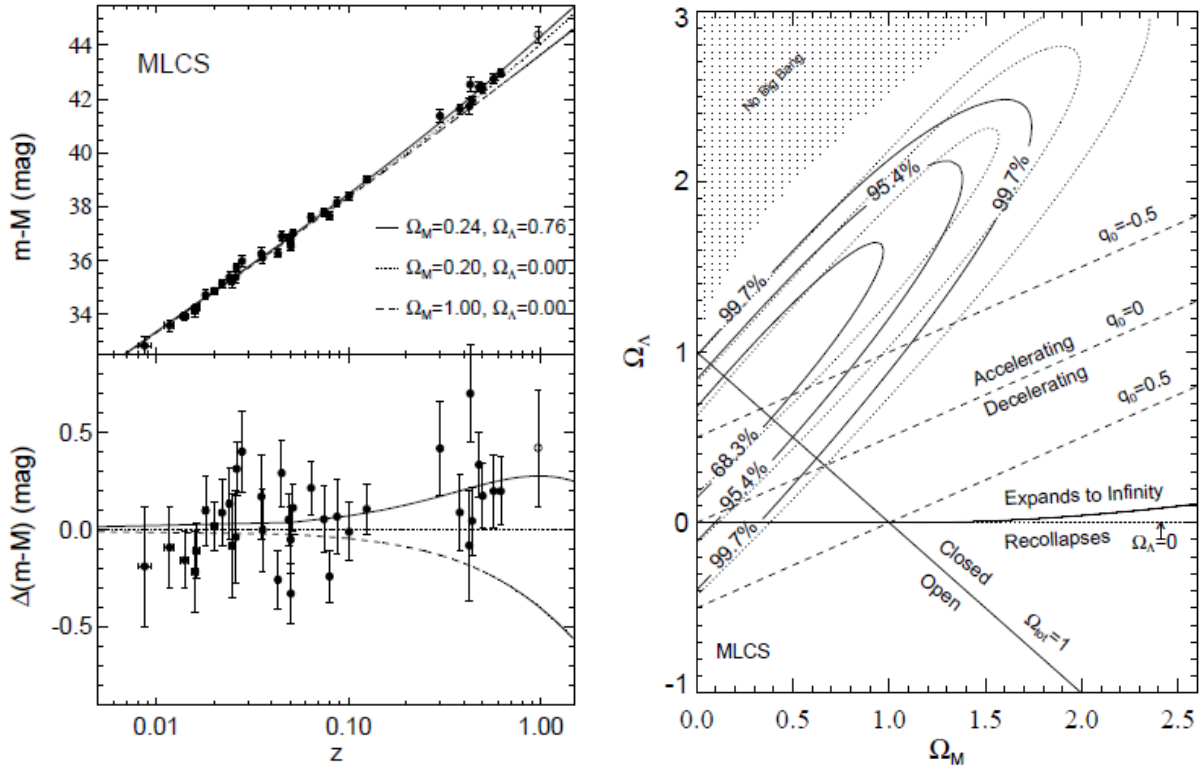

Fig. 1.7: Riess *et al.* determine the luminosity distance (including $K-$correction; redshift correction) via multi-color light curve shape (MLCS) method. The left-upper panel shows the Hubble diagram for type Ia supernovae samples. The best fit for a flat cosmology results in, $\Omega_M = 0.24$, $\Omega_\Lambda = 0.76$. The left-bottom panel indicates the difference between data and models with $\Omega_M = 0.20$, $\Omega_\Lambda = 0$, and the vertical line indicates empty universe with $\Omega_K = 1$. The open symbol is SN 1997ck (z=0.97), which lacks spectropic classification and a color measurement. The right panel shows the $(\Omega_M, \Omega_\Lambda)$ plane from type Ia supernovae. The solid contours are results from the MLCS method. The data of the dotted contours are the result excluding the unclassified SN 1997ck (z=0.97). This figure indicates that current universe is in the accelerated expansion phase. [11]

1.2 The Friedmann-Lemaître Model

The evolution of the universe is derived from the Einstein equation

$$R_{\mu\nu} - \frac{1}{2} g_{\mu\nu} R = 8\pi G \left(T_{\mu\nu} - \frac{\Lambda}{8\pi G} g_{\mu\nu} \right) \equiv 8\pi G \tilde{T}_{\mu\nu}, \tag{1.1}$$

where $g_{\mu\nu}$ is the metric tensor, $T_{\mu\nu}$ is the energy momentum tensor, $R_{\mu\nu}$ is the Ricci tensor, R is the scalar curvature, $\tilde{T}_{\mu\nu}$ is the energy momentum tensor including Λ-term as the dark energy, and G is the gravitational constant.

To solve (1.1) , we assume the following Cosmological Principle, and the fluid property:

- Universe is homogeneous and isotropic

$$ds^2 = dt^2 - a(t)^2 \left[\frac{dr^2}{1-kr^2} + r^2(d\theta^2 + \sin^2\theta d\phi^2) \right]. \tag{1.2}$$

- Constituents can be regarded as the perfect fluid

$$T_{\mu\nu} = \mathrm{diag}(\rho, P, P, P). \tag{1.3}$$

Where, ρ and P are the total energy density and the pressure, $a(t)$ is the scale factor and k is the curvature constant. We take the unit system where $c = 1$.

The left and right hand sides of the Einstein equation represent geometric structure of the space and the matter field. We can obtain an important equation from the conservation law $\nabla_\mu T^{\mu 0} = 0$,

$$\dot{\rho} + 3\frac{\dot{a}}{a}(\rho + p) = 0, \tag{1.4}$$

where the dot indicates ordinary derivative with respect to time. This equation describes density evolution. To solve (1.4), the equation of state ($w = P/\rho$) should be defined. In statistically thermal equilibrium, such thermodynamical variables are defined as follows;

$$n = g \int \frac{d^3p}{(2\pi\hbar)^3} f(\boldsymbol{p}) \tag{1.5}$$

$$\rho = g \int \frac{d^3p}{(2\pi\hbar)^3} E(\boldsymbol{p}) f(\boldsymbol{p}) \tag{1.6}$$

$$P = g \int \frac{d^3p}{(2\pi\hbar)^3} \frac{|\boldsymbol{p}|^2}{3E(\boldsymbol{p})} f(\boldsymbol{p}) \tag{1.7}$$

with use of Fermi-Dirac distribution function or Bose-Einstein distribution function (μ is the chemical potential);

$$f(\boldsymbol{p}) = \left[\exp\left(\frac{E(\boldsymbol{p}) - \mu}{k_\mathrm{B} T} \right) \pm 1 \right]^{-1}. \tag{1.8}$$

The value of EoS w can be evaluated by using the above statistical quantities n and P. Here, n, $\boldsymbol{p}$, $E(\boldsymbol{p})$, g are number density, momentum, energy, internal degree of freedom,

respectively.

Notwithstanding these quantities, following definitions, are commonly used as the manner of cosmology;

$$\begin{cases} w = 0 & \text{(For dust, matter component as the non-relativistic particles; } \rho_m) \\ w = 1/3 & \text{(For radiation as the (ultra) relativistic particles; } \rho_\gamma) \\ w = -1 & \text{(For dark energy as the cosmological constant; } \rho_\Lambda) \end{cases}$$

The Einstein equation reduces to,

$$H^2 = \left(\frac{\dot{a}}{a}\right)^2 = \frac{8\pi G}{3}\left(\rho + \frac{\Lambda}{8\pi G}\right) - \frac{k}{a^2}, \tag{1.9}$$

$$\frac{\ddot{a}}{a} = -\frac{4\pi G}{3}(\rho + 3P), \tag{1.10}$$

where H is the Hubble parameter. Energy density ρ consists of matter, radiation, and cosmological constant ($\rho = \rho_m + \rho_\gamma + \rho_\Lambda$).

Additionally, density parameters (Ω_i) are often defined using critical density at present $\rho_{crit0} \equiv 3H_0^2/8\pi G$. Rewriting (1.9) using ρ_{crit0} and EoS w we get,

$$H^2 = {H_0}^2\left(\frac{\Omega_{m0}}{a^3} + \frac{\Omega_{\gamma 0}}{a^4} + \frac{\Omega_{k0}}{a^2} + \Omega_{\Lambda 0}\right), \tag{1.11}$$

or equivalently,

$$H^2 = {H_0}^2\left(\Omega_{m0}(1+z)^3 + \Omega_{\gamma 0}(1+z)^4 + \Omega_{k0}(1+z)^2 + \Omega_{\Lambda 0}\right), \tag{1.12}$$

where $\Omega_i = \rho_i/\rho_{crit}$ is the energy density parameter and $\Omega_k = -k/H_0^2$ is the density parameter for the curvature, the subscript 0 indicates that physical quantities are evaluated at the present epoch, z is the cosmological redshift ($z = a_0/a - 1$), respectively. The critical density parameter is

$$\rho_{crit0} = \frac{3H_0}{8\pi G} \simeq 1.88 \times 10^{-29} h^2 \text{ g/cm}^3, \tag{1.13}$$

where h defined as $h = H_0/(100 \text{ km/s/Mpc})$ which is the dimensionless Hubble parameter. By exploring the existence of the unique parameter set, we can check the correctness of Big Bang model and clarify how the universe evolves.

1.3 Big Bang Model and its Predictions

Big Bang model succeed in describing the evolution of the universe accurately. Moreover, this theory predicts scientifically verifiable hypothesis, which has been remarkably consistent with many observations.

1.3.1 Big Bang Nucleosynthesis (BBN)

One of the most important successes of the Big Bang model is that primordial abundances of light elements can be quantitatively predicted. Light elements, such as D ^{3}He, ^{4}He and ^{7}Li, are synthesized in Big Bang nucleosynthesis (BBN). Big Bang nucleosynthesis is based on the simple assumptions of validity of Cosmological Principle. This theory predicts that light elements of D, ^{3}He, ^{4}He and ^{7}Li/H were synthesized during the first three minutes in the BBN epoch. BBN has good agreement with the primordial abundances which are estimated by observational data. Standard BBN model has the only one free parameter, baryon-to-photon ratio $\eta = n_b/n_\gamma$, where n_b and n_γ is the number density of baryon and photon. It is noted that the primordial value of η differs from the present value of η because of the electron-positron annihilation (see 'Neutrino decoupling and pair annihilation'). Before the electron-positron annihilation epoch, $(11/4)\eta$ represents the baryon-to-photon ratio. The baryon density parameter is related to the density parameter Ω_{b0};

$$\eta = \frac{n_b}{n_\gamma} = \frac{\rho_{crit0}}{\bar{m} n_{\gamma 0}} = 2.731 \times 10^{-8} \Omega_{b0} h^2, \tag{1.14}$$

where $n_{\gamma 0}$ is the number density of CMB photons. We adopt the present temperature of the CMB photon of $T_\gamma = 2.725$ K [12, 13] and averaged mass $\bar{m} = 1.675 \times 10^{-24}$ g which is adopted in *Public Algorithm Evaluation the Nucleosynthesis of Primordial Elements* (PArthENoPE) [14]. It is note that A. Coc precisely estimated the averaged mass $\bar{m}$ [15];

$$\begin{aligned} \bar{m} &= m_{\rm p}(1 - Y_{\rm p}) + \frac{m_\alpha}{4} Y_{\rm p} \\ &= (1.6735 - 0.0119 Y_{\rm p}) \times 10^{-24} {\rm g}, \end{aligned}$$

where $\bar{m}$, $m_{\rm p}$, m_α and $Y_{\rm p}$ are the averaged mass, proton mass, ^{4}He mass and the mass fraction of ^{4}He.

Thermal equilibrium epoch

At the high temperature $T_\gamma > 3.0$ MeV, neutrinos, neutrons, protons, electrons, positrons and photons are in the thermal equilibrium. This phase is dominated by the radiation component. The total energy density of radiation component (ρ_{rad}) is

$$\rho_{rad} = \rho_\gamma + \rho_{e^-} + \rho_{e^+} + \rho_{\nu_e} + \rho_{\bar{\nu}_e} + \rho_{\nu_\mu} + \rho_{\bar{\nu}_\mu} + \rho_{\nu_\tau} + \rho_{\bar{\nu}_\tau}, \tag{1.15}$$

where each term of the right hand side indicates the energy density of photons, electrons, positrons, electron and anti-electron neutrinos, muon and anti-muon neutrinos, tauon and anti-tauon neutrinos, respectively. These energy components are estimated using (1.6) as

$$\rho_\gamma = 2 \cdot \frac{\pi^2}{30} \frac{(k_{\rm B}T)^4}{(\hbar c)^3} \equiv a_r T_\gamma^4 \tag{1.16}$$

$$\rho_\nu = \frac{7}{8} \cdot \frac{\pi^2}{30} \frac{(k_{\rm B}T)^4}{(\hbar c)^3} = \frac{7}{16} a_r T_\nu^4 \tag{1.17}$$

$$\rho_e = \frac{7}{8}\, 2 \cdot \frac{\pi^2}{30} \frac{(k_{\rm B}T)^4}{(\hbar c)^3} = \frac{7}{8} a_r T_e^4 \tag{1.18}$$

where a_r is the radiation constant ($a_r = \pi^2 k_{\rm B}/15\hbar^3$). Here, the scale factor dependence on the temperature can be written, $\rho_\gamma \propto T^4 \propto a^{-4}$. From the thermal equilibrium condition ($T_\gamma = T_\nu = T_{\rm e}$),

$$\rho_{rad} = \left(\frac{11}{4} + \frac{7}{8} N_\nu^{\rm eff} \right) a_r \left(\frac{T_{\nu 0}}{a} \right)^4, \tag{1.19}$$

where $N_\nu^{\rm eff}$ is the effective neutrino number and the standard theory of particle physics predicts $N_\nu^{\rm eff} = 3.046$ [16]. It includes the effects of (i) non-instantaneous neutrino decoupling and (ii) neutrino oscillations. $T_{\nu 0}$ is the present neutrino temperature.

In addition, neutrons and protons are in the nuclear statistical equilibrium via weak interactions;

$$\mathrm{n} \longleftrightarrow \mathrm{p} + \mathrm{e}^- + \bar{\nu}_{\rm e}, \tag{1.20}$$

$$\mathrm{n} + \nu_{\rm e} \longleftrightarrow \mathrm{p} + \mathrm{e}^-, \tag{1.21}$$

$$\mathrm{n} + \mathrm{e}^+ \longleftrightarrow \mathrm{p} + \bar{\nu}_{\rm e}, \tag{1.22}$$

where n, p, e^-, e^+, ν_e, $\bar{\nu}_e$ are neutrons, protons, electrons, positrons, electron neutorinos and anti-electron neutrinos, respectively.

The reaction rates for the weak interactions can be calculated as follows;

$$\begin{aligned}\lambda &= \sigma(E)v_{\rm in} \\ &= \frac{1}{\tau\lambda_0}\int\left(\prod_{\rm i:Lepton}\frac{4\pi\, p_{\rm i}^2 dp_{\rm i}}{(2\pi\hbar)^3}f_{\rm i}\right)\left(\prod_{\rm f:Lepton}\frac{4\pi\, p_{\rm f}^2 dp_{\rm f}}{(2\pi\hbar)^3}(1-f_{\rm f})\right)\delta(E_{\rm i}-E_{\rm f}),\end{aligned} \tag{1.23}$$

where, $\sigma(E)$, $v_{\rm in}$ and τ are the scattering cross section and velocity of incident particle and lifetime of the specific nuclei. Here, p, f and E are the momentum and distribution function and total energy of leptons, and subscription 'i' ('f') denotes the initial (final) state of particles. Two terms $\delta(E_{\rm i}-E_{\rm f})$ and $(1-f_{\rm f})$ come from the energy conservation law and Fermi blocking factor.

The reaction rates corresponding to (1.23) are written in the following formulae [17];

$$\lambda_{\rm n\to pe\nu} = \frac{1}{\tau\lambda_0}\int_1^q d\epsilon\frac{\epsilon(\epsilon-q)^2(\epsilon^2-1)^{1/2}}{[1+\exp(-\epsilon u)][1+\exp((\epsilon-q)u_\nu)]}, \tag{1.24}$$

$$\lambda_{\rm n\nu\to pe} = \frac{1}{\tau\lambda_0}\int_q^\infty d\epsilon\frac{\epsilon(\epsilon-q)^2(\epsilon^2-1)^{1/2}}{[1+\exp(-\epsilon u)][1+\exp((\epsilon-q)u_\nu)]}, \tag{1.25}$$

$$\lambda_{\rm ne\to p\nu} = \frac{1}{\tau\lambda_0}\int_1^\infty d\epsilon\frac{\epsilon(\epsilon+q)^2(\epsilon^2-1)^{1/2}}{[1+\exp(\epsilon u)][1+\exp(-(\epsilon+q)u_\nu)]}, \tag{1.26}$$

$$\lambda_{\rm pe\nu\to n} = \frac{1}{\tau\lambda_0}\int_1^q d\epsilon\frac{\epsilon(\epsilon-q)^2(\epsilon^2-1)^{1/2}}{[1+\exp(\epsilon u)][1+\exp((q-\epsilon)u_\nu)]}, \tag{1.27}$$

$$\lambda_{\rm pe\to n\nu} = \frac{1}{\tau\lambda_0}\int_q^\infty d\epsilon\frac{\epsilon(\epsilon-q)^2(\epsilon^2-1)^{1/2}}{[1+\exp(\epsilon u)][1+\exp((q-\epsilon)u_\nu)]}, \tag{1.28}$$

$$\lambda_{\rm p\nu\to ne} = \frac{1}{\tau\lambda_0}\int_1^\infty d\epsilon\frac{\epsilon(\epsilon+q)^2(\epsilon^2-1)^{1/2}}{[1+\exp(-\epsilon u)][1+\exp((q+\epsilon)u_\nu)]}, \tag{1.29}$$

where τ is the neutron lifetime, $u = m_{\rm e}/T_\gamma$, $u_\nu = m_{\rm e}/T_\nu$, $\epsilon = E_{\rm e}/m_{\rm e}$, $q = \Delta m_{\rm np}/m_{\rm e}$. λ_0 is definded as

$$\lambda_0 = \int_1^q d\epsilon\ \epsilon(\epsilon-q)^2(\epsilon^2-1)^{1/2} \simeq 1.63609, \tag{1.30}$$

where it is defined to satisfy $\lambda_{n\to pe\nu}\to\tau^{-1}$ when $T_\gamma\to 0$ and $T_\nu\to 0$. In other words, it is introduced to adjust $\lambda_{n\to pe\nu}$ to the experimental value of neutron lifetime at the low temperature (see Fig. 1.8). On the other hand, the other reaction rates converge to $\lambda\to 0$.

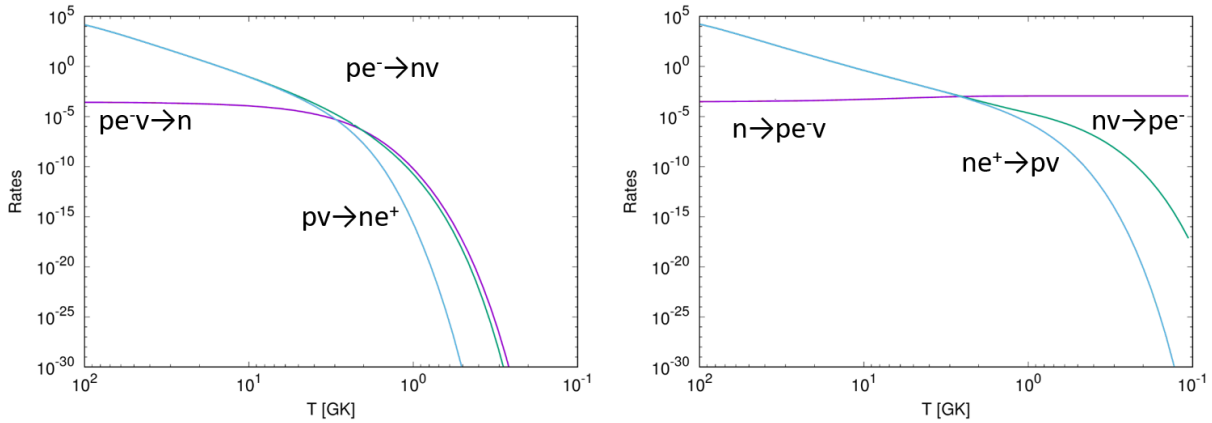

Fig. 1.8: The relation between reaction rates λ and the photon temperature T.

Neutrino decoupling and pair annihilation

When the temperature drops to $T_\gamma \simeq 1.5$ MeV, weak interactions freeze out and neutrinos decouple from the other particles. After the neutrino decoupling, neutrinos behaves free particles and the momentum distribution conserves by themselves. Then the temperature drops to $T_\gamma \simeq 0.7$ MeV, electron-positron annihilation begins via the following reaction:

$$\mathrm{e}^+ + \mathrm{e}^- \longrightarrow \gamma + \gamma.$$

Energy from electron-positron pairs flows in photons via pair annihilation. The annihilation is completed at $T_\gamma \simeq 0.4$ MeV. At this epoch, the total energy density of radiation component becomes

$$\rho_{rad} = \rho_\gamma + \rho_{\nu_e} + \rho_{\bar{\nu}_e} + \rho_{\nu_\mu} + \rho_{\bar{\nu}_\mu} + \rho_{\nu_\tau} + \rho_{\bar{\nu}_\tau}. \tag{1.31}$$

To estimate the temperature evolution of photons and neutrinos, entropy conservation law is used. The entropy $s(a,T)$ is defined as follows,

$$\frac{S(a,T)}{V} \equiv s(a,T) \equiv \sum_{i:\text{particle}} \frac{1}{T_i}\left(\rho_i + P_i\right). \tag{1.32}$$

Where the entropy per unit co-moving volume is conserved because of its independency from the cosmic expansion. In this situation, electron and positron should not be treated as relativistic particles, that is, entropy of electron-positron pairs are evaluated using (1.6) and (1.7);

$$\begin{aligned} s_{\rm e}(a, T_\gamma) &= \frac{1}{T_\gamma}(\rho_{\rm e} + P_{\rm e}) \\ &= \frac{1}{T_\gamma}\frac{g_{\rm e^-} + g_{\rm e^+}}{(2\pi)^3}\int_0^\infty dp_{\rm e}\left[4\pi p_{\rm e}^2\left(\sqrt{m_{\rm e}^2 + \boldsymbol{p}_{\rm e}^2} + \frac{1}{3}\frac{\boldsymbol{p}_{\rm e}^2}{E_{\rm e}}\right)\frac{1}{1+\exp(E_{\rm e}/k_{\rm B}T_\gamma)}\right] \\ &= \frac{1}{T_\gamma}\frac{2}{\pi^2}(k_{\rm B}T_\gamma)^4\,\mathcal{S}_{\rm e}\left(\frac{m_{\rm e}}{k_{\rm B}T_\gamma}\right) \end{aligned} \tag{1.33}$$

where, g_i is the internal degree of freedom, $E = \sqrt{m_e^2 + p^2}$, and we define $\mathcal{S}_{\rm e}$ as

$$\mathcal{S}_{\rm e}(x) \equiv \int_0^\infty y^2 dy\left(\sqrt{x^2+y^2} + \frac{1}{3}\frac{y^2}{\sqrt{x^2+y^2}}\right)\frac{1}{1+\exp(\sqrt{x^2+y^2})}. \tag{1.34}$$

We have to consider conservation law only for photons and electron-positron pairs since they are interacting sufficiently;

$$\begin{aligned} s &= \frac{4}{3}a_r T_\gamma^3\left[1 + \left(\frac{4}{3}a_r T_\gamma^3\right)^{-1}\cdot\frac{1}{T_\gamma}\frac{2}{\pi^2}(k_{\rm B}T_\gamma)^4\mathcal{S}_{\rm e}\right] \\ &= \frac{4}{3}a_r T_\gamma^3\left[1 + \frac{45}{2\pi^4}\mathcal{S}_{\rm e}\right] \\ &= \frac{4}{3}a_r T_\gamma^3\mathcal{J}\left(\frac{m_{\rm e}}{k_{\rm B}T_\gamma}\right) \end{aligned} \tag{1.35}$$

$\mathcal{J}(x)$, which is the entropy of photons plus electron-positron pairs in unit of entropy of the photons, is defined as,

$$\mathcal{J}(x) \equiv 1 + \frac{45}{2\pi^4}\mathcal{S}_{\rm e}(x). \tag{1.36}$$

Adopting (1.35) and conservation law (1.32) for before and after the pair annihilation

period, we obtain the following relations;

$$
\begin{aligned}
& s_{\rm bef} = s_{\rm aft} \\
\Longleftrightarrow \quad & \frac{11}{3} a_r T_{\rm bef}^3 = \frac{4}{3} a_r T_{\rm aft}^3 \mathcal{J} \\
\Longleftrightarrow \quad & \frac{11}{3} a_r T_\nu^3 = \frac{4}{3} a_r T_\gamma^3 \mathcal{J} \\
\Longleftrightarrow \quad & T_\nu = \left(\frac{4}{11}\right)^{1/3} T_\gamma \left[\mathcal{J}\left(\frac{m_{\rm e}}{k_{\rm B} T}\right)\right]^{1/3}
\end{aligned}
\tag{1.37}
$$

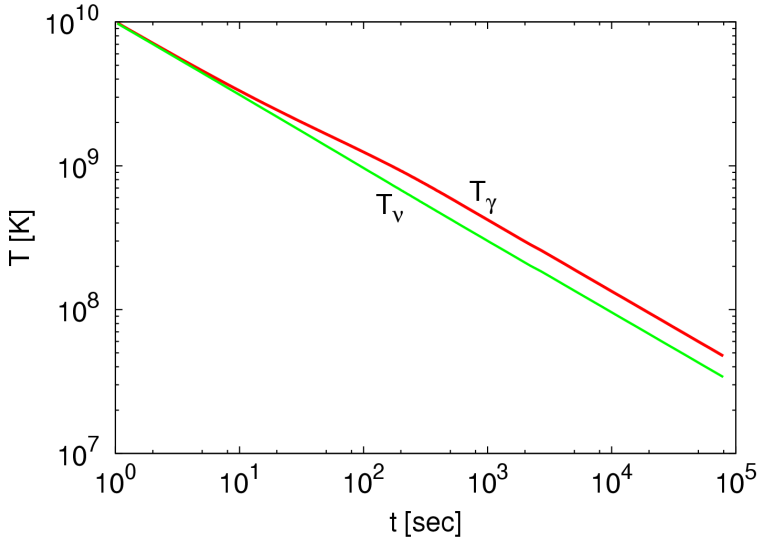

Fig. 1.9: Photon (T_γ) and neutrino (T_ν) temperature evolution.

If massless neutrinos completely decoupled from photons, the neutrino temperature T_ν always proportional to the inverse of the scale factor a^{-1} (see Fig. 1.9). The subscripts 'bef' and 'aft' indicate the entropy of before electron-positron pair annihilation and after the annihilation, respectively. It is noted that the neutrino temperature in the reaction rates (1.24)-(1.29) should be estimated using the relations during this period.

Light elements synthesis

When the temperature falls to $T_\gamma \simeq 0.1$ MeV, light element synthesis begins (see Fig. 1.10).

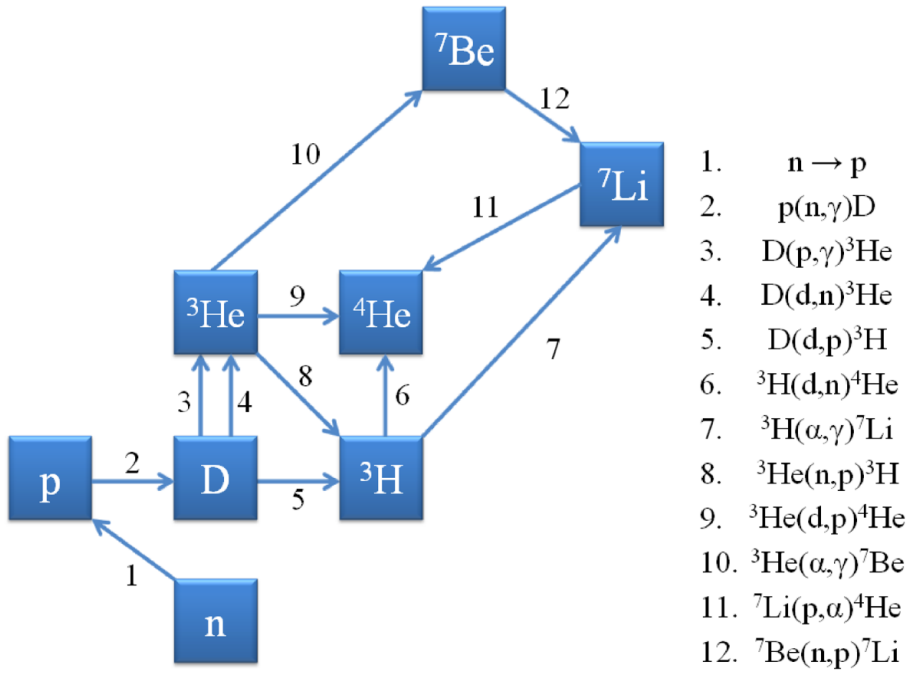

Fig. 1.10: The most important reaction network for Big Bang nucleosynthesis.

1.3.2 Observation of light elements

Helium-4

We show the [O/H]-Y(^{4}He) plane and the variations for observational values in Fig. 1.11. The blue points with error bars represent the abundance in the HII region. The solid curve indicates the most probable path obrained from the chemical evolution calculation. The primordial abundance of ^{4}He is obtained by taking the limit of [O/H]= 0. Observational values in recent years tend to have the consistency with the BBN calculation results. Helium-4 that exists in the universe is mostly synthesized during BBN, but in the star's evolution process. Hydrogen is burned by p-p chain in the deeper region, and ^{4}He is synthesized. Therefore, these quantities are included in the observational values, in the Low-z region where the heavy elements are small. If the element synthesis inside the star is not active, the composition of ^{4}He produced by BBN remains as it is. Therefore, estimation of ^{4}He has been done from direct observation of ^{4}He or recombination line of hydrogen in the HII region outside the galaxy with small amount of metal. However, the estimation of ^{4}He in the HII region outside galaxy involves indeterminacy due to the

uncertainty of the observation and the complexity of the physical process in the HII region. For example, it is difficult to measure the temperature, electron density and optical depth of the region.

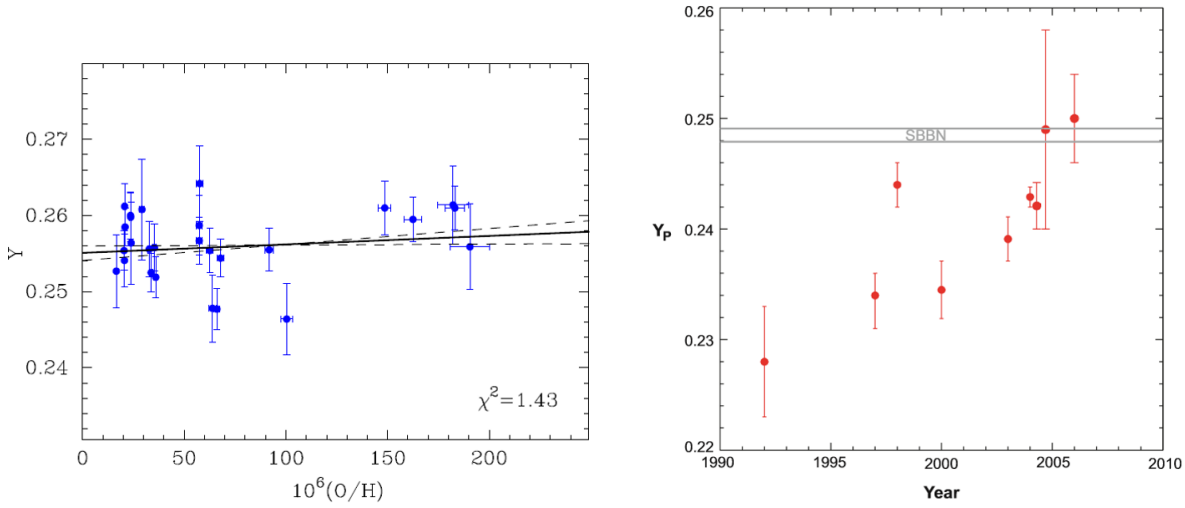

Fig. 1.11: Left: Estimation of the primordial abundane of ^{4}He [18]. Right: Changes in observed values of Helium-4 [19].

Deuterium

Since the composition ratio of deuteron strongly depends on baryon-to-photon ratio η, it is an element also called 'baryometer'. Deuteron is synthesized only in the early universe during BBN, it can be considered to decrease due to the destructive reaction inside the stars (D(p,γ)^{3}He). Therefore, D+^{3}He has been considered to give the upper limit of deuteron. However, the generation process of ^{3}He in the star is not known in detail, and its evaluation is difficult. Therefore, the composition of deuteron is currently estimated by observing the absorption line from QSO at high redshift. Since QSO is a primitive galaxy at the beginning of galaxy formation, it can be a source of information for early universe. We show the chemical evolution of deuteron in the left panel of Fig. 1.12. The solid red curve is calculated using the Times code [20]. We input the BBN production of deuteron since the low metallicity region ([O/H]< -1.5) reflects the BBN production. During the evolution of galaxies, deuteron has been destructed and its abundance decrease. It indicates that the observational value at the region of [O/H]< -1.5 is compatible with the BBN production. The right panel in Fig. 1.12 shows the wide absorption line of hydrogen

and deuteron. The sharp absorption line (∼4907Å at the upper panel) represents the line of $Si_{III}\lambda$ 1206.5, which is used to estimate the redshift of the absorption line from QSO.

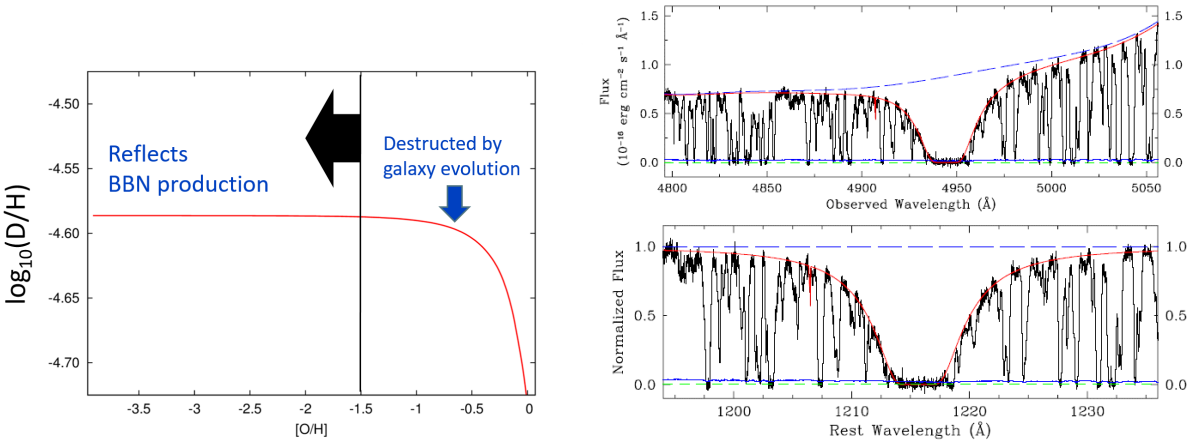

Fig. 1.12: Left: Chemical evolution of deuterium. Right: Absorption lines [21].

Lithium-7

The observation of ^{7}Li/H is carried out for the halo stars of the population III with a small amount of metal. ^{7}Li is burned in the evolution process of the star and its amount decreases; in older galaxies with a small amount of metal, it includes the early universe of BBN. It is estimated that the generated ^{7}Li remains. ^{7}Li/H has been observed since 'Spite plateau' was predicted on the [^{7}Li/H]-[Fe/H] plane. The primordial value is obtained by calculating the ^{7}Li value of zero metalicity on the [^{7}Li/H]-[Fe/H] plane after considering the depletion of ^{7}Li in the observation data. In Fig. 1.13, the green curve is calculated using the Times code [20], and the blue and red points with error bars are the estimated value of ^{7}Li for each star. The purple and dark green points indicate the averaged values in 28 dwarfs (Sbordone *et al.*), and in 18 dwarfs (Korn *et al.*). Korn *et al.* consider the significant depletion and/or destruction for ^{7}Li abundance during the lifetime of Population II stars.

In Fig. 1.14 the observational results of ^{4}He and D, and BBN results are consistent with CMB constraints on baryon-to-photon ratio or baryon density. In addition, ^{4}He and D results give the reasonable extent for the baryon density.

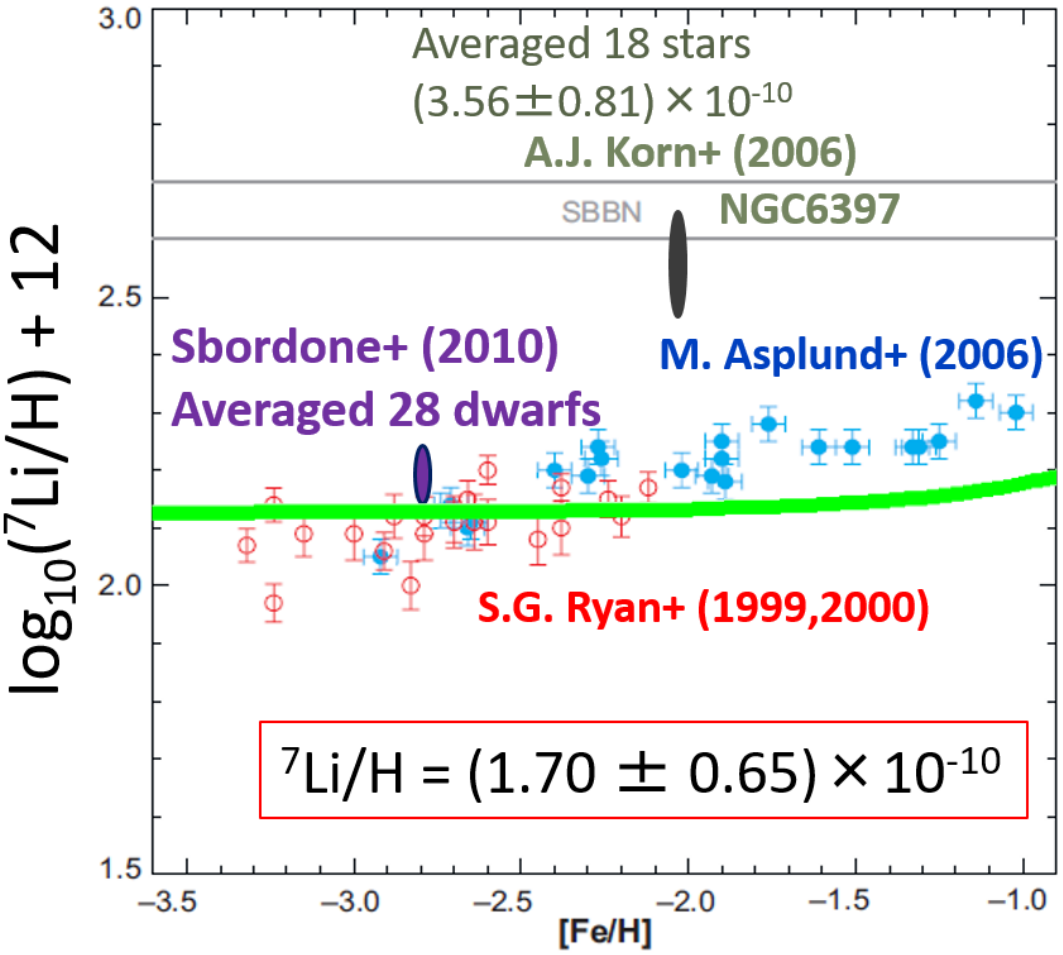

Fig. 1.13: Chemical evolution of lithium-7 and its observational values [19].

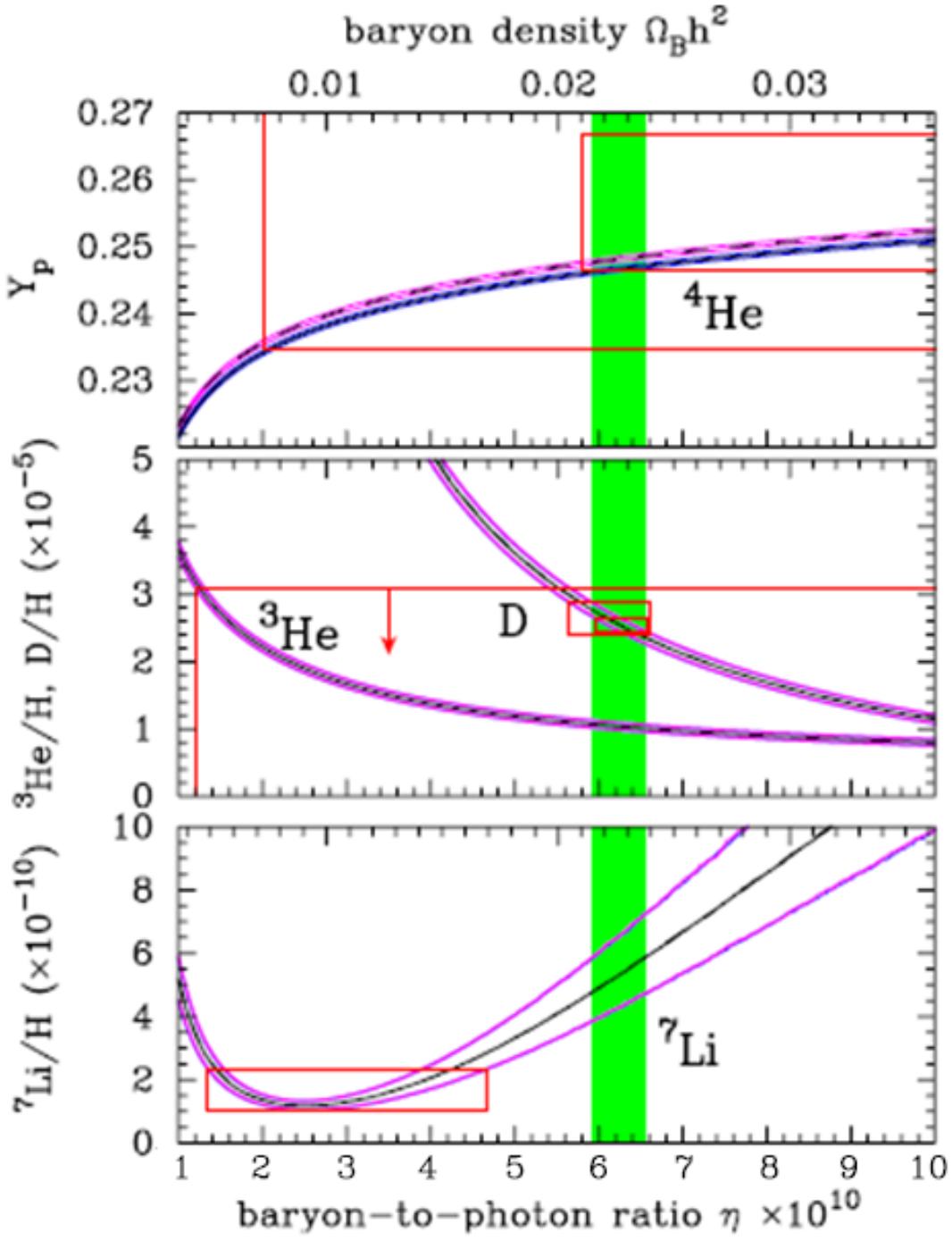

Fig. 1.14: The black curves indicate that abundance of light elements, ^{4}He(Y_p), D, ^{3}He and ^{7}Li which are predicted by the standard Big Bang nucleosynthesis. Blue lines are calculated with neutron lifetime $\tau_n = 878.5 \pm 0.8$ s and purple lines are calculated with $\tau_n = 885.7 \pm 0.8$ s. And these lines are including uncertainties of reaction rates. Red boxes show the 2σ errors of observational prediction and the vertical lines come from the constraints on baryon density. The green vertical band indicates the constrains on baryon density from WMAP [22].

1.3.3 Magnitude-redshift relation

The key idea of the precise measurements of the magnitude-redshift relation ($m - z$ relation) is to adopt the distance ladder. It is the sequential method in determining the distance from the earth to astrophysical objects. A direct measurement is possible only for those objects that are close enough to observer. The techniques in determining distances are based on various correlations in stellar objects. Several measurements rely on a standard candle, such as type Ia supernovae, which has a known luminosity. At present, there is no unified method to measure the distance for distant objects. It is necessary to measure the distance of the nearby object in some method, and then referencing it and obtains the distance of more distant objects. This process is called 'distance ladder'.

Hence, $m - z$ relation plays a key role in determining the cosmological parameters. The cosmological distance measurements or estimations, concerning with the magnitude, enormously depend on the cosmological redshift, curvature, density parameters and Hubble parameter. Distance is measured by the luminosity of stellar objects such as Cepheid variables and type Ia supernova. These objects are known as the standard candle. Additionally recent study makes it possible to use gamma-ray bursts as the standard candle. The quantity of the distance, which is measured by the luminosity, is called luminosity distance (d_L). This quantity is affected by cosmological redshift directly and the spectrum is shifted. The redshift is caused by the expansion of the universe, so that the relation between magnitude and redshift ($m-z$ relation) is one of the most important observational quantity to evaluate how the universe evolves.

1.3.4 Measurements of magnitude-redshift relation

Cepheid variables

The stars outside the Galaxy are dark and it is difficult to measure the spectrum and luminosity. We need to explore the bright stars what we can observe. In Magellanic nebulae, bright stars are found which changes the luminosity periodically from $10^3 L_\odot$ to $10^6 L_\odot$. These stars are called 'Cepheid variables' and the period is about 1$\sim$135 days. It changes the luminosity because of their expansion and contraction in the envelope. Moreover, it is discovered that the longer the period of $\log P$, the brighter the absolute magnitude M (see Fig. 1.15). Using the relation between period and absolute magnitude,

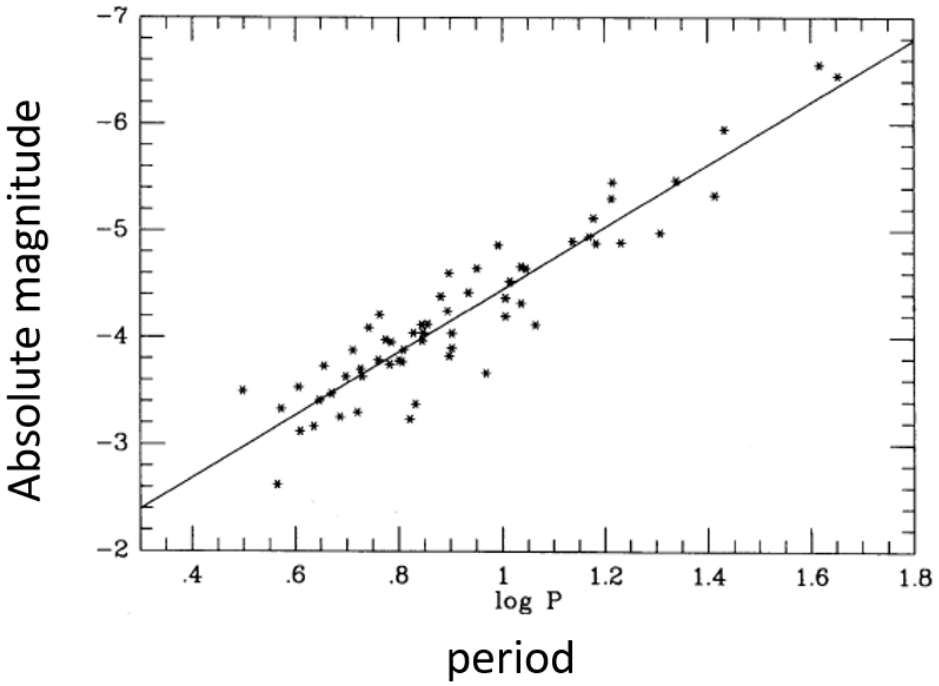

Fig. 1.15: Correlation between period and absolute magnitude (luminosity) of Cepheid variables [23]. Since we can obtain the absolute magnitude from the period, we estimate the distance to the star, which becomes the first 'ladder'.

the distance of more distant Cepheid can be estimated.

Type Ia supernova

There is a popular phenomenon called supernova explosion. There are many kinds of type for supernova explosions, such as type Ia, type Ib, type Ic and, type II supernovae. In particular, type Ia supernova has luminosity about $10^{12}L_{\odot}$, and the luminosity only slightly depends on indivisual stars. Moreover, it is discovered that there is a relation between the peak luminosity M_B and the change rate of the luminosity after 15 days Δm_{15}. This relation is called $M - \Delta m_{15}$ relation or Phillips relation (see Fig. 1.16). Many observational results have been accumulated using this relation. Therefore, the compilation data are available up to the redshift $z \sim$1.5 for type Ia supernovae.

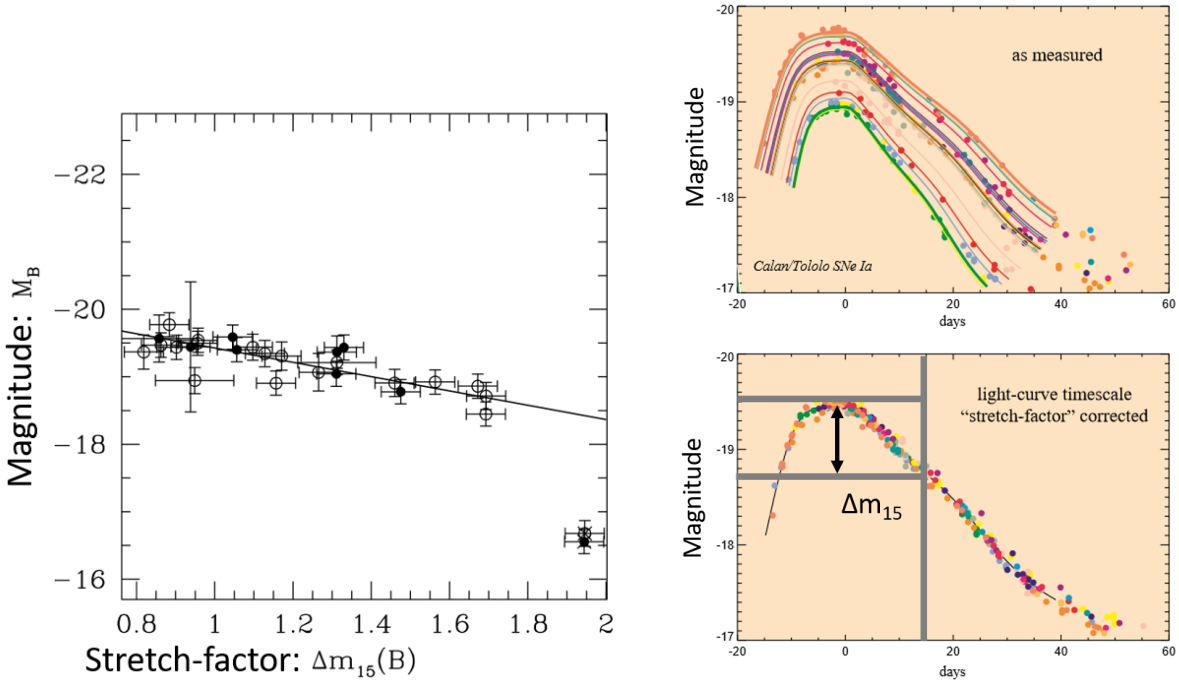

Fig. 1.16: Left: Correlation between magnitude and Δm_{15} of type Ia supernova [24]. Right: Correction of the light curve of type Ia supernovae by redshift and Phillip relation [25].

Gamma ray burst

Gamma ray burst is the brightest celestial phenomenon and the luminosity is reached to $10^{20} L_\odot$. There are two candidates of gamma ray bursts: gravitational collapse of star and neutron stars merger. However, the mechanism is not well understood. Recently, the gamma ray bursts have been enthusiastically studied [26–29] and it gradually turned out that gamma ray bursts have some features on their own. For instance, Amati relation represents the relation between the isotropic energy and peak energy [27, 28].

1.4 Problems in the Present Cosmology

Recent observations indicate that our universe is flat and has turned into accelerated expansion phase at the present epoch [11, 30–33]. Some cosmological models have been introduced to examine the characteristics of the present acceleration [34–39]. The most simple one is the ΛCDM model, which includes Λ term as a dark energy. The Λ term leads to the negative pressure, and moderate the universe for acceleration. This is the standard model of the present cosmology having a dark sector which consists of dark energy and dark matter. Dark matter and dark energy should be around 25% and 70% at the present epoch, respectively [30].

Up to now, the ΛCDM model is almost consistent with many observations of CMB and SN Ia [31, 40], with the exception of the typical estimations of the vacuum energy which are many orders larger than the observed one [41]. Recently, many observational results have been accumulated about SN Ia. Therefore, the compilation data are available up to the redshift $z \sim 1.5$. We have a great interest of investigating the feature of dark energy (DE) around small redshift region. While CMB includes the area of very large redshift compared to the one of SNe Ia, we may have to interpolate the behavior between them if we study DE quantitatively. As a consequence, the data $z \geq 1.5$ would become important to constrain the behavior of DE in a wide range of cosmological epoch.

Recently, the GRBs have been enthusiastically studied [26–29] to investigate the behavior of DE and the expansion rate at high redshift range. As a consequence, we can discuss the density evolution of DE in detail.

Clarifying the properties of DE is one of the most important issues in cosmology, and especially modifying an EoS and/or a gravitational field is the most popular method. Although these are methods to represent the features of DE, it is presumed that DE belongs to dynamical phenomena. Some theoretical dark energy models have been proposed to describe the energy density evolution. For instance, models of quintessence, phantom, quintom, k-essence, Chaplygin gas and so on, belong to non-standard DE models [34–38, 42]. On the other hand, some models which include the modified EoS of dark energy give more direct method. We can categorize above models as follows: (i) Cosmological constant ($w = -1$). (ii) DE with constant but $w \neq -1$. (iii) Dynamical DE with $w > -1$ (Quintessence-like models). (iv) Dynamical DE with $w < -1$ (Phantom-like

models). (v) Dynamical DE which crosses the phantom barrier of $w = -1$ (Crossing models).

Recent observational results indicate that EoS of DE accrosses the barrier of $w = -1$, so called phantom barrier [43–46]. Some theoretical models, which accross the phantom divide, have been extensively studied [47,48]. On the other hand, a modified EoS is easier to handle the density evolution of DE, and it is beneficial to understand the asymptotic behaviour of DE to examine whether the crossing exists or not.

In the present work, we investigate how DE should be categorized by modifying the EoS directly. We adopt a special EoS whose functional form has two limiting values of parameters. In addition, with use of the observational results such as SN Ia and gamma-ray burst (GRB), we constrain specific parameters in EoS of DE over a wide range of the redshift around $1 < (z + 1) < 10$.

Big Bang nuleosynthesis provides substantial clues for investigating physical conditions in the early universe. Standard BBN produces about 25% of the mass of the Universe in the form of ^{4}He, which has been considered to be in good agreement with its observed abundance in a variety of astronomical objects.

The produced amount of ^{4}He depends strongly on a fraction of neutrons at the onset of nucleosynthesis, but is not very sensitive to the baryon-to-photon ratio $\eta(\eta = n_b/n_\gamma; \eta_{10} = 10^{10}\eta)$. Hence the produced amount of ^{4}He is used to explore the expansion rate during BBN, which ca be related to the effective number of neutrino flavors. In addition to ^{4}He, significant amounts of D, ^{3}He, and ^{7}Li are also produced. Because of its strong dependence on η, the abundance of D is crucial in determining η and consequently the density parameter of baryons Ω_b.

In spite of the apparent success of standard BBN (SBBN), recent observed light elements, which are considered to be primordial, have been controversial. Large discrepancies for ^{4}He observations emerge between different observers and modelers of observations: rather high values of ^{4}He have been reported for H II regions in blue compact galaxies. It is noted that the primordial abundance of ^{4}He is deduced from extrapolation to zero metallicity. The deuterium abundance has been observed in absorption systems toward high -redshift quasars. It should be noted that the value of D has been believed to limit the present baryon density. A low value of ^{7}Li observed in Population II stars reported by Bonifacio et al. is considered to be due to depletion and/or destruction during the

lifetimes of stars from a high primordial value.

Recently, the lifetime of neutrons has been updated from the previous adopted value of 885.7 ± 0.8 s which has been used commonly in BBN calculations consistent with the observed abundances of ^{4}He and D. However, the latest compilation by Beringer et al. determined the mean life to be 880.1 ± 1.1 s, which may suggest an inconsistency between BBN and observational values. This indicates a further inconsistency with the η deduced by *Planck*.

The apparent spread in the observed abundances of ^{4}He should give rise to an inconsistent range of η. Apart from observational uncertainties, we have no reliable theories beyond the standard theory of elementary particle physics. It is assumed in standard BBN that there are three flavors of massless neutrinos which are not degenerate. However it was suggested by Harvey and Kolb that lepton asymmetry could be large even when baryon asymmetry is small. The magnitude of the lepton asymmetry is of particular interest in cosmology and particle physics. Related to neutrino oscillations, investigations of BBN have been revised with the use of nonstandard models. As presented by Wagoner *et al.* and Beaudet and Goret, the abundances of light elements are modified by neutrino degeneracy; it could be necessary and crucial to search consistent regions in η within a framework of BBN with degenerate neutrinos by comparing it with the latest observation of the abundances of ^{4}He and D.

If neutrinos are degenerate, the excess density of neutrinos causes speedup in the expansion of the Universe, leaving more neutrons and eventually leading to enhanced production of ^{4}He. On the other hand, degenerate electron neutrinos shift β equilibrium to less or more neutrons and hence change the abundance production of ^{4}He. The latter effect is more significant than the former. In the present paper we investigate BBN by including degenerate neutrinos and using up-to-date nuclear data. Referring to several sets of combinations for recent observed abundances of ^{4}He and D, we derive consistent constraints between η and the degeneracy parameter.

2 Big Bang Nucleosynthesis

2.1 Observed Abundance of Light Elements

There exist very large spreads in some observed abundances of light elements due to different observational methods. Let us describe how we adopt the observed primordial abundances. The primordial abundance of ^{4}He can be measured from observations of the helium and hydrogen emission lines from low-metallicity blue compact dwarf galaxies. Izotov *et al.* reported the ^{4}He abundance from a subsample of 111 HII regions as follows [49]:

$$Y_p = 0.254 \pm 0.003. \tag{2.1}$$

The observational value of ^{4}He has large uncertainty, because the abundance could be appreciated to having the zero metallicitiy in terms of an extrapolation by a model of the chemical evolution of galaxies. An alternative low value of the average was reported by Aver *et al.* [50]

$$Y_p = 0.2464 \pm 0.0097, \tag{2.2}$$

which has a very large spread in errors.

Deuterium is the most crucial element to determine η because of the strong and monotonic dependence on η. Its primordial abundance is determined from metal-poor absorption systems toward high-redshift quasars. Cooke *et al.* have performed measurements at redshift $z = 3.06726$ toward QSO SDSS J1358+6522 [21]. Additionally, they have analyzed all of the known deuterium absorption-line systems that satisfy a set of strict criteria,

$$\mathrm{D/H} = (2.53 \pm 0.04) \times 10^{-5}. \tag{2.3}$$

This value corresponds to the baryon density $\Omega_b h^2 = 0.02202 \pm 0.00046$ which is consistent with the results of the *Planck* observation. Here h is the Hubbule constant in units of 100

km/s/Mpc.

We should note that the observed abundance of ^{7}Li in Population II stars is given by Sbordone *et al.* [51] to be

$$^7\mathrm{Li/H} = (1.58 \pm 0.31) \times 10^{-8}, \tag{2.4}$$

which has been advocated to be rather low compared with BBN. While considering significant depletion and/or destruction during the lifetimes of Population II stars, Korn *et al.* derived a high primordial abundance, [52]

$$^7\mathrm{Li/H} = (2.75 - 4.17) \times 10^{-10}, \tag{2.5}$$

the value which is still too low to be reconciled with the result of BBN. It is noted that Li can be produced together with Be and B through spallation of CNO nuclei by cosmic ray protons and α particles. About 10% of ^{7}Li could be due to cosmic-ray processes, leaving the remainder as primordial. Among a variety of observational data, we here pick up only representatives of ^{4}He and D.

2.2 Standard BBN and Reaction Rates

In general, reaction rate is averaged by Maxwell-Boltzmann distribution;

$$N_A\langle\sigma v\rangle = N_A \left(\frac{8}{\pi\mu k_\mathrm{B}^3 T_\gamma^{\,3}}\right)^{1/2} \int_0^\infty \sigma(E) E \exp\left(-\frac{E}{k_\mathrm{B}T_\gamma}\right) dE,$$

where N_A, v, σ and μ are the Avogadro number, relative velocity, cross section and reduced mass. The reaction cross section of charged particle are shown as

$$\sigma(E) = \frac{S(E)\exp(-2\pi\zeta)}{E},$$

where $S(E)$ is the S-factor, and ζ is the Sommerfeld parameter which is given by the following formula;

$$\zeta = Z_1 Z_2 \left(\frac{e^2}{\hbar c}\right)\left(\frac{\mu c^2}{2E}\right)^{1/2},$$

here, Z_i is the charge in unit of elementary charge e. On the contrary, the reaction cross section with neutrons is

$$\sigma(E) = \frac{R(E)}{v},$$

where $R(E)$ is the transition probability and v is the velocity of incident particle.

2.2.1 Latest obsrvational data and BBN calculation

First of all, twelve reactions and corresponding literature, which greatly influence the final production amount of elements in BBN, are shown in Table 2.1. We performed BBN calculation with use of BBN code (Hashimoto and Arai [53]). All reactions are given in Appendix A(Table A.2).

Table 2.1: BBN main paths and the references.

1	n $\leftrightarrow$ p	(1.24)-(1.29)	7	T(d,n)^{4}He	DE04
2	p(n,γ)D	An06	8	^{3}He(d,p)^{4}He	DE04
3	^{3}He(n,p)T	DE04	9	^{7}Li(p,α)^{4}He	DE04
4	D(p,γ)^{3}He	DE04	10	T(α,γ)^{7}Li	DE04
5	D(d,n)^{3}He	DE04	11	^{3}He(α,γ)^{7}Be	DE04
6	D(d,p)T	DE04	12	^{7}Be(n,p)^{7}Li	DE04

We apply DE04 [54] for reaction network, which are the nuclear reaction rates derived using the R-matrix analysis. It has been recommended conventionally for the main paths of nucleosynthesis. We adopt 880.1 ± 1.1 s [55] for neutron lifetime, which is one of the most important physical quantity and enormously affects the ^{4}He abundance.

In Fig. 2.1, we show the main result of standard Big Bang nucleosynthesis with use of DE04 [54]. From the top panel, the figure shows the ^{4}He mass fraction ($Y_{\rm p}$) and number fraction of deuteron and ^{7}Li comparison to proton (H).

Figure 2.1 indicates three points,

- Lithium problem still remains as the serious problem.
- The result of Izotov (2013) is consistent with that of Aver (2013), but is not consistent with observational result of deuteron by Cooke (2014) and *Planck* 2013 [56].
- BBN result has no answer for the baryon-to-photon ratio using the results of (2.1) and (2.3).

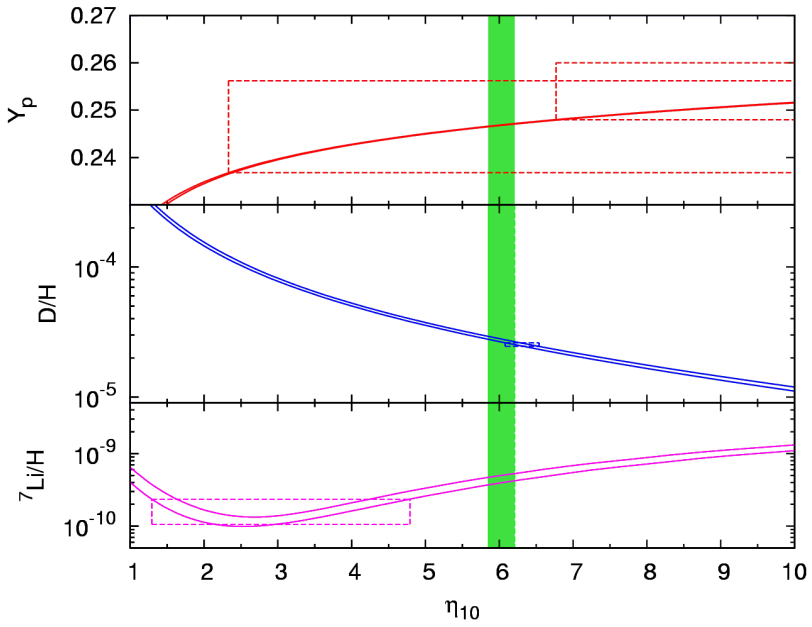

Fig. 2.1: Dependence of light elements abundances on η_{10} using DE04 [54] reaction rates. We apply $\tau_{\rm n} = 880.1$ for the neutron lifetime [55]. Vertical band is the constraints on baryon-to-photon ratio from *Planck* 2013 [56]. Indivisual error bands indicate 2σ confidence level.

We focus on the last two problems because they are the more serious problem than the lithium problem. As the first step of the improvement, we adopted the nuclear reaction rate of NACRE-II compiled by incorporating the experiment result of recent years, and BBN calculation was carried out considering the uncertainties in nuclear reaction rates. We apply NACRE-II for D(p,γ)^{3}He, D(d,n)^{3}He, D(d,p)T, T(d,n)^{4}He, ^{3}He(d,p)^{4}He, ^{7}Li(p,α)^{4}He, T(α,γ)^{7}Li and ^{3}He(α,γ)^{7}Be, respectively. The results are shown in Fig. 2.2 and Table 2.2.

Table 2.3 is the result of calculation using $\eta = 6.19 \times 10^{-10}$. It indicates that the reaction paths significantly affects abundances. At first, let us discuss the final abundances of deuteron and ^{7}Li. Compared to the reaction rate of DE04, NACRE-II reaction rate consumes deuteron -2.3% via D(d,p)T. D(p,γ)^{3}He has the opposite tendency which causes an increase of deuteron by $+0.7\%$. Together with these two reactions, NACRE-II reaction rates have the tendency of consuming more deuterons. NACRE-II reaction rate has the tendency of producing more ^{7}Li via D(p,γ)^{3}He(α,γ)^{7}Be(,e$^+\nu_{\rm e}$)^{7}Li.

Focusing on the box of D/H, the result using NACRE-II is smaller in error with the observed value of *Planck* 2013 than in the case of using DE04, resulting in a more consistent result. Also, when determining η_{10} from ^{4}He, we obtain the small difference of the baryon-to-photon ratio $\delta\eta_{10} \sim -0.07$. Therefore, the influence of nuclear reaction rate [54] and [57] is not so large. It is reasonable to evaluate the results of BBN using only the value of η_{10} obtained from D and the nuclear reaction rate of NACRE-II, which are consistent with *Planck* satellite.

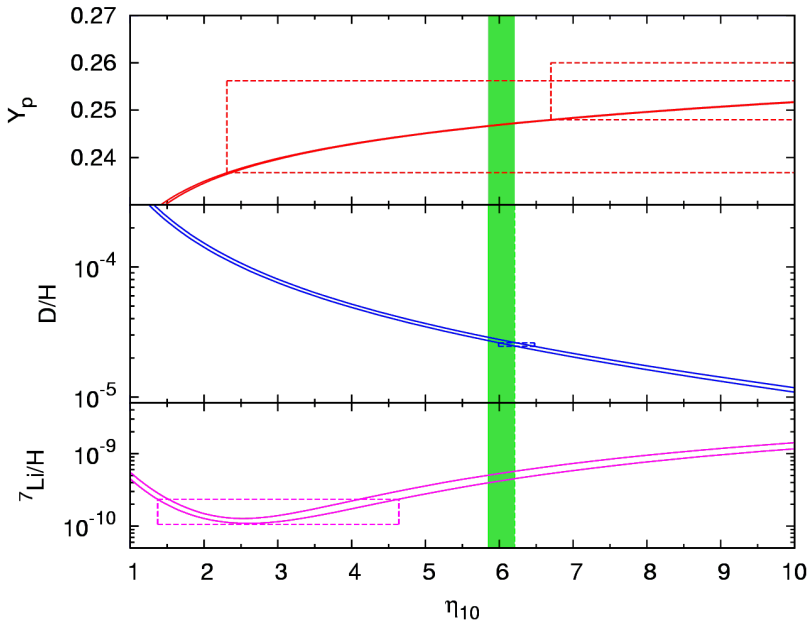

Fig. 2.2: η dependency of light elements abundances using NACRE-II reaction rates. We apply $\tau_{\rm n} = 880.1$ s for the neutron lifetime. Vertical band is the constraints on baryon-to-photon ratio from *Planck* 2013. Each error bars indicate 2σ confidence level.

Table 2.2: Constraints on η_{10} from ^{4}He and D observation using DE04 and NACRE-II.

	DE04	NACRE-II	observation
D	$\eta_{10} = 6.08 - 6.54$	$\eta_{10} = 5.99 - 6.48$	Cooke+ 2013
$Y_{\rm p}$	$\eta_{10} \geq 6.77$	$\eta_{10} \geq 6.70$	Izotov+ 2013
$Y_{\rm p}$	$\eta_{10} \geq 2.33$	$\eta_{10} \geq 2.31$	Aver+ 2013

Table 2.3: Percentage changes of ^{4}He mass fraction and D and ^{7}Li abundances.

	$\delta Y_{\rm p}$	δD	δ^7Li
D (p,γ)^{3}He	-0.01	+0.7	-1.2
D(d,n)^{3}He	-0.02	-0.2	+1.0
D(d,p)T	+0.05	-2.3	+0.3
T(d,n)^{4}He	-0.03	0.0	0.0
^{3}He(d,p)^{4}He	-0.02	+0.1	+0.6
T(α,γ)^{7}Li	+0.01	0.0	0.0
^{3}He(α,γ)^{7}Be	+0.01	0.0	+6.0
^{7}Li(p,α)^{4}He	+0.02	0.0	+0.1

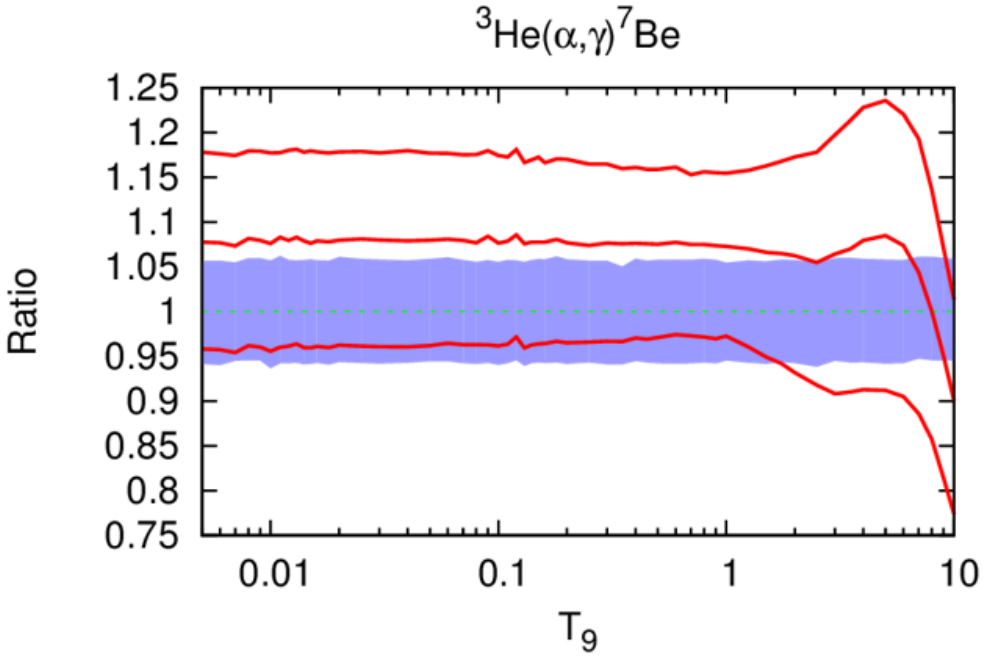

Fig. 2.3: Differences in nuclear reaction rates between DE04 and NACRE-II. Green dot and blue band indicate the DE04 rates and its uncertainties. The red solid lines show the ratio of the reaction rate of NACRE-II to DE04. Top, middle and bottom lines indicate upper limit, adopted value, and lower limit, respectively.

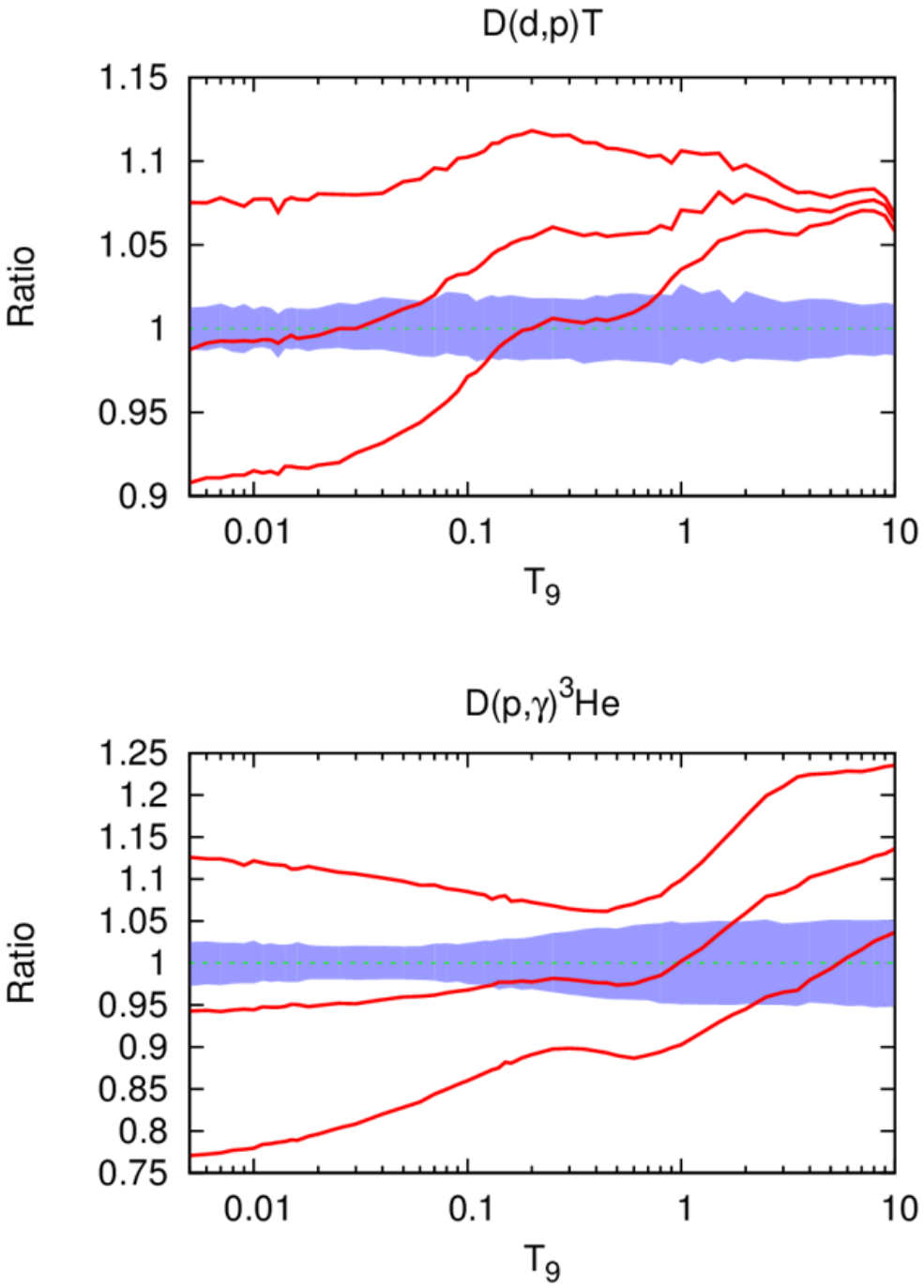

Fig. 2.4: Differences in nuclear reaction rates between DE04 and NACRE-II. Green dot and blue band indicate the DE04 rates and its uncertainties. The red solid lines show the ratio of the reaction rate of NACRE-II to DE04. Top, middle and bottom lines indicate upper limit, adopted value, and lower limit, respectively.

The update of reaction rate does not reduce the discrepancies between the BBN results and observations. Hence, we study the dependency of neutron lifetime. The neutron lifetime is one of the most important physical quantities which affect the ^{4}He abundance. Table 2.4 shows how the neutron lifetime affects the BBN result. The lifetime of 885.7 s is the previous evaluation by A. Serebrov *et al.* [58].

Table 2.4: Neutron lifetime and constraints on η_{10} from observations using with NACRE-II.

	$\tau_n = 880.1$ s	$\tau_n = 885.7$ s	observation
D	$\eta_{10} = 6.08 - 6.54$	$\eta_{10} = 6.09 - 6.56$	Cooke+ 2013
$Y_{\rm p}$	$\eta_{10} \geq 6.77$	$\eta_{10} \geq 6.00$	Izotov+ 2013
$Y_{\rm p}$	$\eta_{10} \geq 2.33$	$\eta_{10} \geq 4.48$	Aver+ 2013

In fact, the evaluated lifetime enormously depends on the method of measurement. At present, measurements are performed by using two methods; proton-counting method and neutron-counting method [59]. The results by these two methods have large discrepancy in neutron lifetime (see Fig. 2.5).

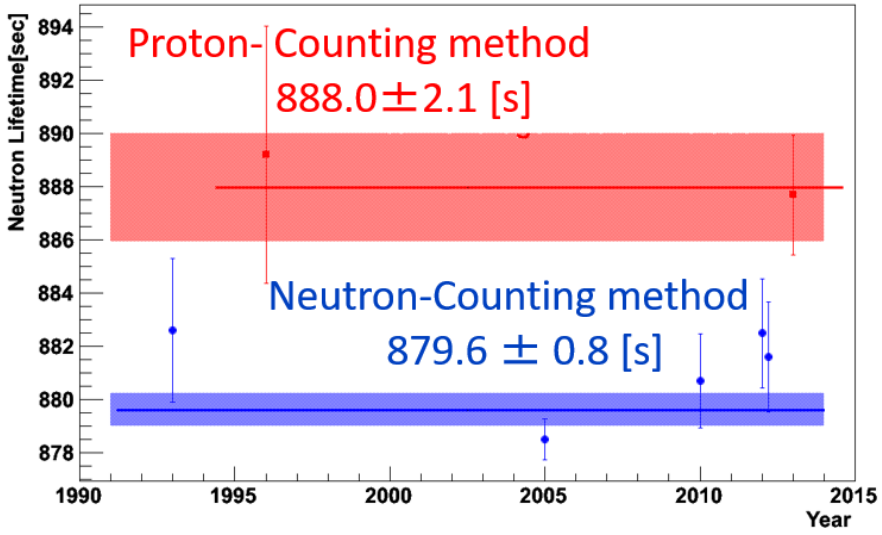

Fig. 2.5: Neutron lifetime that has been measured from 1990 to 2015.

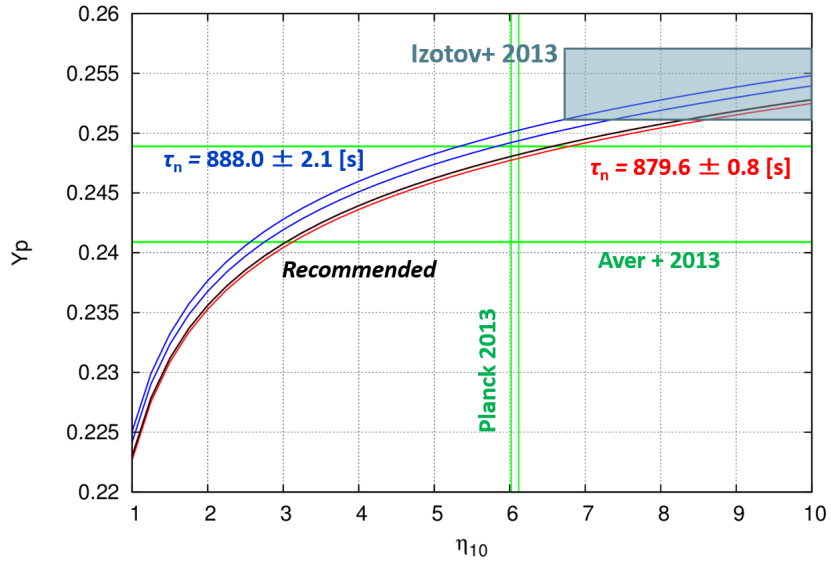

Fig. 2.6: Helium abundances and the neutron lifetime.

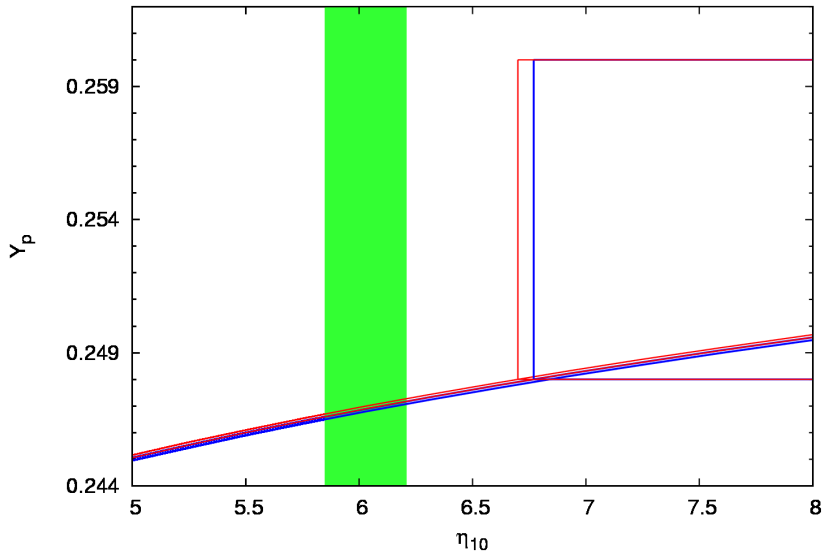

Fig. 2.7: Difference of Y_p between DE04 and NACRE-II. The red and blue lines represent the result of NACRE-II and DE04. The boxes and vertical band indicate the constaints on baryon-to-photon ratio η, and the constraint from *Planck*.

We show the neutron lifetime dependence on the ^{4}He mass fraction in Fig. 2.6. Even if the proton-counting method gives the neutron lifetime precisely, the ^{4}He problem remains. Moreover, there arises the new problem that baryon-to-photon ratio, which is estimated from Aver (2013) results, is inconsistent with the result of *Planck*. Consequently, the standard Big Bang nucleosynthesis failed to reproduce the observational result (see Fig. 2.7) if we adopt the result of Izotov (2013) [49] and 880.1 ± 1.1 s for neutron lifetime.

2.2.2 Puzzle in the standard BBN

As we mentioned above, standard BBN fails to find a consistent range of η for the observed values given in (2.1) and (2.3). Hence, a non-standard model is revisited. The behaviour of the cosmological model depends on the particle model and/or the model of gravitation. Namely, there are two methods for modification. For instance, there are several non-standard models, such as models including sterile neutrinos [60], X-particles [61–67], extra-neutrino generation [68, 69], axions [70], or chemical potential [71, 72] for the case of modifying particle properties. Brans-Dicke [73–75], $f(R)$-gravity [76], decaying-Λ [75, 77], and inhomogeneous models [78] are classified as those modifying the gravitational theory [42, 79, 80].

2.3 Lepton Asymmetry

In our universe there is the baryon asymmetry where baryonic matter exists and anti baryonic matter does not exist. Charge neutrality for baryons binds the electron number and proton number, this limits the degree of baryon asymmetry. On the other hand, neutrino sector can take a large asymmetry because neutrinos are the neutral particle. Standard BBN deals with the baryon asymmetry, but not lepton asymmetry. As a model to reproduce such a situation, there is a model considering the neutrino chemical potential [71, 72].

When the temperature is $T_\gamma \simeq 1.5$ MeV, neutrino decouples from the other particles so that the momentum distriburion conserves. The number densities of neutrinos and anti-neutrinos whose momentum is in the range of $p \sim p + dp$ are described by following distribution functions;

$$n_{\nu_e}(p)d^3p = \frac{4\pi p^2}{(2\pi\hbar)^3}\left[\exp\left(\frac{p-\mu_{\nu_e}}{k_B T}\right)+1\right]^{-1}, \tag{2.6}$$

$$n_{\bar{\nu}_e}(p)d^3p = \frac{4\pi p^2}{(2\pi\hbar)^3}\left[\exp\left(\frac{p+\mu_{\bar{\nu}_e}}{k_B T}\right)+1\right]^{-1}, \tag{2.7}$$

where we regard neutrino as massless particle and introduce the electron neutrino chemical

potential μ_{ν_e}. The quantity of extra neutrino number density N_e is written as

$$N_e = \int dp[n_{\nu_e}(p) - n_{\bar{\nu}_e}(p)] = 4\pi \left(\frac{k_B T}{2\pi\hbar}\right)^3 \mathcal{N}\left(\frac{\mu_\nu}{k_B T}\right), \tag{2.8}$$

$$\mathcal{N}(x) = \int_0^\infty y^2 dy \left[\frac{1}{\exp(y-x)+1} - \frac{1}{\exp(y+x)+1}\right]. \tag{2.9}$$

The extra neutrino number is conserved ($N_e a^3 = $ const.) and neutrino's temperature always proportional to the inverse of the scale factor ($T_\nu \propto a^{-1}$) because they behave as the free particle, then the quantity of N_e/T_ν^3 takes a constant value. We can conclude that (2.9) is independent of the neutrino temperature. It is beneficial to introduce the degeneracy parameter,

$$\xi_i \equiv \frac{\mu_{\nu_i}}{k_B T_{\nu_i}}, \tag{2.10}$$

where subscript i is for the electron-, muon-, tauon- neutrino. The degree of lepton asymmetry is evaluated by integrating (2.9). Corresponding to the baryon asymmetry parameter (η), this quantity is defined as;

$$\eta_\nu = \frac{n_{\nu_i} - n_{\bar{\nu}_i}}{n_\gamma} = \frac{1}{12\zeta(3)} \left(\frac{T_{\nu_i}}{T_\gamma}\right)^3 (\pi^2 \xi_i + {\xi_i}^3), \tag{2.11}$$

where we assumed that neutrinos have the Fermi-Dirac distribution (see Appendix C).

Dolgov *et al.* (2002 [81],2004 [82, 83]) reveals about the degeneracy parameters that

(i) Even if the neutrino mixing angles are small during the BBN epoch, the chemical potential of each generation of neutrino has the same value due to neutrino oscillation (strong-mixing case).

(ii) Under an exotic condition such as the case where neutrinos interact with majoron, the mixing is suppressed and each chemical potential can be determined independently, that is $\xi_e \neq \xi_\mu \neq \xi_\tau$ (no-mixing case).

The degeneracy parameter affects BBN in the following two points:

- The neutrino energy density is increased as the absolute magnitude of degeneracy parameter is increased.
- The neutrino distribution function sensitively depends on the degeneracy parameter.

The former effect makes the expansion rate of the universe faster, and the time scale of BBN is decreased. The reduction of the time scale results in an increase of ^{4}He abundance. Using (1.6) the energy density of the neutrino can be written as

$$\rho_{\nu_i} = \frac{4\pi}{(2\pi\hbar c)^3 c^2} \int_0^\infty dE \frac{E^3}{\exp[(E \pm \mu_{\nu_e})/k_{\rm B}T] + 1}, \tag{2.12}$$

where plus is for neutrinos and minus is for anti-neutrinos. The energy density including the extra neutrinos is

$$\begin{aligned} \rho_{\nu_i} + \rho_{\bar{\nu}_i} &= \frac{\pi^2}{15}\left(\frac{(k_{\rm B}T)^4}{\hbar^3 c^5}\right) \sum_i \left[\frac{7}{8} + \frac{15}{4}\left(\frac{\xi_i}{\pi}\right)^2 + \frac{15}{8}\left(\frac{\xi_i}{\pi}\right)^4\right] \\ &= a_r T_\nu^4 \sum_i \left[\frac{7}{8} + \frac{15}{4}\left(\frac{\xi_i}{\pi}\right)^2 + \frac{15}{8}\left(\frac{\xi_i}{\pi}\right)^4\right]. \end{aligned} \tag{2.13}$$

The total energy of the radiation component before the electron-positron pair annihilation is

$$\rho_{\rm rad} = \left[\frac{11}{4} + \sum_i \left(\frac{7}{8} + \frac{15}{4}\left(\frac{\xi_i}{\pi}\right)^2 + \frac{15}{8}\left(\frac{\xi_i}{\pi}\right)^4\right)\right] a_r \left(\frac{T_\nu}{a}\right)^4, \tag{2.14}$$

and after the electron-positron annihilation is

$$\rho_{\rm rad} = \left[1 + \left(\frac{4}{11}\right)^{4/3} \sum_i \left(\frac{7}{8} + \frac{15}{4}\left(\frac{\xi_i}{\pi}\right)^2 + \frac{15}{8}\left(\frac{\xi_i}{\pi}\right)^4\right)\right] a_r \left(\frac{T_\nu}{a}\right)^4. \tag{2.15}$$

Here, we set $N_{\rm eff} = 3$ as the neutrino generation.

We show the time evolution of the energy density in Fig. 2.8. It is noted that the energy density of neutrinos is increased as the absolute magnitude of ξ_e is increased as seen in (2.15).

The latter effect changes the weak interaction rates concerning the ratio of neutrons and protons. The reaction rates for n $\longleftrightarrow$ p reactions are written by equations from (2.16) to (2.21) with the degeneracy parameters of electron neutrinos:

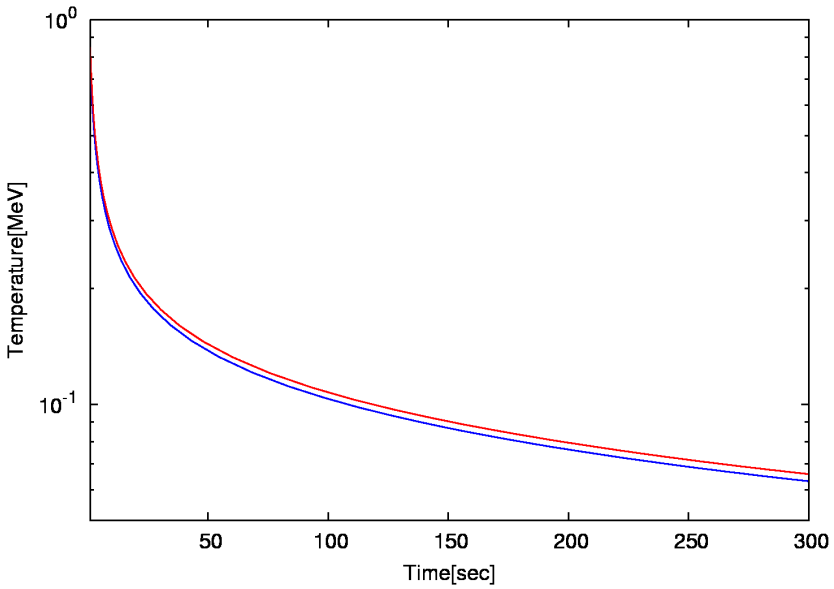

Fig. 2.8: Expansion rate with varing $\xi_{\rm e}$ (Red: $\xi_e = 0$, Blue: $|\xi_{\rm e}| = 1.0$).

$$\lambda_{\rm n\to pe\nu} = \frac{1}{\tau\lambda_0}\int_1^q d\epsilon \frac{\epsilon(\epsilon-q)^2(\epsilon^2-1)^{1/2}}{[1+\exp(-\epsilon z)][1+\exp((\epsilon-q)z_\nu+\xi_e)]}, \tag{2.16}$$

$$\lambda_{\rm n\nu\to pe} = \frac{1}{\tau\lambda_0}\int_q^\infty d\epsilon \frac{\epsilon(\epsilon-q)^2(\epsilon^2-1)^{1/2}}{[1+\exp(-\epsilon z)][1+\exp((\epsilon-q)z_\nu-\xi_e)]}, \tag{2.17}$$

$$\lambda_{\rm ne\to p\nu} = \frac{1}{\tau\lambda_0}\int_1^\infty d\epsilon \frac{\epsilon(\epsilon+q)^2(\epsilon^2-1)^{1/2}}{[1+\exp(\epsilon z)][1+\exp(-(\epsilon+q)z_\nu+\xi_e)]}, \tag{2.18}$$

$$\lambda_{\rm pe\nu\to n} = \frac{1}{\tau\lambda_0}\int_1^q d\epsilon \frac{\epsilon(\epsilon-q)^2(\epsilon^2-1)^{1/2}}{[1+\exp(\epsilon z)][1+\exp((q-\epsilon)z_\nu+\xi_e)]}, \tag{2.19}$$

$$\lambda_{\rm pe\to n\nu} = \frac{1}{\tau\lambda_0}\int_q^\infty d\epsilon \frac{\epsilon(\epsilon-q)^2(\epsilon^2-1)^{1/2}}{[1+\exp(\epsilon z)][1+\exp((q-\epsilon)z_\nu-\xi_e)]}, \tag{2.20}$$

$$\lambda_{\rm p\nu\to ne} = \frac{1}{\tau\lambda_0}\int_1^\infty d\epsilon \frac{\epsilon(\epsilon+q)^2(\epsilon^2-1)^{1/2}}{[1+\exp(-\epsilon z)][1+\exp((q+\epsilon)z_\nu+\xi_e)]}, \tag{2.21}$$

Particularly, when neutrons and protons are in thermal equilibrium, the n/p ratio are changed because of the degeneracy parameter of electron neutrino:

$$\frac{n_{\rm n}}{n_{\rm p}} = \exp\left[-\frac{\Delta m_{\rm np}}{k_{\rm B}T} - \xi_e\right], \tag{2.22}$$

where $\Delta m_{\rm np}$ indicates the mass difference of neutron and proton. In this work, we assumed

that only the electron neutrino has the chemical potential.

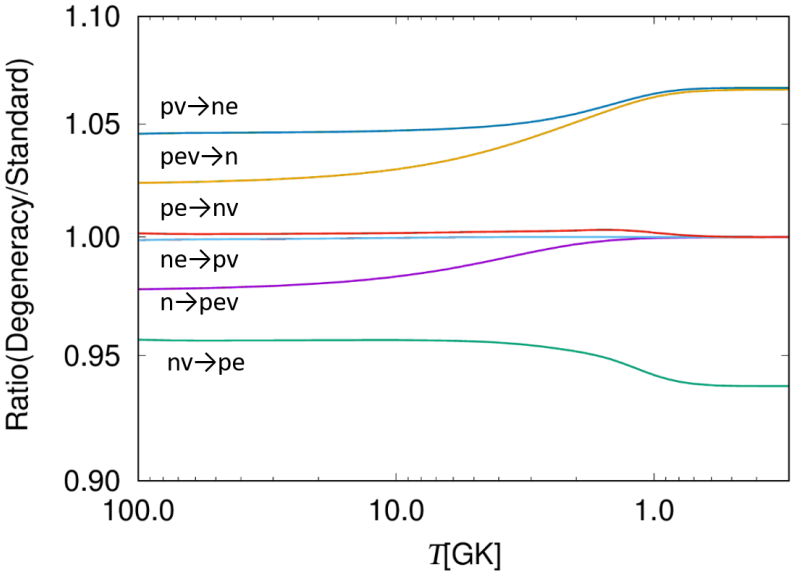

Fig. 2.9: Effect of ξ_e on the reaction rates between neutrons and protons. The ratios corresponds to the case of $\xi_e = -0.046$ compared to the standard model of $\xi_e = 0$.

We show the effect of ξ_e on the reaction rates between conversions of neutrons and protons in Fig. 2.9. It shows the ratios between including and excluding ($\xi_e = 0$) chemical potential. We note that the weak interaction rates without chemical potential are shown in Fig. 1.8. The ratio between neutrons and protons is one of the most important value for BBN calculation. Since neutrons and protons are in thermal equilibrium at $T_\gamma > 20$ GK, the reaction rates determine the ratio. In high temperature, $T_\gamma > 2$ GK, the ratio between neutrons and protons are determined by the reactions of $p\nu \to ne$, $n\nu \to pe$, $pe \to n\nu$, and $ne \to p\nu$ (see Fig. 1.8). Combining the result of Fig. 2.9, it can be concluded that the change ratios between neutrons and protons are dominated by the former two reactions $p\nu \to ne$ and $n\nu \to pe$.

The change of reaction rates before the starting point of BBN ($T_\gamma > 3$ GK) mainly affects the abundance of ^{4}He. The positive (negative) chemical potential makes ^{4}He increase (decrease). We show the calculational results of the chemical potential dependency in Fig. 2.10. Also, Fig. 2.11 indicates the effects for each element. The final abundance of ^{4}He are strongly affected by the chemical potential, but the parameter of baryon-to-photon ratio η_{10} is numerically degenerated. The degeneration is solved by analysing

together with the observational result of deuteron. The final abundance of deuteron is slightly affected by the chemical potential but not baryon-to-photon ratio η_{10}. As a result, the degeneracy parameter ξ_e and baryon-to-photon ratio ($\eta_{10} = \eta \times 10^{-10}$) are constrained from the analysis of $Y_p \oplus$ D/H (see Fig. 2.12).

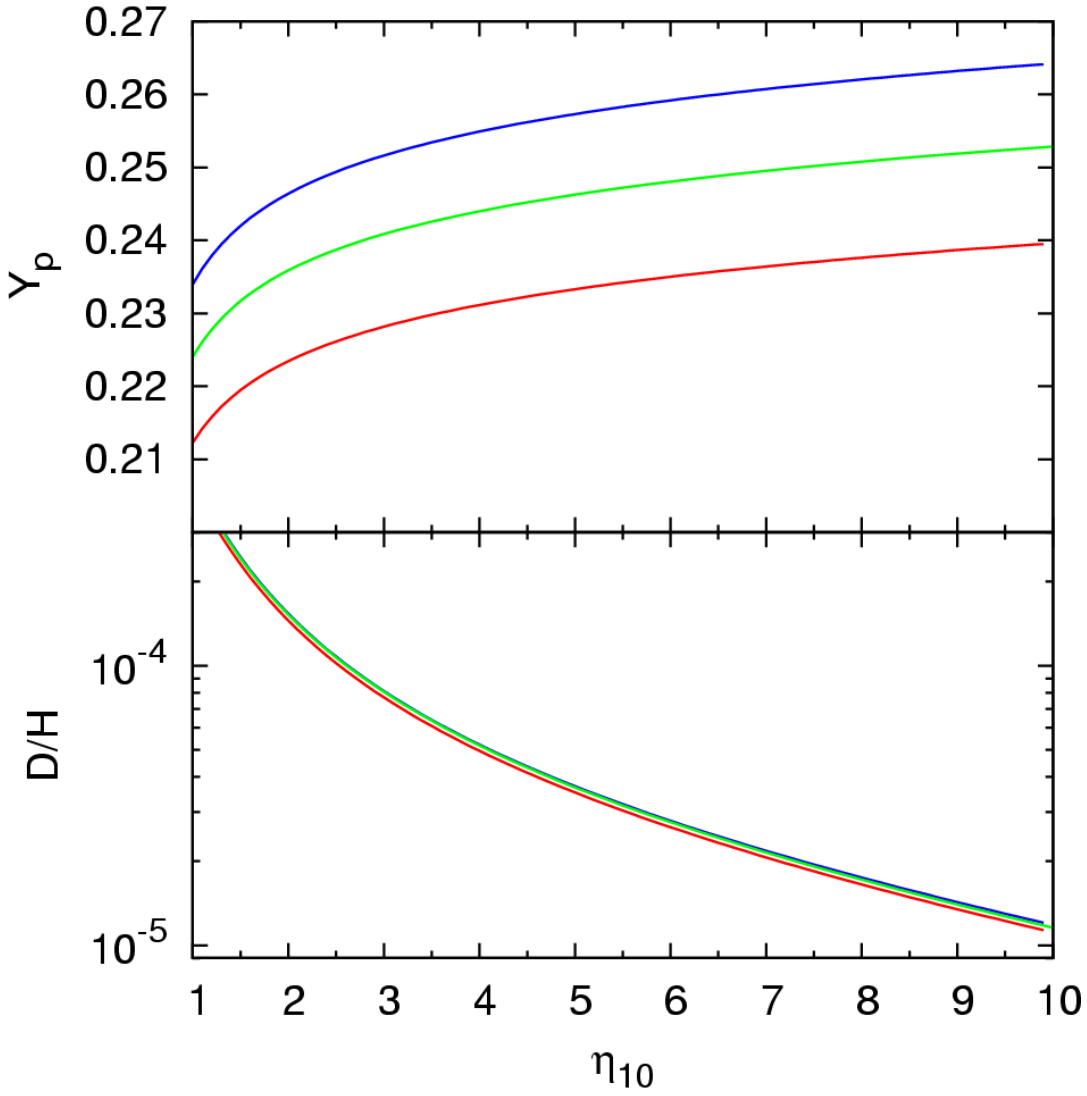

Fig. 2.10: Dependence of Y_p and D/H on ξ_e (Blue: $\xi_e = -0.1$, Green: $\xi_e = 0.0$, Red: $\xi_e = 0.1$).

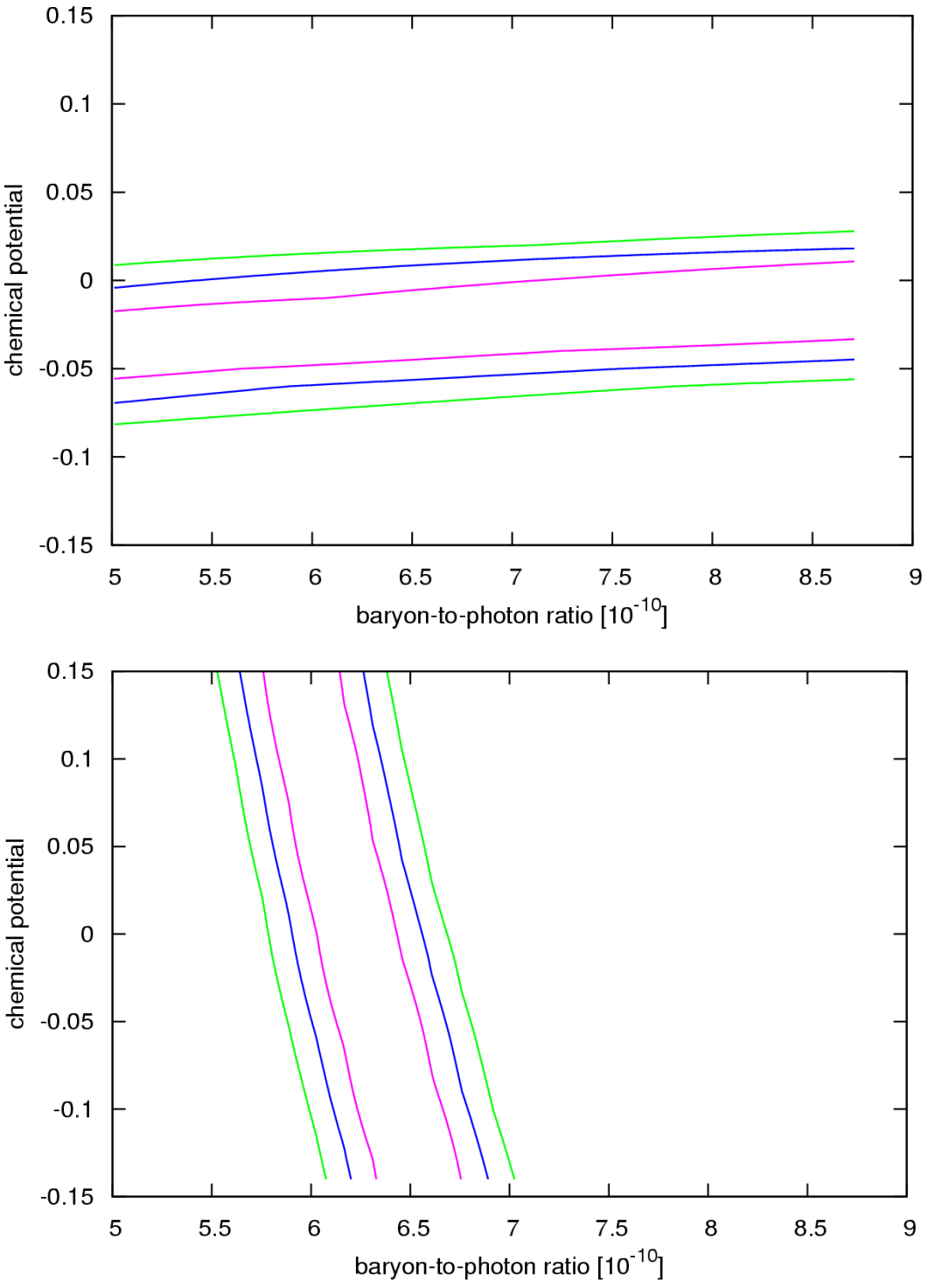

Fig. 2.11: The upper and lower panels show the limit from the observatonal result of Y_p (Izotov *et al.* [49]) and D/H (Cooke *et al.* [21]). Contours with 1σ, 2σ, and 3σ confidence levels from $Y_{\rm p}$ and D/H.

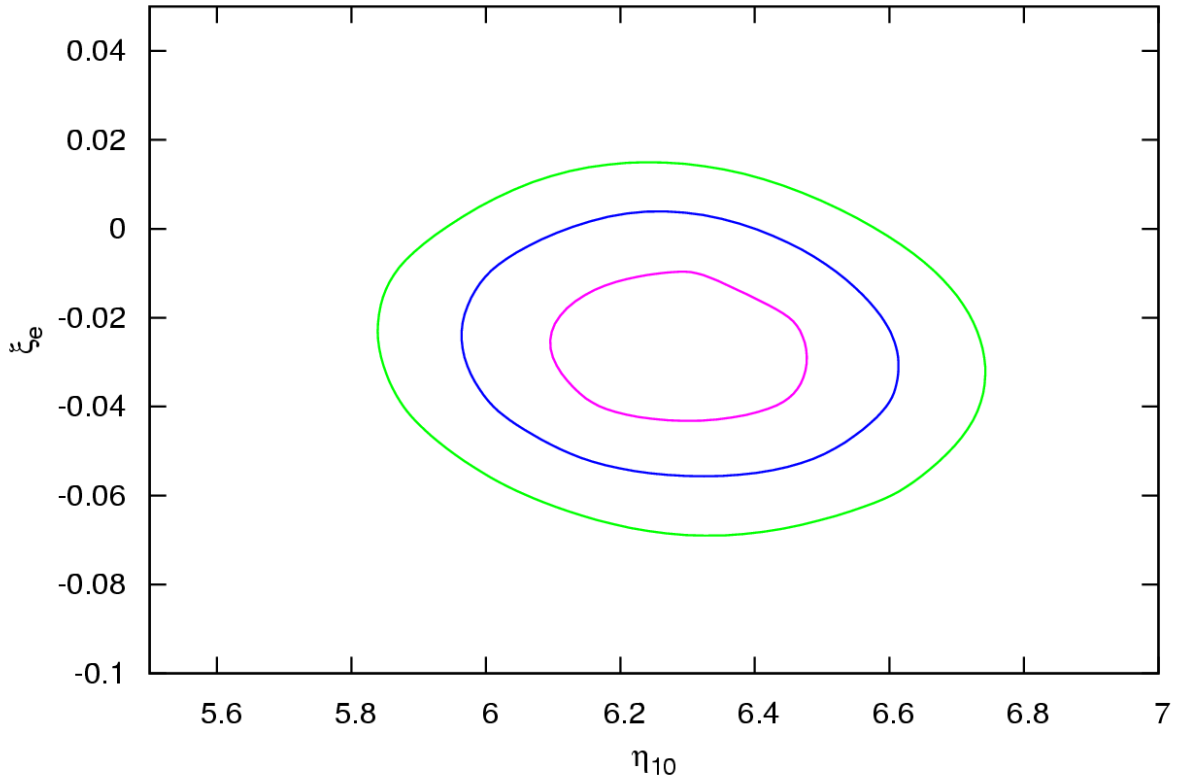

Fig. 2.12: Contours with 1σ, 2σ, and 3σ confidence levels from $Y_{\rm p}\oplus$D/H.

The latest results

We perform BBN calculation using our code which includes 14 nuclides and 48 paths (see Table A.1). Moreover, our code includes the Coulomb correction for the interaction between neutrons and protons (see Appendix B).

In recent years, estimation method of light elements is improved, particularly for ^{4}He. Traditionally, the emission lines, which are employed to evaluate abundance of ^{4}He, are in the visible wavelength range, and the number of suitable lines is limited. Furthermore, there are large systematic uncertainties in helium abundance because of the degeneracy of physical parameters, such as density and temperature. Recently, Izotov *et al.* estimated ^{4}He abundance including He$_{\rm I}\lambda$10830Å emission line. The 10830Å line of ^{4}He strongly depends on the electron density, which results in breaking the degeneracy with temperature. They presented ^{4}He abundance by using near-infrared spectropic observation of the

line in 45 low-metallicity H II regions [18](ITG14):

$$Y_{\rm p} = 0.2551 \pm 0.0022. \tag{2.23}$$

An alternative low value of the average was reported by Aver *et al.* [84](AOS15):

$$Y_{\rm p} = 0.2449 \pm 0.0040, \tag{2.24}$$

which is the results of 31 sets of observations including $\mathrm{He_I}\lambda 10830$Å emission line.

The mean value of the D/H data (15 measurements) gives a same order value as an alternative estimate [21] of the primordial deuterium abundance [85]:

$$\mathrm{D/H} = (2.55 \pm 0.19) \times 10^{-5}. \tag{2.25}$$

We show the constraints on baryon-to-photon ratio from these observations in Fig. 2.13. The results of ITG14 gives a quite different constraint for baryon-to-photon ratio, and the large discrepancy between these observations became larger. Therefore, we recalculate the model of lepton asymmetry, and represent (η, ξ) plane in Fig. 2.14. ITG14 excludes the standard BBN with 3σ confidence level.

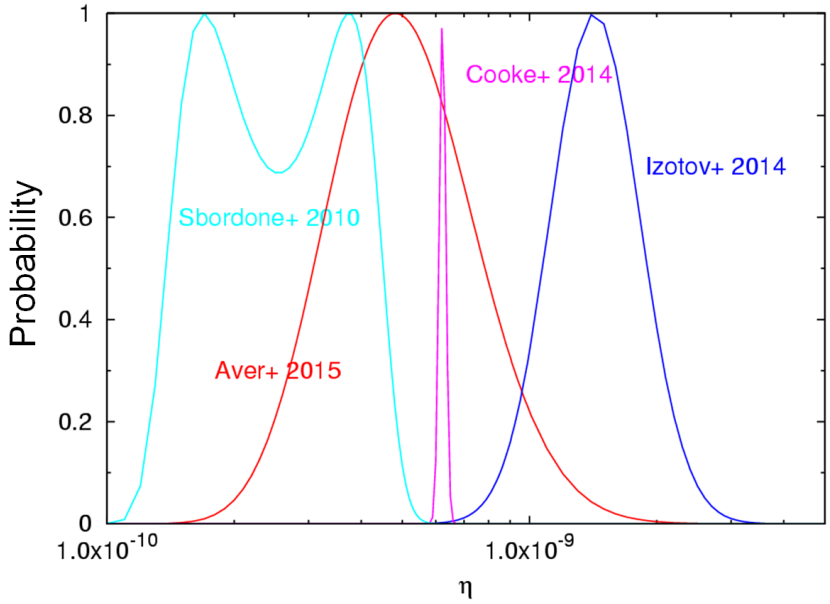

Fig. 2.13: Probability function of each observational result as a function η.

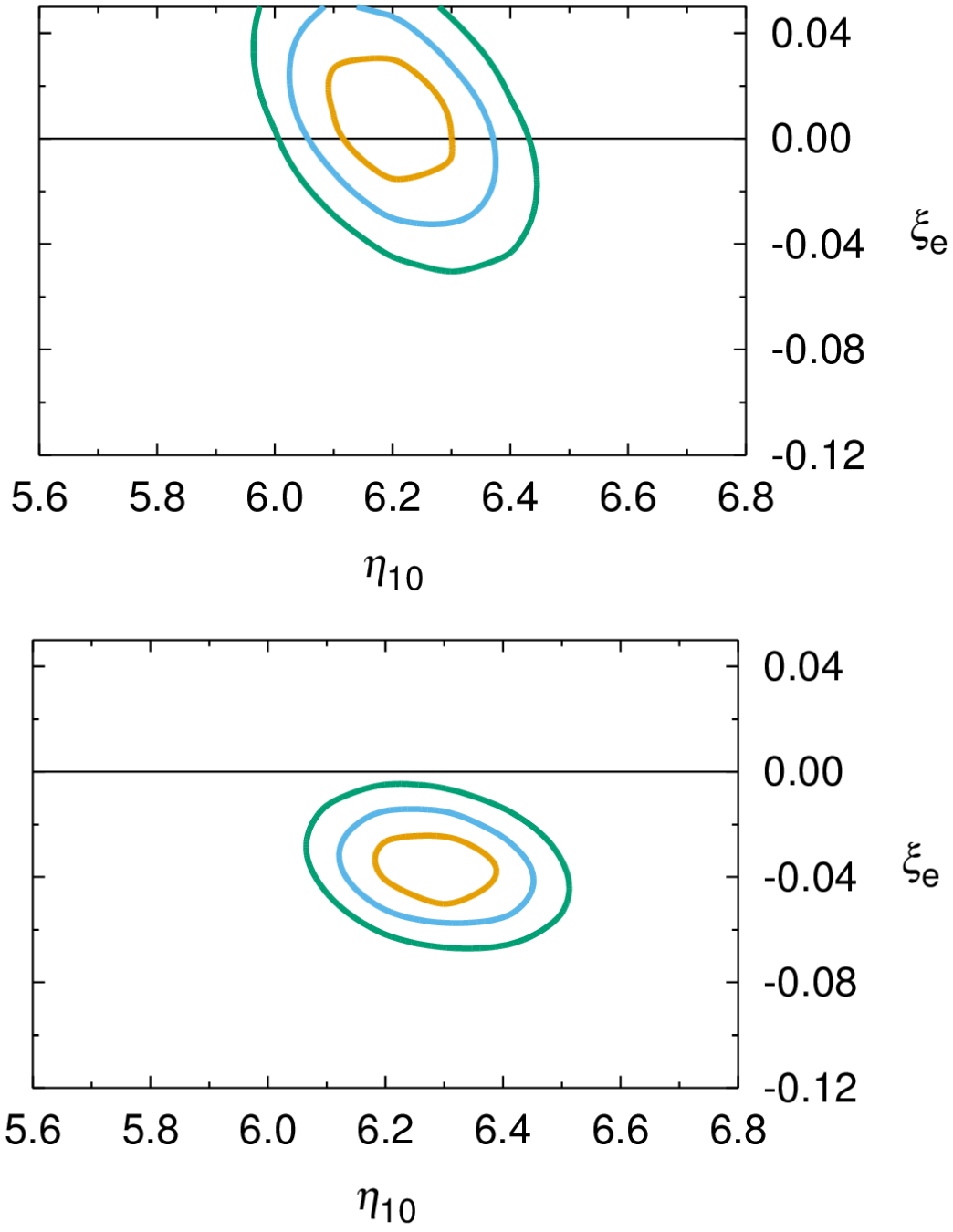

Fig. 2.14: Contours with 1σ, 2σ, and 3σ confidence levels from $Y_{\rm p}\oplus$D/H. The upper and lower contours are the results by using AOS15 and ITG14. We use a result of the primordial abundance by Cooke *et al.*(2014) for both the contours.

2.4 Concluding Remarks

In this study, standard BBN and non-standard BBN were calculated for BBN considering lepton asymmetry. In addition to the nuclear reaction rates (DE04) determined by Descouvemont *et al.* (2004), which is the nuclear reaction rate conventionally recommended BBN in the standard model, we applied the latest NACRE-II (2013) to the BBN. We adopted the latest estimated value of 880.1 ± 1.1 s and also the previous one of 885.7 s for the neutron lifetime. Furthermore, we used the Monte Carlo method to include the ambiguity caused by these nuclear reaction rate errors.

Compared with DE04, NACRE-II which includes the latest nuclear reaction rates has a small experimental errors. Regarding the production amount of D, the results using NACRE-II were found to be more consistent with η deduced from observations by *Planck* 2013, as compared to DE04.

As a result of computations using the latest value 880.1 ± 1.1 s as the neutron lifetime for the standard BBN, the effect on η_{10} due to the difference in nuclear reaction rates [54,57] was $\delta\eta_{10} \sim 0.07$, and we cannot find any change in BBN. Also, taking into account the uncertainty of the nuclear reaction rates, the value of η cannot be determined from the value of ^{4}He.

In order to examine the consistency with Izotov *et al.* (^{4}He observation), we adopted the lepton asymmetry as non-standard BBN. For nuclear reaction rates we adopted NACRE-II [57] whose restriction on η_{10} obtained from D is close to that obtained from *Planck* 2013.

Lepton asymmetry is introduced by introducing a chemical potential for neutrino. The two effects of the chemical potential are; one affects the expansion coefficient, the other is the temperature in the early universe which exceeds 10^{10} K. The chemical potential causes the effect on the n/p ratio. Especially, the latter greatly influence, which greatly influence the composition ratio of ^{4}He. As a result, we have obtained the parameters: $-3.4 \times 10^{-2} < \xi_e < -1.8 \times 10^{-2}$ and $6.17 < \eta_{10} < 6.38$ (1σ C.L.). This is also consistent with the result obtained by CMB observations $5.85 < \eta_{10} < 6.21$ (2σ C.L.) [56].

We considered the lepton asymmetry as non-standard BBN, but there are other models assuming unknown particles assumption and those with modified gravitational field theory. Even if observation shows that the lepton asymmetry is not so large, it may be

possible to incorporate the same effect by modification of gravity field theory or assumption of unknown particles. In order to solve the deviation from the standard model, it is necessary to study modified gravity field theory, new particle model, non-uniformity of the cosmic baryonic matter distribution.

3 Equation of State of Dark Energy

We consider that the energy-momentum tensor consists of two fluids ($\rho = \rho_{\rm de} + \rho_{\rm m}$): (i) $\rho_{\rm m}$: non-relaivistic matter component as cold dark matter, (ii) $\rho_{\rm de}$: DE with unknown properties. To study the characteristic feature of DE, we adopt a specific EoS of DE, that is, $w_{\rm de}$ or $w_{de}(a)$ in EoS which has been proposed by Hannested and Mörtsell [38],

$$w_{\rm de}(a) = \frac{\omega a^\beta + \gamma}{a^\beta + 1}, \tag{3.1}$$

where the scale factor a in this EoS is normalized at the time of $\rho_{\rm m} = \rho_{\rm de}$ and β is always positive. Positive (negative) β shows the anterograde (retrograde) evolution in terms of the scale factor. In our choice, $w_{\rm de}(a)$ converges to ω at large a and equals to γ at the origin. We show the time evolution of dark energy and matter components in Fig. 3.1. This EoS can reproduce many kind of DE models mentioned in § 1.4.

In the present work, we consider the matter and DE as parts of the energy-momentum tenosor, and these are conserved independently,

$$\dot{\rho_{\rm de}} + 3H(1 + w_{\rm de})\rho_{\rm de} = 0, \tag{3.2}$$

$$\dot{\rho_{\rm m}} + 3H\rho_{\rm m} = 0, \tag{3.3}$$

where subscripts 'de' and 'm' indicate DE and matter, respectively. With use of EoS and the continuity equations for matter and DE, (3.2) and (3.3) can be integrated to obtain the energy density evolution,

$$\rho_{\rm m}(a) = \rho_{\rm m}(a_*)\left(\frac{a}{a_*}\right)^{-3}, \tag{3.4}$$

$$\rho_{\rm de}(a) = \rho_{\rm de}(a_*)\left(\frac{a}{a_*}\right)^{-3}\psi(a),$$

$$\psi(a;a_*) \equiv \exp\left(-3\int_1^{a/a_*}\frac{w_{\rm de}(x/a_*)}{x}dx\right) = \left(\frac{a}{a_*}\right)^{-3\gamma}\left(\frac{a^\beta+1}{a_*^\beta+1}\right)^{-3(\omega-\gamma)/\beta}, \tag{3.5}$$

where a_* is the present value of the scale factor, and is not a free parameter but is

determined by solving the following equation with a given $\Omega_{\rm m,0}$,

$$\psi(a=1;a_*)=\frac{\Omega_{\rm m,0}}{1-\Omega_{\rm m,0}}. \tag{3.6}$$

Equivalently, a_* is the solution of $\Omega_{\rm m,0}/(1-\Omega_{\rm m,0})=a_*^{3\gamma}[(a_*^\beta+1)/2]^{-3(\omega-\gamma)/\beta}$. We note that $\rho_{\rm de}=\rho_{\rm m}$ at $a=1$.

The density parameters are defined as follows,

$$\Omega_{\rm m}(a) = \frac{\rho_{\rm m}(a)}{\rho_{\rm m}(a)+\rho_{\rm de}(a)}, \tag{3.7}$$

$$\Omega_{\rm de}(a) = \frac{\rho_{\rm de}(a)}{\rho_{\rm m}(a)+\rho_{\rm de}(a)}. \tag{3.8}$$

Indeed, $\Omega_{\rm m}=\Omega_{\rm de}=1/2$ at $a=1$. With the above quantities, the Hubble parameter can be written as follows,

$$H(a)=H(a_*)\left(\frac{a}{a_*}\right)^{-3/2}\left[\Omega_{\rm m}(a_*)+\Omega_{\rm de}(a_*)\psi(a;a_*)\right]^{1/2}. \tag{3.9}$$

Type Ia supernova is the well known probe of DE due to the measurement of observations of the magnitude-redshift relation up to $z\simeq 1.5$ [86, 87]. They are utilized to limit the cosmological parameters. In particular, observations for type Ia supernovae have led to constain the Hubble constant or the density fraction of DE. To constrain the cosmological parameters, we adopt the *Supernova Union2.1* compilation [40] and *Supernova Legacy Survey (SNLS)* [88] data. Moreover, recent analysis of observations indicates that GRBs can also become a prove of DE. Therefore, we employ the redshift-luminosity distance relation obtained from GRB observations which are estimated by J. Liu and H. Wei [89]. Cosmological formulas for the luminosity distance $d_{\rm L}$ and distance moduli μ (the difference between the apparent and absolute magnitude) are obtained as a function of the scale factor a as follows,

$$d_{\rm L}(a) = \frac{1}{a}\int_1^a \frac{dx}{x^2H(x)}, \tag{3.10}$$

$$\mu(a) = 5\log_{10}(d_{\rm L}(a)/10\ {\rm pc}), \tag{3.11}$$

where μ is usually shown as a function of the redshift parameter z.

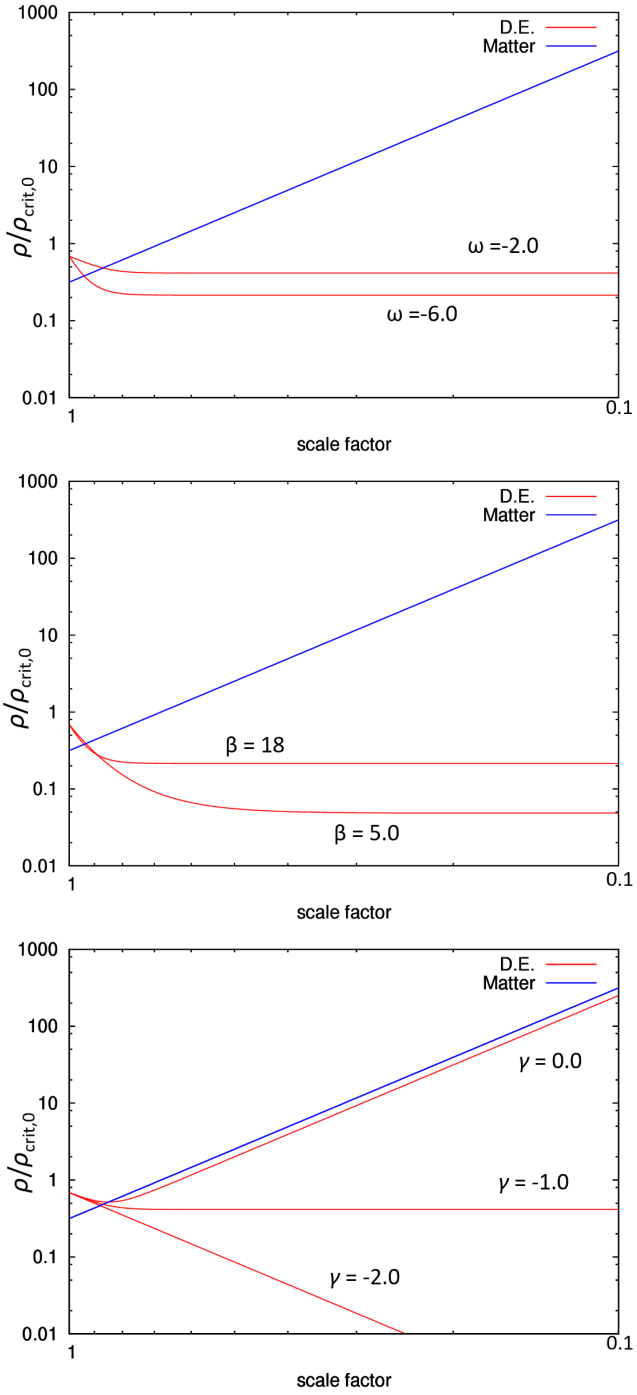

Fig. 3.1: These panels show the evolution of dark energy and matter density. Top, middle, bottom panels show ω, β, and γ dependency of dark energy.

3.1 Computational Method of Cosmological Parameters

To constrain the present cosmological parameters, following variables are defined,

$$w_0 = w_{\rm de}(a_*), \quad w_a = \left.\frac{dw_{\rm de}}{da}\right|_{a=a_*}, \quad H_0 = H(a_*),$$
$$\Omega_{\rm de,0} = \Omega_{\rm de}(a_*), \quad \Omega_{\rm m,0} = \Omega_{\rm m}(a_*), \quad z+1 = \frac{a_*}{a}. \tag{3.12}$$

where the subscript 0 represents their present values, respectively. Here, $(z+1)$ is exactly an unity at present.

We investigate three specific cases for models of dark energy: (i) vEoS: a variable EoS model which has 5 free parameters; $\Omega_{\rm m,0}$ (equivalently $\Omega_{\rm de,0}$), β, ω, γ and H_0. (ii) cEoS: constant EoS model in which ω is always equal to γ, in this case β makes no sence. (iii) C.C: standard ΛCDM model which consists of cosmological constant and cold dark matter.

To find the best fit values we calculate χ^2 as follows,

$$\chi^2 = \sum_{i=(\rm SNe,GRBs)}^{N} \frac{[d_{{\rm L},i}{}^{\rm th}(a;\omega,\gamma,\beta,\Omega_{\rm m,0},H_0) - d_{{\rm L},i}{}^{\rm obs}(a)]^2}{\sigma^2_{{\rm obs},i}(a)}.$$

Where N is the total number of observational data of type Ia supernovae and GRBs. We can evaluate the best fit values of parameters by minimamizing χ^2 values.

We apply Markov Chain Monte Carlo (MCMC) method to constrain the parameters of models. Here, we define a proposal distribution function $q(\boldsymbol{x}'|\boldsymbol{x})$ which is an arbitrary function, and a target distribution $\pi(\boldsymbol{x})$. The proposal distribution function works better or worse for the convergence steps.

First, we set initial values $\boldsymbol{x}^{(0)} = (x_1^{(0)}, x_2^{(0)}, \cdots, x_N^{(0)})$ and the step length $\boldsymbol{dx}^{(0)} = (dx_1^{(0)}, dx_2^{(0)}, \cdots, dx_N^{(0)})$. Second, we predict the next value $\boldsymbol{x}^{(n+1)}$ and the step length

$\boldsymbol{dx}^{(n+1)}$,

$$
\begin{aligned}
x_i^{(n+1)} &= \begin{cases} x_i^{(n)} + \epsilon_i^{(n)} dx_i^{(n)} & (\ u \leq \alpha(\boldsymbol{x}^{(n)}, \boldsymbol{x}^{(n-1)})\ ) \\ x_i^{(n)} & (\text{otherwise}) \end{cases} \\
dx_i^{(n+1)} &= \begin{cases} \frac{|\boldsymbol{dx}^{(n)}| \epsilon_i^{(n)} dx_i^{(n)}}{\sqrt{\sum_i (\epsilon_i^{(n)} dx_i^{(n)})^2}} & (\ u \leq \alpha(\boldsymbol{x}^{(n)}, \boldsymbol{x}^{(n-1)})\ ) \\ dx_i^{(n)} & (\text{otherwise}) \end{cases}
\end{aligned}
$$

where u is the uniformed random number, $\alpha(\boldsymbol{x}^{(n)}, \boldsymbol{x}^{(n-1)}) = \min\{1, \frac{\pi(\boldsymbol{x}^{(n-1)}) q(\boldsymbol{x}^{(n)}|\boldsymbol{x}^{(n-1)})}{\pi(\boldsymbol{x}^{(n)}) q(\boldsymbol{x}^{(n-1)}|\boldsymbol{x}^{(n)})}\}$ is the acceptance probability, $\pi(\boldsymbol{x}^{(n)})$ and $\pi(\boldsymbol{x}^{(n-1)})$ are the $\exp(-\chi^2/2)$ values of each step. $\boldsymbol{\epsilon}$ are random numbers according to the normal distribution. In the present work, we assume $q(\boldsymbol{x}|\boldsymbol{x}^{(n-1)}) = q(\boldsymbol{x}^{(n-1)}|\boldsymbol{x})$ beacuse of the assumption of detailed balance, and $\alpha(\boldsymbol{x}^{(n)}, \boldsymbol{x}^{(n-1)})$ is reduced to a simple formula: $\alpha(\boldsymbol{x}^{(n)}, \boldsymbol{x}^{(n-1)}) = \min\{1, \pi(\boldsymbol{x}^{(n-1)})/\pi(\boldsymbol{x}^{(n)})\}$. We preserve the data point of $x^{(n)}$ for the case of $u \leq \alpha(\boldsymbol{x}^{(n)}, \boldsymbol{x}^{(n-1)})$, and the next predicted value is $x_i^{(n+1)} = x_i^{(n)} + dx_i$.

Note that we set the norm of $\boldsymbol{dx}$ as a constant value in N-dimensional parameter space and $\boldsymbol{dx}$ is redefined when $\boldsymbol{x}^{(n+1)} \neq \boldsymbol{x}^{(n)}$. Moreover, the step length $\epsilon_i^{(n)} dx_i^{(n)}$ are weighted by normal distribution function.

We set 100 bins from the minimum to the maximum value for each x_i, and we performed the MCMC calculation till $\pi(\boldsymbol{x})$ are converged.

3.2 Type Ia Supernovae and Gamma Ray Bursts Constraint on Dark Energy Models

3.2.1 Best fit parameters

As the first evaluation, we search for the best fit parameters for each model. We show the best fit parameters and χ^2 values for each model in TABLE 3.1. Particularly, in vEoS model, we have found that the parameter β takes the range as $\beta > 20$, and ω prefers less than -1 and γ prefers greater than -1. This indicates that the feature of DE should be changed drastically. Both H_0 and $\Omega_{\mathrm{m},0}$ seem to be consistent with the *Planck* 2015 results. Furthermore, the energy density of DE is only slightly affected from these

parameters of the early stage in the universe. Since DE cannot become the candidate to solve the cosmological constant problem, the value of the (effective) EoS may be increased by some unknown mechanisms in the earlier epoch.

Table 3.1: Best fit parameters for three models and corresponding χ^2 values.

Parameter	vEoS	cEoS	C.C.
ω	-1.02	-1.03	-1
γ	-0.873	-1.03	-1
β	> 20	–	–
H_0	70.1	69.9	69.8
$\Omega_{\mathrm{m},0}$	0.2801	0.2993	0.2897
w_0	-1.02	-1.03	-1
w_a	-1.73×10^{-6}	0	0
$\chi^2_{\mathrm{min}}(\Delta\chi^2)$	726.9	728.9(+2.0)	729.4(+2.5)
Number of free parameters	5	3	2

β is the arbitrary value and $\omega = \gamma$ for the models of cEoS and C.C.

3.2.2 Markov Chain Monte Carlo method and constraints on dark energy models

For the next step, we apply MCMC method to obtain a reliable reagion for each parameter as shown in Fig. 3.2. This result indicates that DE should change the property from quintessence-like to phantom-like field at $z \sim 0.3$ (see Fig. 3.3). From the result that $w_a \sim 0$ and β is very large, it would be more important to search the turning point ($z \sim 0.3$) than to evaluate the slope of EoS at present. In fact, some models whose (effective) EoS gives the similar condition are constructed in terms of the modified gravitational theory (e.g., [48, 90, 91]).

Let us discuss the convergency of the MCMC method. Since the acceptance rate is affected by not only the proposal distributions $q(\boldsymbol{x}|\boldsymbol{x}^{(n-1)})$ but also dispersion parameters (or step lengths), dispersion parameters for each Gaussian should be estimated in burn-in period. Theoretically, it is known that an ideal acceptance rate of the random walk algorithm in N-dimensions is about 23.4% [92]. However, our method does not need the evaluation of dispersions but we have to determine only $|\boldsymbol{dx}^{(0)}|$, and step lengths are redefined automatically depending on the previous accepted step of $\epsilon_i dx_i$. In the present

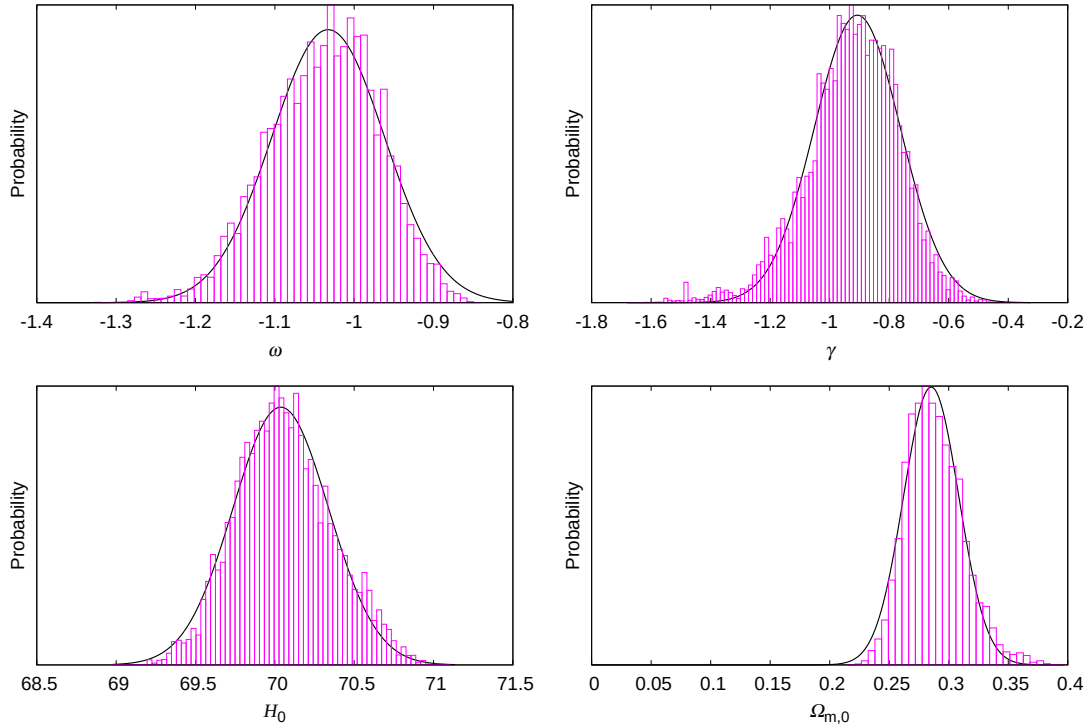

Fig. 3.2: Posterior distributions for ω, γ, H_0 and $\Omega_{m,0}$. The boxes and lines show data points and the plausible functions as Gaussian, respectively. These constraints come from the type Ia supernovae and GRBs observations.

study acceptance rate was $\sim 25\%$. Therefore, our method with the parameter settings has operated rather well.

We have investigated the properties of DE by analysing the observational data sets of type Ia supernovae and GRBs as shown in Fig. 3.4, where we note that the difference due to parameters given in Table 3.1 is very small even for $z \sim 10$.

In order to compare models in Table 3.1 with the standard model (C.C.), we adopt Akaike information criteria (AIC) [93]. AIC is applied to the models with a different number of free parameters. We will define AIC such as $\mathrm{AIC} = \chi^2_{\mathrm{min}} + 2n$, where n is the number of free parameters. Here, we define the difference between C.C. and the other model i as $\Delta(\mathrm{AIC})_i = (\mathrm{AIC})_i - (\mathrm{AIC})_{\mathrm{C.C.}}$. The negative value of $\Delta(\mathrm{AIC})_i$ proves the priority of the model i compared to the C.C. In previous studies, type Ia supernovae data indicate that w_{de} may cross the -1 barrier. However, we find that $\Delta(\mathrm{AIC})_{\mathrm{vEoS}} = 3.5$ and $\Delta(\mathrm{AIC})_{\mathrm{cEoS}} = 1.5$, and therefore we cannot have clear evidence (see Table 7 and 8) for

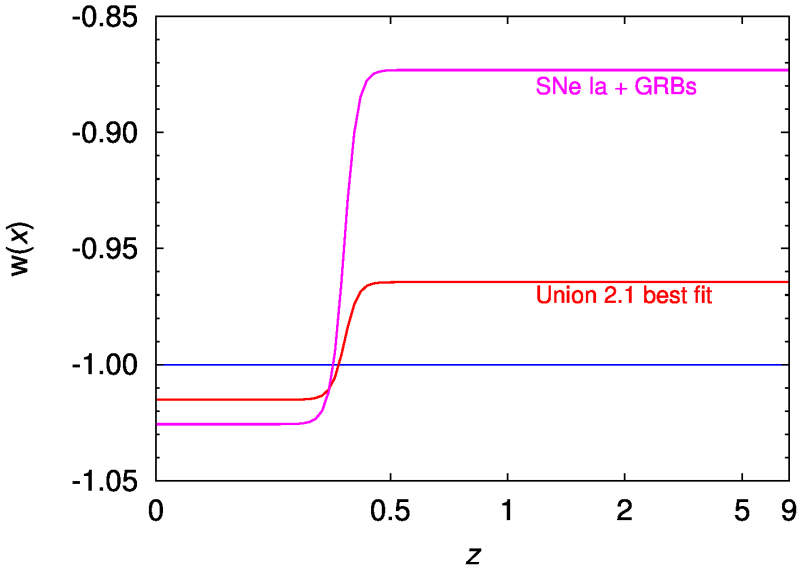

Fig. 3.3: EoS of DE as a function of time. Holizontal line (blue) shows cosmological constant and curved line (purple) shows variable EoS with best fit parameters. We find that DE changes its property from quintessence-like in the early time to phantom-like field in the present epoch at $z \sim 0.3$ or equivalently $a \sim 0.75$.

the time dependency of DE.

Fig. 3.5 shows the probability distribution on the plane of (ω, γ). We define 68% C.L. and 95% C.L. such as $\Delta\chi^2 = 2.30$ and $\Delta\chi^2 = 6.18$, respectively. The area on a plane of γ against ω is divided into four square regions. Q and P denote quintessence-like and phantom-like models. The crossing whose DE evolves from Q to P is indicated by Q$\rightarrow$P. P$\rightarrow$Q shows that the crossing proceeds oppositely. If the parameter set (ω, γ) exists in the upper right region, DE always behaves quintessence. The lower left region belongs to phantom. The percentages denote the integrated probability in each separated (squared) region. This indicates that the model whose DE evolves from $w_{\rm de} < -1$ to $w_{\rm de} > -1$ (P$\rightarrow$Q) is excluded in 2.4 σ confidence level.

On the other hand, we can conclude that the transition from $w_{\rm de} > -1$ to $w_{\rm de} < -1$ would occur rapidly around $z \sim 0.3$ if the crossing exists (see Fig. 3.3). Some crossing models have been already constructed (e.g., [48,90,91]), and the EoS changes from $w_{\rm de} > -1$ to $w_{\rm de} < -1$ moderately in these models. Our results may indicate that the alternation would occur more instantly, because β should be taken a large value.

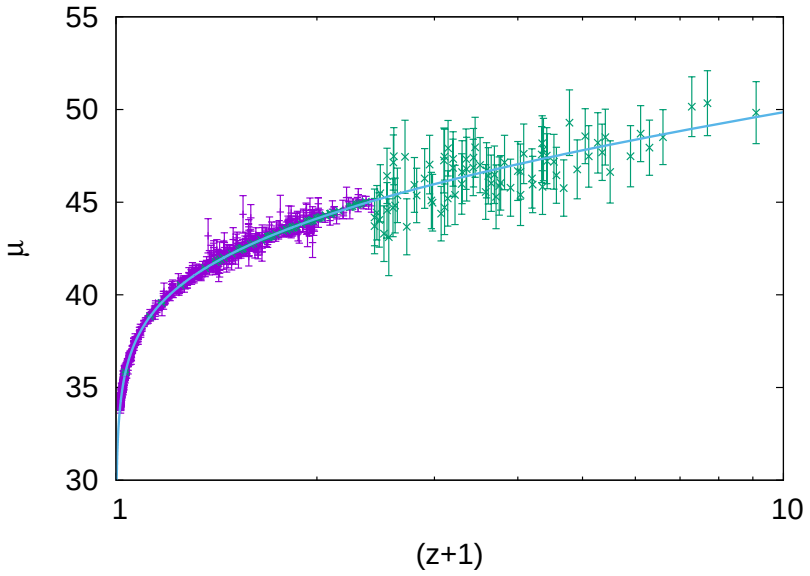

Fig. 3.4: Magnitude-redshift relation for the vEoS model. The observational data are given with error bars; purple: type Ia supernovae [40, 88], green: GRBs [89].

Finally, we obtain the following results with 68% C.L. : $\omega = -1.03 \pm 0.11$, $\gamma = -0.91 \pm 0.14$, $H_0 = 70.0 \pm 0.3$ and $\Omega_{m,0} = 0.285 \pm 0.023$.

3.3 Concluding Remarks

The value of H_0, Ω_m, Ω_Λ, and $w_{\rm de}(a)$ are consistent with the Planck 2015 results (XIII) of the ΛCDM model [31](TT,TE,EE+lowP+lensing). On the contrary, for the Planck result (XIV, Fig. 5) [94] assuming EoS to be represented a first-order of Taylor expansion of $w(z)$, EoS evolves from $w_{\rm de} < -1$ to $w_{\rm de} > -1$. The redshift dependency of the EoS is completely opposite direction compared with our result.

Other investigations [38, 40] indicate that EoS evolves from $w_{\rm de} > -1$ to $w_{\rm de} < -1$, which are the same tendency compared with our result. Hannestad et al. [38] adopt CMBFAST package. They insist that it is hard to constrain more than two parameters from 157 "gold" samples of type Ia supernova data only. Therefore, they utilize SN Ia + LSS (SDSS and 2 degree Field Galaxy Survey; 2dFGRS) + CMB (WMAP) data. However, latest 695 SN Ia data [40, 88] can constrain five parameters, and gives sumaller value ($\chi^2_{\rm min}$/d.o.f. = 0.97) than that by Hannestad et al. ($\chi^2_{\rm min}$/d.o.f. = 1.10; SNI-a best

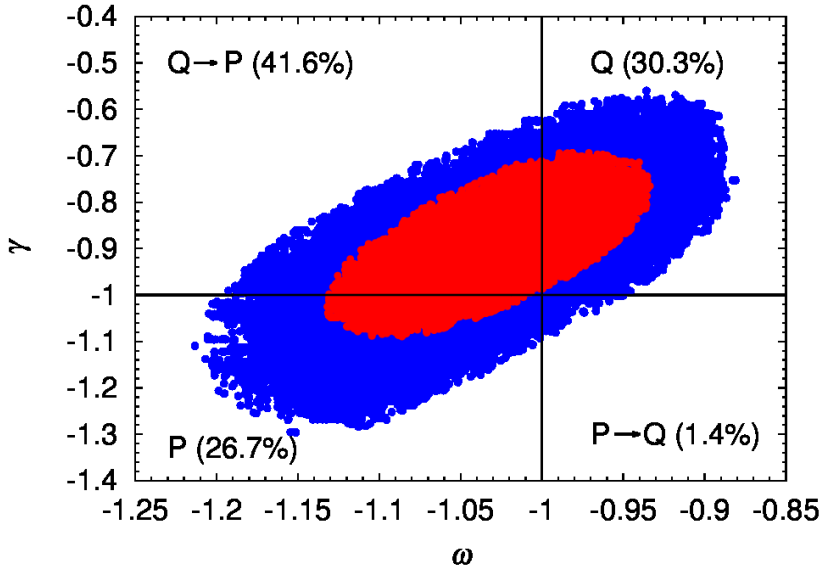

Fig. 3.5: Constraints obtained from probability distribution on ω and γ; 68% C.L. and 95% C.L. correspond to red and blue regions, respectively. The area on a plane of γ against ω is divided into four square regions. Q and P denote quintessence-like and phantom-like models. The crossing whose DE evolves from Q to P is indicated by Q→P. P→Q shows that the crossing proceeds oppositely.

fit model in Table 2 [38]). Combining 695 type Ia supernovae and 138 gamma ray bursts data analysis result in a smaller value χ^2/d.o.f. = 0.87. In conclusion, we succeed in constraining five parameters with no presumption of parameter range.

Our results of w_a in (3.12) are consistent with those obtained from Union 2.1 (see Tables 7 and 8 in [40]) whose data is limitted to type Ia supernovae. Our studies with use of only SNIa data [40] give $w_{\rm de} \simeq -1.02$ for $z < 0.3$ and $w_{\rm de} \simeq -0.97$ for $z \sim 0.5$ with $\Omega_m = 0.277$. Using the values w_0 and w_a given in [40] (w_zCDM and SNe+CMB in Table 7), the EoS value is around $w \sim -0.96$ at $z = 0.5$ with $\Omega_m = 0.273$ [40].

In the present work, an equality epoch concerning matter and dark energy is changed by $\delta z \sim +1.5$ compared to the case of C.C. due to inclusion of type Ia supernovae and gamma ray bursts observations, which affects the formation of the first object.

4 Summary and Discussions

In addition to the nuclear reaction rate (DE04) determined by Descouvemont *et al.* (2004), which is the nuclear reaction rate conventionally encouraged by BBN in the standard model, we applied the latest NACRE-II (2013) to the BBN. We adopted the latest estimated value of 880.1 ± 1.1 s and also the previous one of 885.7 s for the lifetime of the neutron. Furthermore, we used the Monte Carlo method to include the ambiguity caused by these nuclear reaction rate errors.

Compared with DE04, NACRE-II which includes the latest nuclear reaction rates have a small experimental errors. Regarding the production amount of D, the results using NACRE-II were found to be more consistent those with DE04 for η deduced from the observations by *Planck* 2013.

As a result of computations using the latest value 880.1 ± 1.1 s as the neutron lifetime for the standard BBN, the effect on η_{10} due to the difference in nuclear reaction rates [54,57] was $\delta\eta_{10} \sim 0.07$, and we cannot find any change in BBN. Also, taking into account the uncertainty of the nuclear reaction rates, the value of η cannot be determined from the value of ^{4}He.

In order to examine the consistency with Izotov *et al.* (^{4}He observation), we adopted Lepton asymmetry as non-standard BBN. For nuclear reaction rates we adopted NACRE-II [57] whose restriction on η_{10} obtained from D is close to that obtained from *Planck* 2013.

Lepton asymmetry is introduced by giving the neutrino a chemical potential. The two effects of the chemical potential are; one affects the expansion coefficient, the other is the temperature in the early universe which exceeds 10^{10} K. This causes the effect on the n/p ratio. Especially, the influence of the latter is large, which greatly influence the composition ratio of ^{4}He. As a result, we have obtained the parameters: $-3.4 \times 10^{-2} < \xi_e < -1.8 \times 10^{-2}$ and $6.17 < \eta_{10} < 6.38$ (1σ C.L.). This is also consistent with the result obtained by CMB observations $5.85 < \eta_{10} < 6.21$ (2σ C.L.) [56].

We considered Lepton asymmetry as non-standard BBN, but there are other models using unknown particles assumption and modified gravitational field theory. Even if observation shows that the lepton asymmetry is not so large, it may be possible to incorporate the same effect by modification of gravity field theory or assumption of unknown

particles. In order to solve the deviation from the standard model, it is necessary to study modified gravity field theory, new particle model, non-uniformity of the cosmic baryonic matter distribution.

The value of H_0, Ω_m, Ω_Λ, and $w_{\rm de}(a)$ are consistent with the Planck 2015 results (XIII) of the ΛCDM model [31](TT,TE,EE+lowP+lensing). On the contrary, for the Planck result (XIV, Fig. 5) [94] assuming EoS to be represented a first-order of Taylor expansion of $w(z)$, EoS evolves from $w_{\rm de} < -1$ to $w_{\rm de} > -1$. The redshift dependency of the EoS is completely opposite direction compared with our result.

Other investigations [38, 40] indicate that EoS evolves from $w_{\rm de} > -1$ to $w_{\rm de} < -1$, which are the same tendency compared with our result. Hannestad et al. [38] adopt CMBFAST package. They insist that it is hard to constrain more than two parameters from 157 "gold" samples of type Ia supernova data only. Therefore, they utilize SN Ia + LSS (SDSS and 2 degree Field Galaxy Survey; 2dFGRS) + CMB (WMAP) data. However, latest 695 SN Ia data [40, 88] can constrain five parameters, and gives sumaller value ($\chi^2_{\rm min}$/d.o.f. = 0.97) than that by Hannestad et al. ($\chi^2_{\rm min}$/d.o.f. = 1.10; SNI-a best fit model in Table 2 [38]). Combining 695 type Ia supernovae and 138 gamma ray bursts data analysis result in a smaller value χ^2/d.o.f. = 0.87. In conclusion, we succeed in constraining five parameters with no presumption of parameter range.

Our results of w_a in (3.12) are consistent with those obtained from Union 2.1 (see Tables 7 and 8 in [40]) whose data is limitted to type Ia supernovae. Our studies with use of only SNIa data [40] give $w_{\rm de} \simeq -1.02$ for $z < 0.3$ and $w_{\rm de} \simeq -0.97$ for $z \sim 0.5$ with $\Omega_m = 0.277$. Using the values w_0 and w_a given in [40] (w_zCDM and SNe+CMB in Table 7), the EoS value is around $w \sim -0.96$ at $z = 0.5$ with $\Omega_m = 0.273$ [40].

In the present work, an equality epoch concerning matter and dark energy is changed by $\delta z \sim +1.5$ compared to the case of C.C. due to inclusion of type Ia supernovae and gamma ray bursts observations, which affects the formation of the first object.

A Reaction Rates Adopted in BBN Calculations

Table A.1: Adopted reaction rates in our code.

	Reaction	Ref.		Reaction	Ref.
1	n $\longleftrightarrow$ p	(1.24)-(1.29)	26	^{3}He (t,d)^{4}He	SMITH10
2	n (p,γ)D	An06	27	^{6}Li (n,α)T	CF88
3	D (p,γ)^{3}He	NACRE-II	28	^{7}Be (n,α)^{4}He	WAG
4	T (α,γ)^{7}Li	NACRE-II	29	^{6}Li (p,α)^{3}He	PT05
5	D (d,γ)^{4}He	SMITH10	30	^{9}Be (p,α)^{6}Li	CF88
6	T (p,γ)^{4}He	SMITH10	31	^{10}Be (p,α)^{7}Li	WAG
7	^{6}Li (p,γ)^{7}Be	NACRE	32	^{8}Li (α,p)^{11}Be	WAG
8	D (α,γ)^{6}Li	NACRE	33	^{3}He (t,α)D	CF88
9	D (n,γ)T	NK06	34	^{4}He (d,t)^{3}He	CF88
10	^{3}He (n,γ)^{4}He	KA02	35	^{7}Li (p,d)^{6}Li	MAFO
11	^{6}Li (n,γ)^{7}Li	JZ10	36	^{7}Li (d,p) ^{8}Li	MAFO
12	^{7}Li (n,γ)^{8}Li	KA02	37	^{7}Li (t,n)^{9}Be	BK91
13	^{8}Li (n,γ)^{9}Li	WIES	38	^{7}Li (t,d)^{8}Li	HI09
14	^{9}Be (n,γ)^{10}Be	WAG	39	^{8}Li (p,d)^{7}Li	MAFO
15	^{10}Be (n,γ)^{11}Be	WIES	40	^{8}Li (d,n)^{9}Be	MAFO
16	T (p,γ)^{4}He	CF88	41	^{7}Be (n,d)^{6}Li	MAFO
17	^{4}He (d,γ)^{6}Li	MB11	42	^{9}Be (n,t)^{7}Li	BK91
18	^{3}He (d,p) ^{4}He	NACRE-II	43	^{9}Li $\longrightarrow$ 2^{4}He + n	WC12
19	D (d,n)^{3}He	NACRE-II	44	^{6}Li $\longrightarrow$ ^{4}He + p + n	CF88
20	D (d,p) T	NACRE-II	45	^{9}Be $\longrightarrow$ 2^{4}He + n	WC12
21	T (d,n)^{4}He	NACRE-II	46	T $\longleftrightarrow$ ^{3}He	EC
22	^{7}Li (p,α)^{4}He	NACRE-II	47	^{9}Li $\rightarrow$ ^{9}Be	WC12
23	^{3}He(α,γ)^{7}Be	NACRE-II	48	^{7}Be $\rightarrow$ ^{7}Li	EC
24	T (p,n)^{3}He	DE04			
25	^{7}Li (p,n)^{7}Be	DE04			

An06 [95], NACRE-II [57], SMITH10 [96], NACRE [97], NK06 [98], KA02 [99], JZ10 [100], WAG [101], CF88 [102], MB11 [103], DE04 [54], PT05 [104], MAFO [105], BK91 [106] HI09 [107], WC12 [108].

Table A.2: Adopted reaction rates in Hashimoto and Arai code.

	Reaction	Ref.		Reaction	Ref.		Reaction	Ref.
1	D(p,γ)^{3}He	DE04*	31	^{10}B(p,α)^{7}Be	CF88	61	^{7}Li(d,n)^{4}He^{4}He	CF88
2	D(d,γ)^{4}He	SMITH10	32	^{10}B(α,n)^{13}N	CF88	62	^{7}Be(d,p)^{4}He^{4}He	CF88
3	D(d,n)^{3}He	DE04*	33	^{11}B(p,γ)^{12}C	CF88	63	^{9}Be(p,d)^{4}He^{4}He	CF88
4	D(d,p)T	DE04*	34	^{11}B(p,n)^{11}C	CF88	64	^{11}Be(p,α)^{4}He^{4}He	CF88
5	T(p,γ)^{4}He	SMITH10	35	^{11}B(α,n)^{14}N	CF88	65	^{7}Li(t,nn)^{4}He^{4}He	CF88
6	T(p,n)^{3}He	DE04*	36	^{11}B(α,p)^{14}C	CF88	66	^{7}Li(^{3}He,np)^{4}He^{4}He	CF88
7	T(d,n)^{4}He	DE04*	37	^{12}C(p,γ)^{13}N	CF88	67	^{7}Be(t,np)^{4}He^{4}He	CF88
8	^{3}He(d,p)^{4}He	DE04*	38	^{12}C(α,γ)^{16}O	CF88	68	^{7}Be(^{3}He,pp)^{4}He^{4}He	CF88
9	^{3}He(t,d)^{4}He	SMITH10	39	^{12}C(α,n)^{15}O	CF88	69	^{4}He(np,γ)^{6}Li	CF88
10	^{4}He(d,γ)^{6}Li	SMITH10	40	^{13}C(p,γ)^{14}N	CF88	70	^{4}He(αn,γ)^{9}Be	CF88
11	^{4}He(t,γ)^{7}Li	DE04*	41	^{13}C(p,n)^{13}N	CF88	71	p(n,γ)D	An06
12	^{4}He(t,n)^{6}Li	SMITH10	42	^{13}C(α,n)^{16}O	CF88	72	D(n,γ)T	WAG
13	^{3}He(α,γ)^{7}Be	DE04*	43	^{14}C(p,γ)^{15}N	CF88	73	^{3}He(n,γ)^{4}He	WAG
14	^{4}He(α,γ)^{8}Be	SMITH10	44	^{14}C(p,n)^{14}N	CF88	74	^{6}Li(n,γ)^{7}Li	WAG
15	^{6}Li(p,γ)^{7}Be	SMITH10	45	^{14}C(α,γ)^{18}O	CF88	75	^{7}Li(n,γ)^{8}Li	WAG
16	^{6}Li(p,α)^{3}He	SMITH10	46	^{13}N(p,γ)^{14}O	CF88	76	^{10}B(n,γ)^{11}B	WAG
17	^{6}Li(α,γ)^{10}B	SMITH10	47	^{14}N(p,γ)^{15}O	CF88	77	^{6}Li(n,α)T	WAG
18	^{7}Li(p,n)^{7}Be	DE04*	48	^{14}O(p,n)^{14}O	CF88	78	^{7}Be(n,α)^{4}He	WAG
19	^{7}Li(p,γ)^{8}Be	SMITH10	49	^{14}N(α,γ)^{18}F	CF88	79	n(e$^+$,ν)p	Wag73
20	^{7}Li(p,α)^{4}He	SMITH10	50	^{14}N(α,n)^{17}F	CF88	80	p(e,ν)n	Wag73
21	^{7}Li(α,γ)^{11}B	SMITH10	51	^{15}N(p,γ)^{16}O	CF88	81	p(p,e$^-$)D	Wag73
22	^{7}Li(α,n)^{10}B	SMITH10	52	^{15}N(p,n)^{15}O	CF88	82	^{3}He(p,e$^-$)^{4}He	Wag73
23	^{7}Be(p,γ)^{8}B	SMITH10	53	^{15}N(p,α)^{12}C	CF88	83	^{3}He(e$^-$,ν)T	Wag73
24	^{7}Be(α,γ)^{11}C	SMITH10	54	^{15}N(α,γ)^{19}F	CF88	84	^{7}Be(e$^-$,ν)^{7}Li	Wag73
25	^{8}Be(α,γ)^{12}C	CF88	55	^{15}N(α,n)^{18}F	CF88			
26	^{9}Be(p,γ)^{10}B	CF88	56	^{16}O(p,α)^{13}N	CF88			
27	^{9}Be(p,n)^{9}B	CF88	57	D(p,n)pp	CF88			
28	^{9}Be(p,α)^{6}Li	CF88	58	T(t,nn)^{4}He	CF88			
29	^{9}Be(α,n)^{12}C	CF88	59	^{3}He(t,np)^{4}He	CF88			
30	^{10}B(p,γ)^{11}C	CF88	60	^{3}He(^{3}He,pp)^{4}He	CF88			

Wag73 [109]. Note that DE04* is updated to NACRE-II.

The NACRE-II reaction rate tables for the main path in BBN

Table A.3: ^{3}He(α,γ)^{7}Be

T	Adopted	lower limit	upper limit				
0.005	5.14E-25	4.57E-25	5.62E-25	0.16	9.98E-04	8.93E-04	1.08E-03
0.006	3.79E-23	3.37E-23	4.14E-23	0.18	2.28E-03	2.04E-03	2.47E-03
0.007	1.17E-21	1.04E-21	1.28E-21	0.2	4.62E-03	4.14E-03	5.02E-03
0.008	1.99E-20	1.77E-20	2.17E-20	0.25	1.89E-02	1.70E-02	2.05E-02
0.009	2.17E-19	1.93E-19	2.37E-19	0.3	5.49E-02	4.93E-02	5.94E-02
0.01	1.70E-18	1.51E-18	1.86E-18	0.35	1.28E-01	1.15E-01	1.38E-01
0.011	1.03E-17	9.13E-18	1.12E-17	0.4	2.54E-01	2.29E-01	2.74E-01
0.012	5.03E-17	4.48E-17	5.50E-17	0.45	4.54E-01	4.09E-01	4.89E-01
0.013	2.09E-16	1.86E-16	2.28E-16	0.5	7.44E-01	6.72E-01	8.02E-01
0.014	7.51E-16	6.68E-16	8.20E-16	0.6	1.67E+00	1.51E+00	1.80E+00
0.015	2.40E-15	2.14E-15	2.63E-15	0.7	3.16E+00	2.86E+00	3.39E+00
0.016	6.96E-15	6.20E-15	7.60E-15	0.8	5.30E+00	4.79E+00	5.70E+00
0.018	4.56E-14	4.06E-14	4.98E-14	0.9	8.17E+00	7.38E+00	8.79E+00
0.02	2.30E-13	2.05E-13	2.51E-13	1.	1.18E+01	1.07E+01	1.27E+01
0.025	5.86E-12	5.21E-12	6.39E-12	1.25	2.44E+01	2.19E+01	2.64E+01
0.03	6.88E-11	6.12E-11	7.50E-11	1.5	4.19E+01	3.73E+01	4.57E+01
0.04	2.46E-09	2.19E-09	2.69E-09	1.75	6.40E+01	5.66E+01	7.02E+01
0.05	3.11E-08	2.77E-08	3.39E-08	2.	9.04E+01	7.93E+01	9.98E+01
0.06	2.14E-07	1.91E-07	2.33E-07	2.5	1.54E+02	1.34E+02	1.72E+02
0.07	9.92E-07	8.85E-07	1.08E-06	3.	2.32E+02	1.98E+02	2.61E+02
0.08	3.50E-06	3.13E-06	3.82E-06	3.5	3.21E+02	2.73E+02	3.64E+02
0.09	1.02E-05	9.06E-06	1.11E-05	4.	4.21E+02	3.56E+02	4.79E+02
0.1	2.53E-05	2.26E-05	2.76E-05	5.	6.53E+02	5.49E+02	7.44E+02
0.11	5.62E-05	5.02E-05	6.11E-05	6.	9.15E+02	7.71E+02	1.04E+03
0.12	1.14E-04	1.02E-04	1.24E-04	7.	1.19E+03	1.01E+03	1.36E+03
0.13	2.13E-04	1.90E-04	2.31E-04	8.	1.47E+03	1.26E+03	1.67E+03
0.14	3.75E-04	3.35E-04	4.07E-04	9.	1.74E+03	1.49E+03	1.96E+03
0.15	6.25E-04	5.59E-04	6.80E-04	10.	1.99E+03	1.71E+03	2.24E+03

Table A.4: ^{3}He(d,p)^{4}He

T	Adopted	lower limit	upper limit				
0.001	3.54E-19	3.21E-19	3.87E-19	0.16	5.03E+05	4.61E+05	5.51E+05
0.002	6.14E-13	5.58E-13	6.72E-13	0.18	8.07E+05	7.40E+05	8.84E+05
0.003	6.36E-10	5.78E-10	6.96E-10	0.2	1.22E+06	1.11E+06	1.33E+06
0.004	5.02E-08	4.56E-08	5.49E-08	0.25	2.77E+06	2.53E+06	3.04E+06
0.005	1.11E-06	1.01E-06	1.22E-06	0.3	5.19E+06	4.71E+06	5.69E+06
0.006	1.18E-05	1.07E-05	1.29E-05	0.35	8.51E+06	7.68E+06	9.34E+06
0.007	7.74E-05	7.04E-05	8.47E-05	0.4	1.27E+07	1.14E+07	1.39E+07
0.008	3.64E-04	3.31E-04	3.99E-04	0.45	1.76E+07	1.57E+07	1.93E+07
0.009	1.35E-03	1.23E-03	1.48E-03	0.5	2.31E+07	2.06E+07	2.54E+07
0.01	4.15E-03	3.78E-03	4.54E-03	0.6	3.53E+07	3.13E+07	3.89E+07
0.011	1.11E-02	1.01E-02	1.21E-02	0.7	4.83E+07	4.26E+07	5.33E+07
0.012	2.64E-02	2.40E-02	2.89E-02	0.8	6.12E+07	5.37E+07	6.77E+07
0.013	5.74E-02	5.22E-02	6.29E-02	0.9	7.35E+07	6.42E+07	8.15E+07
0.014	1.16E-01	1.05E-01	1.26E-01	1.	8.49E+07	7.39E+07	9.43E+07
0.015	2.18E-01	1.98E-01	2.39E-01	1.25	1.09E+08	9.40E+07	1.21E+08
0.016	3.89E-01	3.54E-01	4.26E-01	1.5	1.27E+08	1.08E+08	1.42E+08
0.018	1.08E+00	9.87E-01	1.19E+00	1.75	1.39E+08	1.18E+08	1.56E+08
0.02	2.62E+00	2.38E+00	2.87E+00	2.	1.48E+08	1.25E+08	1.67E+08
0.025	1.52E+01	1.39E+01	1.67E+01	2.5	1.57E+08	1.31E+08	1.78E+08
0.03	5.82E+01	5.30E+01	6.37E+01	3.	1.61E+08	1.33E+08	1.83E+08
0.04	4.07E+02	3.71E+02	4.46E+02	3.5	1.61E+08	1.32E+08	1.83E+08
0.05	1.62E+03	1.48E+03	1.77E+03	4.	1.59E+08	1.30E+08	1.82E+08
0.06	4.63E+03	4.23E+03	5.07E+03	5.	1.53E+08	1.24E+08	1.76E+08
0.07	1.07E+04	9.80E+03	1.17E+04	6.	1.46E+08	1.18E+08	1.68E+08
0.08	2.14E+04	1.96E+04	2.35E+04	7.	1.38E+08	1.11E+08	1.59E+08
0.09	3.85E+04	3.52E+04	4.22E+04	8.	1.31E+08	1.05E+08	1.51E+08
0.1	6.38E+04	5.85E+04	6.99E+04	9.	1.24E+08	9.85E+07	1.42E+08
0.11	9.94E+04	9.11E+04	1.09E+05	10.	1.17E+08	9.27E+07	1.34E+08
0.12	1.47E+05	1.35E+05	1.61E+05				
0.13	2.09E+05	1.92E+05	2.29E+05				
0.14	2.88E+05	2.64E+05	3.15E+05				
0.15	3.85E+05	3.53E+05	4.22E+05				

Table A.5: ^{7}Li(p,α)^{4}He

T	Adopted	lower limit	upper limit				
0.001	9.17E-27	7.79E-27	1.12E-26	0.16	4.92E+02	4.42E+02	5.42E+02
0.002	2.38E-19	2.02E-19	2.90E-19	0.18	8.42E+02	7.60E+02	9.25E+02
0.003	9.06E-16	7.71E-16	1.10E-15	0.2	1.34E+03	1.21E+03	1.46E+03
0.004	1.61E-13	1.37E-13	1.96E-13	0.25	3.35E+03	3.05E+03	3.66E+03
0.005	6.41E-12	5.45E-12	7.78E-12	0.3	6.73E+03	6.14E+03	7.31E+03
0.006	1.06E-10	9.02E-11	1.29E-10	0.35	1.17E+04	1.07E+04	1.27E+04
0.007	9.93E-10	8.46E-10	1.20E-09	0.4	1.84E+04	1.68E+04	1.99E+04
0.008	6.28E-09	5.36E-09	7.61E-09	0.45	2.68E+04	2.46E+04	2.91E+04
0.009	2.98E-08	2.55E-08	3.61E-08	0.5	3.71E+04	3.40E+04	4.02E+04
0.01	1.14E-07	9.74E-08	1.38E-07	0.6	6.31E+04	5.78E+04	6.83E+04
0.011	3.68E-07	3.15E-07	4.45E-07	0.7	9.58E+04	8.79E+04	1.04E+05
0.012	1.04E-06	8.89E-07	1.25E-06	0.8	1.35E+05	1.24E+05	1.46E+05
0.013	2.62E-06	2.25E-06	3.16E-06	0.9	1.79E+05	1.65E+05	1.94E+05
0.014	6.04E-06	5.18E-06	7.27E-06	1.	2.29E+05	2.10E+05	2.48E+05
0.015	1.29E-05	1.11E-05	1.55E-05	1.25	3.72E+05	3.41E+05	4.03E+05
0.016	2.58E-05	2.22E-05	3.10E-05	1.5	5.39E+05	4.93E+05	5.84E+05
0.018	8.80E-05	7.56E-05	1.05E-04	1.75	7.25E+05	6.63E+05	7.88E+05
0.02	2.53E-04	2.17E-04	3.01E-04	2.	9.31E+05	8.49E+05	1.01E+06
0.025	2.09E-03	1.80E-03	2.47E-03	2.5	1.40E+06	1.28E+06	1.53E+06
0.03	1.04E-02	8.98E-03	1.23E-02	3.	1.98E+06	1.79E+06	2.17E+06
0.04	1.08E-01	9.30E-02	1.26E-01	3.5	2.68E+06	2.42E+06	2.94E+06
0.05	5.63E-01	4.88E-01	6.52E-01	4.	3.51E+06	3.16E+06	3.85E+06
0.06	1.98E+00	1.72E+00	2.28E+00	5.	5.52E+06	4.97E+06	6.08E+06
0.07	5.40E+00	4.71E+00	6.17E+00	6.	7.86E+06	7.08E+06	8.65E+06
0.08	1.23E+01	1.08E+01	1.40E+01	7.	1.03E+07	9.29E+06	1.13E+07
0.09	2.47E+01	2.16E+01	2.78E+01	8.	1.27E+07	1.14E+07	1.40E+07
0.1	4.48E+01	3.94E+01	5.03E+01	9.	1.49E+07	1.35E+07	1.64E+07
0.11	7.53E+01	6.66E+01	8.42E+01	10.	1.70E+07	1.53E+07	1.86E+07
0.12	1.19E+02	1.06E+02	1.33E+02				
0.13	1.79E+02	1.60E+02	1.99E+02				
0.14	2.60E+02	2.32E+02	2.87E+02				
0.15	3.62E+02	3.25E+02	4.00E+02				

Table A.6: D(d,n)^{3}He

T	Adopted	lower limit	upper limit				
0.001	1.43E-08	1.28E-08	1.58E-08	0.16	7.32E+05	6.70E+05	7.89E+05
0.002	5.95E-05	5.31E-05	6.57E-05	0.18	9.36E+05	8.59E+05	1.01E+06
0.003	3.23E-03	2.89E-03	3.57E-03	0.2	1.16E+06	1.06E+06	1.24E+06
0.004	3.95E-02	3.53E-02	4.36E-02	0.25	1.77E+06	1.64E+06	1.90E+06
0.005	2.34E-01	2.09E-01	2.58E-01	0.3	2.46E+06	2.28E+06	2.63E+06
0.006	9.01E-01	8.05E-01	9.95E-01	0.35	3.20E+06	2.97E+06	3.41E+06
0.007	2.64E+00	2.36E+00	2.91E+00	0.4	3.98E+06	3.70E+06	4.23E+06
0.008	6.38E+00	5.70E+00	7.04E+00	0.45	4.78E+06	4.46E+06	5.08E+06
0.009	1.34E+01	1.20E+01	1.48E+01	0.5	5.59E+06	5.23E+06	5.93E+06
0.01	2.54E+01	2.27E+01	2.80E+01	0.6	7.25E+06	6.80E+06	7.67E+06
0.011	4.44E+01	3.97E+01	4.89E+01	0.7	8.90E+06	8.38E+06	9.40E+06
0.012	7.25E+01	6.49E+01	7.99E+01	0.8	1.05E+07	9.95E+06	1.11E+07
0.013	1.12E+02	1.01E+02	1.24E+02	0.9	1.22E+07	1.15E+07	1.28E+07
0.014	1.67E+02	1.49E+02	1.84E+02	1.	1.37E+07	1.30E+07	1.45E+07
0.015	2.39E+02	2.14E+02	2.63E+02	1.25	1.76E+07	1.66E+07	1.85E+07
0.016	3.31E+02	2.96E+02	3.64E+02	1.5	2.12E+07	2.01E+07	2.23E+07
0.018	5.88E+02	5.27E+02	6.48E+02	1.75	2.46E+07	2.34E+07	2.59E+07
0.02	9.64E+02	8.64E+02	1.06E+03	2.	2.79E+07	2.65E+07	2.93E+07
0.025	2.58E+03	2.31E+03	2.84E+03	2.5	3.39E+07	3.23E+07	3.55E+07
0.03	5.44E+03	4.88E+03	5.97E+03	3.	3.93E+07	3.76E+07	4.10E+07
0.04	1.60E+04	1.44E+04	1.75E+04	3.5	4.43E+07	4.25E+07	4.60E+07
0.05	3.40E+04	3.07E+04	3.73E+04	4.	4.87E+07	4.70E+07	5.05E+07
0.06	6.04E+04	5.45E+04	6.60E+04	5.	5.65E+07	5.48E+07	5.81E+07
0.07	9.52E+04	8.61E+04	1.04E+05	6.	6.26E+07	6.10E+07	6.42E+07
0.08	1.38E+05	1.25E+05	1.51E+05	7.	6.73E+07	6.58E+07	6.88E+07
0.09	1.89E+05	1.72E+05	2.06E+05	8.	7.27E+07	7.11E+07	7.44E+07
0.1	2.48E+05	2.25E+05	2.69E+05	9.	7.72E+07	7.54E+07	7.89E+07
0.11	3.13E+05	2.85E+05	3.40E+05	10.	8.13E+07	8.03E+07	8.40E+07
0.12	3.86E+05	3.51E+05	4.17E+05				
0.13	4.64E+05	4.23E+05	5.02E+05				
0.14	5.48E+05	5.01E+05	5.92E+05				
0.15	6.38E+05	5.83E+05	6.88E+05				

Table A.7: D(d,p)T

T	Adopted	lower limit	upper limit				
0.001	1.45E-08	1.33E-08	1.57E-08	0.16	7.42E+05	7.02E+05	7.87E+05
0.002	6.02E-05	5.52E-05	6.54E-05	0.18	9.44E+05	8.95E+05	1.00E+06
0.003	3.27E-03	3.00E-03	3.55E-03	0.2	1.16E+06	1.10E+06	1.23E+06
0.004	4.00E-02	3.67E-02	4.34E-02	0.25	1.75E+06	1.66E+06	1.84E+06
0.005	2.36E-01	2.17E-01	2.57E-01	0.3	2.38E+06	2.26E+06	2.51E+06
0.006	9.12E-01	8.38E-01	9.89E-01	0.35	3.04E+06	2.89E+06	3.20E+06
0.007	2.67E+00	2.45E+00	2.90E+00	0.4	3.72E+06	3.54E+06	3.91E+06
0.008	6.46E+00	5.94E+00	7.00E+00	0.45	4.41E+06	4.20E+06	4.63E+06
0.009	1.36E+01	1.25E+01	1.47E+01	0.5	5.11E+06	4.87E+06	5.36E+06
0.01	2.57E+01	2.37E+01	2.79E+01	0.6	6.52E+06	6.23E+06	6.82E+06
0.011	4.49E+01	4.13E+01	4.87E+01	0.7	7.93E+06	7.61E+06	8.27E+06
0.012	7.34E+01	6.76E+01	7.96E+01	0.8	9.34E+06	8.99E+06	9.71E+06
0.013	1.14E+02	1.05E+02	1.23E+02	0.9	1.07E+07	1.04E+07	1.11E+07
0.014	1.69E+02	1.56E+02	1.83E+02	1.	1.21E+07	1.17E+07	1.25E+07
0.015	2.42E+02	2.23E+02	2.62E+02	1.25	1.54E+07	1.50E+07	1.59E+07
0.016	3.35E+02	3.09E+02	3.63E+02	1.5	1.86E+07	1.81E+07	1.90E+07
0.018	5.96E+02	5.49E+02	6.45E+02	1.75	2.15E+07	2.11E+07	2.19E+07
0.02	9.77E+02	9.01E+02	1.06E+03	2.	2.43E+07	2.38E+07	2.47E+07
0.025	2.62E+03	2.41E+03	2.83E+03	2.5	2.94E+07	2.89E+07	2.98E+07
0.03	5.51E+03	5.10E+03	5.95E+03	3.	3.40E+07	3.35E+07	3.44E+07
0.04	1.62E+04	1.50E+04	1.74E+04	3.5	3.82E+07	3.77E+07	3.86E+07
0.05	3.46E+04	3.21E+04	3.72E+04	4.	4.21E+07	4.17E+07	4.25E+07
0.06	6.14E+04	5.71E+04	6.59E+04	5.	4.91E+07	4.88E+07	4.95E+07
0.07	9.68E+04	9.02E+04	1.04E+05	6.	5.54E+07	5.51E+07	5.58E+07
0.08	1.41E+05	1.31E+05	1.50E+05	7.	6.10E+07	6.07E+07	6.14E+07
0.09	1.93E+05	1.80E+05	2.06E+05	8.	6.59E+07	6.55E+07	6.63E+07
0.1	2.52E+05	2.37E+05	2.69E+05	9.	7.00E+07	6.96E+07	7.03E+07
0.11	3.19E+05	3.00E+05	3.40E+05	10.	7.33E+07	7.29E+07	7.36E+07
0.12	3.92E+05	3.69E+05	4.17E+05				
0.13	4.72E+05	4.45E+05	5.02E+05				
0.14	5.57E+05	5.26E+05	5.91E+05				
0.15	6.47E+05	6.12E+05	6.87E+05				

Table A.8: D(p,γ)^{3}He

T	Adopted	lower limit	upper limit				
0.001	1.35E-11	1.09E-11	1.62E-11	0.16	1.52E+01	1.37E+01	1.67E+01
0.002	1.87E-08	1.51E-08	2.25E-08	0.18	1.93E+01	1.75E+01	2.12E+01
0.003	6.07E-07	4.93E-07	7.27E-07	0.2	2.37E+01	2.16E+01	2.60E+01
0.004	5.38E-06	4.38E-06	6.43E-06	0.25	3.62E+01	3.31E+01	3.94E+01
0.005	2.52E-05	2.06E-05	3.01E-05	0.3	5.01E+01	4.59E+01	5.44E+01
0.006	8.15E-05	6.67E-05	9.71E-05	0.35	6.52E+01	5.98E+01	7.08E+01
0.007	2.07E-04	1.70E-04	2.47E-04	0.4	8.13E+01	7.45E+01	8.84E+01
0.008	4.47E-04	3.68E-04	5.31E-04	0.45	9.84E+01	9.00E+01	1.07E+02
0.009	8.55E-04	7.04E-04	1.01E-03	0.5	1.16E+02	1.06E+02	1.27E+02
0.01	1.49E-03	1.23E-03	1.77E-03	0.6	1.54E+02	1.40E+02	1.69E+02
0.011	2.43E-03	2.01E-03	2.87E-03	0.7	1.95E+02	1.77E+02	2.14E+02
0.012	3.73E-03	3.09E-03	4.40E-03	0.8	2.38E+02	2.16E+02	2.61E+02
0.013	5.47E-03	4.54E-03	6.45E-03	0.9	2.84E+02	2.57E+02	3.12E+02
0.014	7.73E-03	6.42E-03	9.10E-03	1.	3.32E+02	2.99E+02	3.64E+02
0.015	1.06E-02	8.80E-03	1.24E-02	1.25	4.57E+02	4.12E+02	5.03E+02
0.016	1.41E-02	1.17E-02	1.65E-02	1.5	5.91E+02	5.31E+02	6.52E+02
0.018	2.33E-02	1.95E-02	2.74E-02	1.75	7.30E+02	6.54E+02	8.07E+02
0.02	3.60E-02	3.02E-02	4.22E-02	2.	8.73E+02	7.79E+02	9.68E+02
0.025	8.59E-02	7.25E-02	1.00E-01	2.5	1.17E+03	1.04E+03	1.30E+03
0.03	1.66E-01	1.41E-01	1.93E-01	3.	1.46E+03	1.30E+03	1.63E+03
0.04	4.35E-01	3.73E-01	5.01E-01	3.5	1.76E+03	1.56E+03	1.97E+03
0.05	8.62E-01	7.44E-01	9.86E-01	4.	2.07E+03	1.84E+03	2.30E+03
0.06	1.45E+00	1.26E+00	1.65E+00	5.	2.67E+03	2.39E+03	2.95E+03
0.07	2.20E+00	1.93E+00	2.50E+00	6.	3.27E+03	2.95E+03	3.60E+03
0.08	3.11E+00	2.74E+00	3.51E+00	7.	3.86E+03	3.50E+03	4.23E+03
0.09	4.17E+00	3.69E+00	4.69E+00	8.	4.45E+03	4.05E+03	4.86E+03
0.1	5.37E+00	4.77E+00	6.02E+00	9.	5.02E+03	4.58E+03	5.48E+03
0.11	6.71E+00	5.98E+00	7.49E+00	10.	5.59E+03	5.10E+03	6.08E+03
0.12	8.18E+00	7.31E+00	9.10E+00				
0.13	9.77E+00	8.76E+00	1.08E+01				
0.14	1.15E+01	1.03E+01	1.27E+01				
0.15	1.33E+01	1.20E+01	1.47E+01				

Table A.9: T(α,γ)^{7}Li

T	Adopted	lower limit	upper limit				
0.002	7.06E-21	6.52E-21	7.88E-21	0.16	8.76E-01	8.15E-01	9.73E-01
0.003	1.79E-17	1.65E-17	2.00E-17	0.18	1.43E+00	1.33E+00	1.58E+00
0.004	2.48E-15	2.29E-15	2.77E-15	0.2	2.16E+00	2.01E+00	2.40E+00
0.005	8.21E-14	7.59E-14	9.17E-14	0.25	4.93E+00	4.60E+00	5.46E+00
0.006	1.18E-12	1.09E-12	1.32E-12	0.3	9.14E+00	8.54E+00	1.01E+01
0.007	9.87E-12	9.12E-12	1.10E-11	0.35	1.49E+01	1.39E+01	1.65E+01
0.008	5.68E-11	5.25E-11	6.34E-11	0.4	2.21E+01	2.06E+01	2.44E+01
0.009	2.49E-10	2.30E-10	2.77E-10	0.45	3.07E+01	2.86E+01	3.40E+01
0.01	8.85E-10	8.18E-10	9.88E-10	0.5	4.06E+01	3.79E+01	4.51E+01
0.011	2.68E-09	2.48E-09	2.99E-09	0.6	6.39E+01	5.93E+01	7.13E+01
0.012	7.15E-09	6.61E-09	7.98E-09	0.7	9.12E+01	8.41E+01	1.02E+02
0.013	1.72E-08	1.59E-08	1.92E-08	0.8	1.22E+02	1.11E+02	1.37E+02
0.014	3.78E-08	3.49E-08	4.22E-08	0.9	1.55E+02	1.41E+02	1.75E+02
0.015	7.73E-08	7.15E-08	8.62E-08	1.	1.90E+02	1.72E+02	2.16E+02
0.016	1.49E-07	1.37E-07	1.66E-07	1.25	2.85E+02	2.54E+02	3.26E+02
0.018	4.72E-07	4.36E-07	5.26E-07	1.5	3.87E+02	3.42E+02	4.44E+02
0.02	1.27E-06	1.18E-06	1.42E-06	1.75	4.92E+02	4.32E+02	5.65E+02
0.025	9.25E-06	8.56E-06	1.03E-05	2.	5.99E+02	5.24E+02	6.86E+02
0.03	4.17E-05	3.86E-05	4.65E-05	2.5	8.15E+02	7.13E+02	9.28E+02
0.04	3.70E-04	3.42E-04	4.12E-04	3.	1.03E+03	9.04E+02	1.17E+03
0.05	1.73E-03	1.60E-03	1.92E-03	3.5	1.25E+03	1.11E+03	1.40E+03
0.06	5.55E-03	5.14E-03	6.18E-03	4.	1.46E+03	1.28E+03	1.62E+03
0.07	1.40E-02	1.30E-02	1.56E-02	5.	1.86E+03	1.63E+03	2.04E+03
0.08	3.00E-02	2.78E-02	3.34E-02	6.	2.27E+03	1.99E+03	2.42E+03
0.09	5.68E-02	5.27E-02	6.32E-02	7.	2.51E+03	2.19E+03	2.73E+03
0.1	9.83E-02	9.12E-02	1.09E-01	8.	2.74E+03	2.38E+03	2.96E+03
0.11	1.58E-01	1.47E-01	1.76E-01	9.	2.91E+03	2.51E+03	3.13E+03
0.12	2.41E-01	2.24E-01	2.68E-01	10.	3.02E+03	2.61E+03	3.25E+03
0.13	3.50E-01	3.26E-01	3.90E-01				
0.14	4.90E-01	4.56E-01	5.45E-01				
0.15	6.64E-01	6.18E-01	7.38E-01				

Table A.10: T(d,n)^{4}He

T	Adopted	lower limit	upper limit				
0.001	1.87E-07	1.67E-07	2.09E-07	0.18	1.73E+08	1.60E+08	1.85E+08
0.002	1.37E-03	1.22E-03	1.53E-03	0.2	2.06E+08	1.91E+08	2.21E+08
0.003	9.98E-02	8.90E-02	1.11E-01	0.25	2.83E+08	2.63E+08	3.04E+08
0.004	1.47E+00	1.31E+00	1.64E+00	0.3	3.47E+08	3.23E+08	3.72E+08
0.005	9.93E+00	8.86E+00	1.10E+01	0.35	3.98E+08	3.70E+08	4.25E+08
0.006	4.24E+01	3.78E+01	4.71E+01	0.4	4.36E+08	4.07E+08	4.66E+08
0.007	1.35E+02	1.20E+02	1.50E+02	0.45	4.65E+08	4.34E+08	4.96E+08
0.008	3.49E+02	3.12E+02	3.87E+02	0.5	4.85E+08	4.53E+08	5.17E+08
0.009	7.80E+02	7.01E+02	8.62E+02	0.6	5.10E+08	4.77E+08	5.42E+08
0.01	1.56E+03	1.41E+03	1.71E+03	0.7	5.19E+08	4.86E+08	5.51E+08
0.011	2.85E+03	2.59E+03	3.12E+03	0.8	5.19E+08	4.87E+08	5.50E+08
0.012	4.87E+03	4.44E+03	5.31E+03	0.9	5.13E+08	4.82E+08	5.44E+08
0.013	7.85E+03	7.19E+03	8.53E+03	1.	5.04E+08	4.74E+08	5.34E+08
0.014	1.21E+04	1.11E+04	1.31E+04	1.25	4.76E+08	4.48E+08	5.04E+08
0.015	1.79E+04	1.65E+04	1.93E+04	1.5	4.47E+08	4.21E+08	4.73E+08
0.016	2.56E+04	2.37E+04	2.75E+04	1.75	4.19E+08	3.95E+08	4.43E+08
0.018	4.81E+04	4.48E+04	5.16E+04	2.	3.94E+08	3.71E+08	4.17E+08
0.02	8.30E+04	7.74E+04	8.87E+04	2.5	3.52E+08	3.32E+08	3.72E+08
0.025	2.47E+05	2.32E+05	2.63E+05	3.	3.19E+08	3.00E+08	3.37E+08
0.03	5.70E+05	5.34E+05	6.06E+05	3.5	2.92E+08	2.75E+08	3.09E+08
0.04	1.93E+06	1.81E+06	2.06E+06	4.	2.70E+08	2.54E+08	2.86E+08
0.05	4.62E+06	4.30E+06	4.93E+06	5.	2.37E+08	2.23E+08	2.52E+08
0.06	8.98E+06	8.34E+06	9.63E+06	6.	2.14E+08	2.01E+08	2.27E+08
0.07	1.52E+07	1.41E+07	1.64E+07	7.	1.97E+08	1.84E+08	2.09E+08
0.08	2.34E+07	2.16E+07	2.52E+07	8.	1.83E+08	1.72E+08	1.95E+08
0.09	3.35E+07	3.09E+07	3.61E+07	9.	1.73E+08	1.62E+08	1.84E+08
0.1	4.52E+07	4.17E+07	4.88E+07	10.	1.64E+08	1.54E+08	1.75E+08
0.11	5.85E+07	5.40E+07	6.30E+07				
0.12	7.30E+07	6.73E+07	7.86E+07				
0.13	8.84E+07	8.16E+07	9.52E+07				
0.14	1.05E+08	9.66E+07	1.13E+08				
0.15	1.21E+08	1.12E+08	1.31E+08				
0.16	1.38E+08	1.28E+08	1.49E+08				

B Correction of the Reaction Rate between Protons and Neutrons

In the Big Bang nucleosynthesis, the ratio between protons and neutrons is an important quantity in discussing the composition of ^{4}He. The reaction rate (Wagoner rate) between protons and neutrons [109] is commonly used for the Big Bang nucleosynthesis. We evaluated Wagoner's rate by computing (1.24) -(1.29) formulae (Integrated formulae). The Wagoner's reaction rate includes Coulomb correction which is characterized by the parameter $F_{\rm n}$ whose $F_{\rm n}$ corresponds to the non relativistic case of $\mathcal{G}$ (B.6). We set $F_{\rm n} = 1$ to exclude the effect.

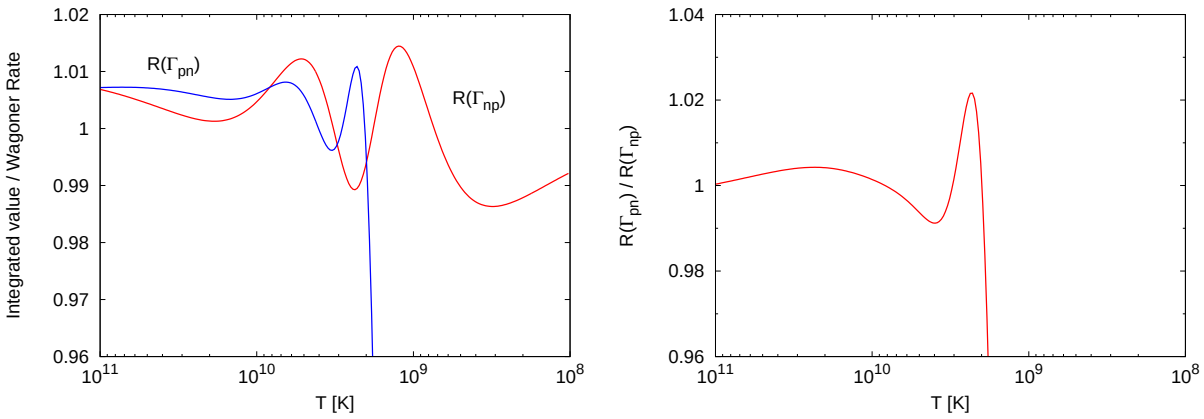

Fig. B.1: Left: R indicates the ratio of Integrated value to Wagoner rate s^{-1} in BBN. Γ_{ij} denotes the $i \to j$ reaction. Red and blue lines indicate p $\to$ n and n $\to$ p. Right: Deviation from thermal equilibrium of neutrons and protons.

Wagoner's reaction rate of n$\longleftrightarrow$p has $\sim$1% accuracy in the range of $1 \times 10^{11} \sim 2 \times 10^9$ K, and p$\longrightarrow$n reaction rate is over estimated in low temperature. However, in the low temperature the abundance of ^{4}He is hardly effected since the heavy nucleon begins to be generated.

Furthermore, radiative and Coulomb correction are written as [17, 96];

$$\mathcal{R}(\beta, y) = 1 + \frac{\alpha}{2\pi} C(\beta, y), \tag{B.1}$$

$$\mathcal{G}(\pm Z, E) \equiv xF(\pm Z, E). \tag{B.2}$$

Here, $x \equiv (E_{\rm e}^2 - m_{\rm e}^2 c^4)^{1/2}/E_{\rm e}$

$$F(\pm Z, E_{\rm e}) = 2(1+s)(2pR)^{2(s-1)} e^{\pm\pi\omega} \left| \frac{\Gamma(s \pm i\omega)}{\Gamma(2s+1)} \right|^2 . \tag{B.3}$$

$$(\text{ with } \quad s = (1-(\alpha Z)^2)^{1/2}, \quad \omega = \pm \alpha Z/x \quad)$$

$$\begin{aligned} C(\beta, y) \simeq\ & 40 + 4(U-1)\left(\frac{y}{3\epsilon} - \frac{3}{2} + \ln 2y\right) + U\left[2(1+\beta^2) + \frac{1}{6}\left(\frac{y}{\epsilon}\right)^2 - 4\beta U\right] \\ & -4\left(\frac{2 + 11\beta + 25\beta^2 + 25\beta^3 + 30\beta^4 + 20\beta^5 + 8\beta^6}{(1+\beta)^6}\right) \end{aligned} \tag{B.4}$$

$$U \equiv \beta^{-1} \tanh^{-1} \beta, \tag{B.5}$$

where β is the velocity of electron per speed of light, y and ϵ are the energies of neutrinos and electrons. α is the fine structure constant, Γ is the Gamma function, and Z is the nuclear charge after the decay. It is noted that electron has the plus sign and positron has minus. R is the nuclear radius; $R = 2.908 \times 10^{-3} A^{1/3} - 2.437 A^{-1/3}$, where A is the nuclear mass number.

Especially, the cases of the neutral particle and non relativistic limit (B.2) reduces to:

$$\begin{aligned} \mathcal{G}(0, E) &= 1, \\ \mathcal{G}(Z, \beta \ll 1) &\rightarrow \frac{2\pi\omega/\beta}{1 - e^{-2\pi\omega/\beta}}. \end{aligned}$$

In our BBN code, the Coulomb correction is performed by multiplying (B.6) by (1.24), (1.25), (1.27), and (1.28). It is noted that (1.26) and (1.29) have no Coulomb correction factor since there are no coulomb interaction between neutrons and positrons, and protons and neutrinos.

C Fermi-Dirac Integral

In this section, we show the solution of the Fermi-Dirac integral with positive/negative chemical potential. The solution is useful to calculate the physical quantities, such as number density and energy density.

Positive chemical potential

At first, we show the solution of the Fermi-Dirac integral with positive chemical potential $\mathcal{F}_{\rm FD+}$.

$$\begin{aligned}\mathcal{F}_{\rm FD+} &= \int_0^\infty dx\ \frac{x^n}{1+\exp(x-\mu)} \quad (\,\mu \geq 0\,) \\ &= \int_0^\mu dx\ \frac{x^n}{1+\exp(x-\mu)} + \int_\mu^\infty \frac{x^n \exp(-x+\mu)}{1+\exp(-x+\mu)} \equiv \mathcal{F}_1 + \mathcal{F}_2 \end{aligned} \tag{C.1}$$

The first term of (C.1) is

$$\begin{aligned}\mathcal{F}_1 &= \int_0^\mu dx\ x^n \left(\sum_{k=0}^\infty \exp[k(x-\mu)]\cdot(-1)^k\right) \\ &= \int_0^\mu dx\ x^n \left(\sum_{0}^\infty \exp(kx)\cdot\exp(-k\mu)\cdot(-1)^k\right) \\ &= \sum_{k=0}^\infty \left(\int_0^\mu dx\ x^n \exp(kx)\right)\exp(-k\mu)\cdot(-1)^k \\ &= \sum_{k=1}^\infty \sum_{l=0}^n \left[\frac{n!}{l!}\frac{(-k)^{l-n}}{k}x^l\exp(kx)\right]_0^\mu \exp(-k\mu)\cdot(-1)^k + \left[\frac{x^{n+1}}{n+1}\right] \\ &= \sum_{k=1}^\infty \sum_{l=0}^n \left[\frac{n!}{l!}\frac{(-k)^{l-n}}{k}\mu^l\right]\cdot(-1)^k - \sum_{k=1}^\infty \left[n!\frac{(-k)^{-n}}{k}\exp(-k\mu)\right]\cdot(-1)^k + \frac{\mu^{n+1}}{n+1}. \end{aligned}$$

The second term of (C.1) is

$$\begin{aligned}
\mathcal{F}_2 &= \int_0^\infty dx\; x^n \exp(-x+\mu)\left(\sum_{k=0}^{\infty}\exp[k(-x+\mu)]\cdot(-1)^k\right) \\
&= \sum_{k=1}^{\infty}\left[\int_\mu^\infty dx\; x^n\exp(-kx)\right]\exp(k\mu)(-1)^{k+1} \\
&= \sum_{k=1}^{\infty}\sum_{l=0}^{n}\left[\frac{n!}{l!}\frac{k^{l-n}}{-k}x^l\exp(-kx)\right]_\mu^\infty \exp(k\mu)(-1)^{k+1} \\
&= -\sum_{k=1}^{\infty}\sum_{l=0}^{n}\left[\frac{n!}{l!}\frac{k^{l-n}}{-k}\mu^l\right](-1)^{k+1} \\
&= \sum_{k=1}^{\infty}\sum_{l=0}^{n}\left[\frac{n!}{l!}\frac{k^{l-n}}{-k}\mu^l\right](-1)^{k}.
\end{aligned}$$

Hence,

$$\begin{aligned}
\mathcal{F}_{\mathrm{FD+}} &= \frac{\mu^{n+1}}{n+1}+\sum_{k=1}^{\infty}\sum_{l=0}^{n}\left[\frac{n!}{l!}\frac{(-k)^{l-n}-k^{l-n}}{k}\mu^l\right](-1)^k \\
&\qquad +\sum_{k=1}^{\infty} n!\left[\frac{(-\exp(-\mu))^k}{k^{n+1}}\right](-1)^{n+1}. \qquad \cdots(\star)
\end{aligned}$$

Moreover, an inifinite series in the second term of $(\star)$ can be written by the Dirichlet-eta function:

(i) The case of mod(n,2)$\equiv$ 0:

$$\begin{aligned}
(\text{Second term}) &= \sum_{k=1}^{\infty}\sum_{p=1}^{n/2}\left[\frac{n!}{(2p-1)!}\frac{-2}{k^{n+1-(2p-1)}}\mu^{2p-1}\right](-1)^k \\
&= \sum_{k=1}^{\infty}\sum_{p=1}^{n/2}\left[2\frac{n!}{(2p-1)}\frac{(-1)^{k-1}}{k^{n+2-2p}\mu^{2p-1}}\right] \\
&= \sum_{p=1}^{n/2}\left[2\frac{n!}{(2p-1)}\eta(n+2-2p)\mu^{2p-1}\right].
\end{aligned}$$

(ii) The case of mod(n,2)$\equiv$ 1:

$$\begin{aligned}
(\text{Second term}) &= \sum_{k=1}^{\infty}\sum_{p=0}^{(n-1)/2}\left[\frac{n!}{(2p)!}\frac{-2}{k^{n+1-2p}}\mu^{2p}\right](-1)^k \\
&= \sum_{k=1}^{\infty}\sum_{p=0}^{(n-1)/2}\left[2\frac{2!}{(2p)!}\frac{(-1)^{k-1}}{k^{n+1-2p}}\mu^{2p}\right] \\
&= \sum_{p=0}^{(n-1)/2}\left[2\frac{n!}{(2p)!}\eta(n+1-2p)\mu^{2p}\right].
\end{aligned}$$

The third term of ($\star$) can be shown;

$$\begin{aligned}
(\text{Third term}) &= -\sum_{k=1}^{\infty}\left[n!\frac{(-k)^{-n}}{k}\exp(-k\mu)\right](-1)^k \\
&= (-1)^{n+1}n!\sum_{k=1}^{\infty}\frac{(-\exp(-\mu))^k}{k^{n+1}} \\
&= (-1)^{n+1}n!\ \mathrm{Li}_{n+1}\left(-e^{-\mu}\right),
\end{aligned}$$

where $\mathrm{Li}_{n+1}\left(-e^{-\mu}\right)$ is the polylogarithm.
Consequently, we obtain the following formulae;

$$\mathcal{F}_{\mathrm{FD}+} = \frac{\mu^{n+1}}{n+1}+\sum_{p=1}^{n/2}\left[2\frac{n!}{(2p-1)}\eta(n+2-2p)\mu^{2p-1}\right]+(-1)^{n+1}n!\ \mathrm{Li}_{n+1}\left(-e^{-\mu}\right)$$

is for mod(n,2)$\equiv$ 0 and

$$\mathcal{F}_{\mathrm{FD}+} = \frac{\mu^{n+1}}{n+1}+\sum_{p=0}^{(n-1)/2}\left[2\frac{n!}{(2p)!}\eta(n+1-2p)\mu^{2p}\right]+(-1)^{n+1}n!\ \mathrm{Li}_{n+1}\left(-e^{-\mu}\right)$$

is for mod(n,2)$\equiv$ 1.

Negative chemical potential

$$\mathcal{F}_{\mathrm{FD}-} = \int_0^{\infty}\frac{x^n}{1+\exp(x+\mu)} \quad (\,\mu\geq 0\,) \tag{C.2}$$

$$
\begin{aligned}
\mathcal{F}_{\mathrm{FD}-} &= \int_0^\infty dx\ x^n \frac{\exp(-x-\mu)}{1+\exp(-x-\mu)} \\
&= \int_0^\infty dx\ x^n \exp(-x-\mu)\left(\sum_{k=0}^{\infty}\exp[k(-x-\mu)]\cdot(-1)^k\right) \\
&= \sum_{k=1}^{\infty}\left[\int_0^\infty dx\ x^n\exp(-kx)\right]\exp(-k\mu)(-1)^{k+1} \\
&= \sum_{k=1}^{\infty}\sum_{l=0}^{n}\left[\frac{n!}{l!}\frac{k^{l-n}}{-k}x^l\exp(-kx)\right]_0^\infty \exp(-k\mu)(-1^{k+1}) \\
&= -\sum_{k=1^\infty}\left[n!\frac{k^{-n}}{-k}\exp(-k\mu)\right](-1)^{k+1} \\
&= -\sum_{k=1}^{\infty} n!\frac{(-\exp(-\mu))^k}{k^{n+1}} \\
&= -n!\mathrm{Li}_{n+1}(-e^{-\mu})
\end{aligned}
$$

Formula

Riemann-zeta function is

$$\zeta(s)=\sum_{k=1}^{\infty}\frac{1}{k^s}.$$

Dirichlet-eta function is

$$\eta(s)=\sum_{k=1}^{\infty}\frac{(-1)^{k-1}}{k^s}=(1-2^{1-s})\zeta(s).$$

Particularly,

$$\eta(1)=\ln 2\ ,\ \eta(2)=\frac{\pi^2}{12}\ ,\ \eta(4)=\frac{7\pi^4}{720}\ ,\ \eta(6)=\frac{31\pi^6}{30240}.$$

Polylogarithm is defined as

$$\mathrm{Li}_s(z)=\sum_{k=1}^{\infty}\frac{z^k}{k^s}\quad(\ |z|<1,\ s,z\in\mathbb{C}\ ).$$

Acknowledgment

I am very grateful to my advisor, Prof. Masa-aki Hashimoto for his proper advices, continuous encouragement, useful discussions and critical reading of this thesis.

I thank Prof. K. Arai, Assistant Prof. H. Yamaoka, Assistant Prof. M. Machida for useful discussions and advices. I greatly appriciate Prof. S. Fujimoto for useful discussions and advices on nucleosynthesis. I am really thankful to Dr. R. Nakamura, Dr. E. P. B. A. Thushari for their continuous encouragement and advices. I thank to the member of our research group, especially I am grateful to Y. Matsuo for giving me technical advises since my era of graduate student. I am also grateful to Y. Kikuchi, K. Hayashida, K. Takagi, Y. Morita, R. Fukuda, S. Komeda, H. Tezuka, K. Mimasu, Y. Ueki, R. Une, T. Nakahara, Y. Taniguchi, Y. Arimura, T. Ohmura, H. Sakemi, M. Nakao and G. Nagano.

References

[1] A. Einstein, Annalen der Physik **354**, 769 (1916).

[2] A. Friedmann, Zeitschrift fur Physik **10**, 377 (1922).

[3] G. Lemaître, Annales de la Société Scientifique de Bruxelles **47**, 49 (1927).

[4] E. Hubble, Contributions from the Mount Wilson Observatory, vol. 3, pp.23-28 **3**, 23 (1929).

[5] G. Gamow, Physical Review **70**, 572 (1946).

[6] R. A. Alpher, H. Bethe, and G. Gamow, Physical Review **73**, 803 (1948).

[7] C. Hayashi, Progress of Theoretical Physics **5**, 224 (1950).

[8] C. Hayashi, Progress of Theoretical Physics Supplement **49**, 248 (1971).

[9] A. A. Penzias and R. W. Wilson, Astrophys. J. **142**, 419 (1965).

[10] Planck Collaboration *et al.*, Astron. Astrophys. **594**, A1 (2016), 1502.01582.

[11] A. G. Riess *et al.*, Astron. J. **116**, 1009 (1998), astro-ph/9805201.

[12] J. C. Mather, D. J. Fixsen, R. A. Shafer, C. Mosier, and D. T. Wilkinson, Astrophys. J. **512**, 511 (1999), astro-ph/9810373.

[13] D. J. Fixsen, Astrophys. J. **707**, 916 (2009), 0911.1955.

[14] O. Pisanti *et al.*, Computer Physics Communications **178**, 956 (2008), 0705.0290.

[15] A. Coc, J.-P. Uzan, and E. Vangioni, J. Cosmol. Astropart. Phys. **10**, 050 (2014), 1403.6694.

[16] G. Mangano *et al.*, Nucl. Phys. B **729**, 221 (2005).

[17] D. A. Dicus *et al.*, Phys. Rev. D **26**, 2694 (1982).

[18] Y. I. Izotov, T. X. Thuan, and N. G. Guseva, Mon. Non. R. Astorn. Soc. **445**, 778 (2014), 1408.6953.

[19] G. Steigman, Annual Review of Nuclear and Particle Science **57**, 463 (2007), 0712.1100.

[20] F. X. Timmes, S. E. Woosley, and T. A. Weaver, Astrophys. J. Suppl. **98**, 617 (1995), astro-ph/9411003.

[21] J. Cooke *et al.*, Astrophys. J. **781**, 16 (2014).

[22] M. Kawasaki and M. Kusakabe, Phys. Rev. D **86**, 063003 (2012), 1204.6164.

[23] W. P. Gieren, T. G. Barnes, III, and T. J. Moffett, Astrophys. J. **418**, 135 (1993).

[24] G. Altavilla *et al.*, Mon. Non. R. Astorn. Soc. **349**, 1344 (2004), astro-ph/0401273.

[25] S. Perlmutter *et al.*, Cosmology From Type IA Supernovae: Measurements, Calibration Techniques, and Implications, in *American Astronomical Society Meeting Abstracts*, , Bulletin of the American Astronomical Society Vol. 29, p. 1351, 1997, astro-ph/9812473.

[26] D. Yonetoku *et al.*, Astrophys. J. **609**, 935 (2004), astro-ph/0309217.

[27] L. Amati *et al.*, Mon. Non. R. Astorn. Soc. **391**, 577 (2008), 0805.0377.

[28] S. Capozziello and L. Izzo, Astron. Astrophys. **519**, A73 (2010), 1003.5319.

[29] M. G. Dainotti, V. F. Cardone, E. Piedipalumbo, and S. Capozziello, Mon. Non. R. Astorn. Soc. **436**, 82 (2013), 1308.1918.

[30] P. A. R. Ade *et al.*, Astron. Astrophys. **571**, A16 (2014), 1303.5076.

[31] P. A. R. Ade *et al.*, ArXiv e-prints (2015), 1502.01589.

[32] S. Perlmutter *et al.*, Astrophys. J. **517**, 565 (1999), astro-ph/9812133.

[33] A. G. Riess *et al.*, Astrophys. J. **607**, 665 (2004), astro-ph/0402512.

[34] T. Chiba, T. Okabe, and M. Yamaguchi, Phys. Rev. D **62**, 023511 (2000), astro-ph/9912463.

[35] R. R. Caldwell, R. Dave, and P. J. Steinhardt, Phys. Rev. Lett.**80**, 1582 (1998), astro-ph/9708069.

[36] M. C. Bento, O. Bertolami, and A. A. Sen, Phys. Rev. D **66**, 043507 (2002), gr-qc/0202064.

[37] C. Gao, F. Wu, X. Chen, and Y.-G. Shen, Phys. Rev. D **79**, 043511 (2009), 0712.1394.

[38] S. Hannestad and E. Mörtsell, J. Cosmol. Astropart. Phys. **9**, 001 (2004), astro-ph/0407259.

[39] R. Nakamura, M.-A. Hashimoto, and K. Ichiki, Phys. Rev. D **77**, 123511 (2008), 0801.0290.

[40] N. Suzuki *et al.*, Astrophys. J. **746**, 85 (2012), 1105.3470.

[41] R. D. Sorkin, Is the cosmological "constant" a nonlocal quantum residue of discreteness of the causal set type?, in *Particles, Strings, and Cosmology-PASCOS 2007*, edited by A. Rajantie, C. Contaldi, P. Dauncey, and H. Stoica, , American Institute of Physics Conference Series Vol. 957, pp. 142–153, 2007, 0710.1675.

[42] Y.-F. Cai, E. N. Saridakis, M. R. Setare, and J.-Q. Xia, Phys. Rep. **493**, 1 (2010), 0909.2776.

[43] H. K. Jassal, J. S. Bagla, and T. Padmanabhan, Mon. Non. R. Astorn. Soc. **405**, 2639 (2010), astro-ph/0601389.

[44] S. Nesseris and L. Perivolaropoulos, J. Cosmol. Astropart. Phys. **1**, 018 (2007), astro-ph/0610092.

[45] P. Wu and H. Yu, Phys. Lett. B**643**, 315 (2006), astro-ph/0611507.

[46] U. Alam, V. Sahni, and A. A. Starobinsky, J. Cosmol. Astropart. Phys. **6**, 008 (2004), astro-ph/0403687.

[47] K. Hirano and Z. Komiya, General Relativity and Gravitation **42**, 2751 (2010), 0912.4950.

[48] Y. Du, H. Zhang, and X.-Z. Li, European Physical Journal C **71**, 1660 (2011), 1008.4421.

[49] Y. Izotov *et al.*, A&A **57**, 558 (2013).

[50] E. Aver *et al.*, J. Cosmol. Astropart. Phys. **11**, 17 (2013).

[51] L. Sbordone *et al.*, 2010 **26**, 552 (2010).

[52] A. J. Korn *et al.*, Nature **442**, 657 (2006), astro-ph/0608201.

[53] M. Hashimoto and K. Arai, Physics Reports of Kumamoto Uiversity **7**, 47 (1985).

[54] P. Descouvemont, A. Adahchour, C. Angulo, A. Coc, and E. Vangioni-Flam, Atomic Data and Nuclear Data Tables **88**, 203 (2004), astro-ph/0407101.

[55] J. Bering *et al.*, Phys. Rev. D **86**, 010001 (2012).

[56] P. A. R. Ade *et al.*, astro-ph (2013), 1311.1657.

[57] Y. Xu *et al.*, Nuclear Physics A **918**, 61 (2013), 1310.7099.

[58] A. Serebrov *et al.*, Physics Letters B **605**, 72 (2005), nucl-ex/0408009.

[59] D. Dubbers and M. G. Schmidt, Reviews of Modern Physics **83**, 1111 (2011), 1105.3694.

[60] K. N. Abazajian *et al.*, ArXiv e-prints (2012), 1204.5379.

[61] M. Kusakabe *et al.*, Astrophys. J. Suppl. **214**, 5 (2014), 1403.4156.

[62] C. Bird, K. Koopmans, and M. Pospelov, Phys. Rev. D **78**, 083010 (2008), hep-ph/0703096.

[63] R. H. Cyburt *et al.*, J. Cosmol. Astropart. Phys. **12**, 037 (2012), 1209.1347.

[64] T. Jittoh *et al.*, Phys. Rev. D **76**, 125023 (2007), 0704.2914.

[65] M. Kamimura, Y. Kino, and E. Hiyama, Progress of Theoretical Physics **121**, 1059 (2009), 0809.4772.

[66] M. Kawasaki, K. Kohri, and T. Moroi, Physics Letters B **649**, 436 (2007), hep-ph/0703122.

[67] K. Kohri and F. Takayama, Phys. Rev. D **76**, 063507 (2007), hep-ph/0605243.

[68] G. Steigman and K. M. Nollett, Physics Procedia **61**, 179 (2015), 1402.5399.

[69] K. M. Nollett and G. Steigman, Phys. Rev. D **91**, 083505 (2015), 1411.6005.

[70] K. J. Bae, H. Baer, and A. Lessa, J. Cosmol. Astropart. Phys. **4**, 041 (2013), 1301.7428.

[71] S. Weinberg, Physical Review **128**, 1457 (1962).

[72] R. V. Wagoner, W. A. Fowler, and F. Hoyle, Astrophys. J. **148**, 3 (1967).

[73] K. Arai, M. Hashimoto, and T. Fukui, Astron. Astrophys. **179**, 17 (1987).

[74] E. P. B. A. Thushari, R. Nakamura, M. Hashimoto, and K. Arai, Astron. Astrophys. **521**, A52 (2010), 1007.1060.

[75] M. Hashimoto, R. Nakamura, S. Gamow, and K. Arai, Nuclear Physics A **758**, 779 (2005).

[76] T. P. Sotiriou and V. Faraoni, Reviews of Modern Physics **82**, 451 (2010), 0805.1726.

[77] R. Nakamura, E. P. B. A. Thushari, M. Ikeda, and M.-a. Hashimoto, CMB constraints on the thermal evolution with a decaying cosmological term, in *American Institute of Physics Conference Series*, edited by S. Kubono *et al.*, , American Institute of Physics Conference Series Vol. 1484, pp. 400–402, 2012.

[78] R. Nakamura, M.-A. Hashimoto, S.-I. Fujimoto, N. Nishimura, and K. Sato, Constraints on the heavy elements production in inhomogeneous Big-Bang nucleosynthesis from light-element observations, in *American Institute of Physics Conference*

Series, edited by I. Tanihara *et al.*, , American Institute of Physics Conference Series Vol. 1269, pp. 378–380, 2010.

[79] T. Clifton, P. G. Ferreira, A. Padilla, and C. Skordis, Phys. Rep. **513**, 1 (2012), 1106.2476.

[80] A. Joyce, B. Jain, J. Khoury, and M. Trodden, Phys. Rep. **568**, 1 (2015), 1407.0059.

[81] A. D. Dolgov, Phys. Rep. **370**, 333 (2002), hep-ph/0202122.

[82] A. D. Dolgov and F. Takahashi, ArXiv High Energy Physics - Phenomenology e-prints (2004), hep-ph/0409299.

[83] A. D. Dolgov and F. Takahashi, Nuclear Physics B **688**, 189 (2004), hep-ph/0402066.

[84] E. Aver, K. A. Olive, and E. D. Skillman, J. Cosmol. Astropart. Phys. **7**, 011 (2015), 1503.08146.

[85] S. A. Balashev, E. O. Zavarygin, A. V. Ivanchik, K. N. Telikova, and D. A. Varshalovich, Mon. Non. R. Astorn. Soc. **458**, 2188 (2016), 1511.01797.

[86] A. G. Riess *et al.*, Astrophys. J. **659**, 98 (2007), astro-ph/0611572.

[87] R. Amanullah *et al.*, Astrophys. J. **716**, 712 (2010), 1004.1711.

[88] A. Conley *et al.*, Astrophys. J. Suppl. **192**, 1 (2011), 1104.1443.

[89] J. Liu and H. Wei, General Relativity and Gravitation **47**, 141 (2015), 1410.3960.

[90] K. Bamba, C.-Q. Geng, S. Nojiri, and S. D. Odintsov, Phys. Rev. D **79**, 083014 (2009), 0810.4296.

[91] Y.-F. Cai, H. Li, Y.-S. Piao, and X. Zhang, Phys. Lett. B**646**, 141 (2007), gr-qc/0609039.

[92] G. O. Roberts, A. Gelman, and W. R. Gilks, The Annals of Applied Probability**7**, 110 (1997).

[93] H. Akaike, IEEE Trans. Automatic Control **19**, 716 (1974).

[94] P. A. R. Ade *et al.*, ArXiv e-prints (2015), 1502.01590.

[95] S. Ando *et al.*, Phys. Rev. C **74**, 025809 (2006).

[96] C. J. Smith and G. M. Fuller, Phys. Rev. D **81**, 06527 (2010).

[97] C. Angulo *et al.*, Nuclear Physics A **656**, 3 (1999).

[98] Y. Nagai *et al.*, Phys. Rev. C **74**, 025804 (2006).

[99] I. Dillmann *et al.*, KADoNiS- The Karlsruhe Astrophysical Database of Nucleosynthesis in Stars, in *Capture Gamma-Ray Spectroscopy and Related Topics*, edited by A. Woehr and A. Aprahamian, , American Institute of Physics Conference Series Vol. 819, pp. 123–127, 2006.

[100] J. Su *et al.*, Chinese Physics Letters **27**, 052101 (2010), 1001.4329.

[101] R. V. Wagoner, Astrophys. J. Suppl. **18**, 247 (1969).

[102] G. R. Caughlan *et al.*, Atomic Data and Nuclear Data Tables **32**, 197 (1985).

[103] A. M. Mukhamedzhanov, L. D. Blokhintsev, and B. F. Irgaziev, Phys. Rev. C **83**, 055805 (2011), 1103.0453.

[104] R. G. Pizzone *et al.*, Astron. Astrophys. **438**, 779 (2005).

[105] R. A. Malaney and W. A. Fowler, Astrophys. J. **333**, 14 (1988).

[106] D. S. Leonard, H. J. Karwowski, C. R. Brune, B. M. Fisher, and E. J. Ludwig, Phys. Rev. C **73**, 045801 (2006), nucl-ex/0601035.

[107] T. Hashimoto *et al.*, Physics Letters B **674**, 276 (2009).

[108] J. K. Tuli, *Weak rates from the Nuclear Wallet Cards* (National Nuclear Data Center, 2004).

[109] R. V. Wagoner, Astrophys. J. **179**, 343 (1973).